Autophagy and Cell Autonomous Neurodegeneration in Niemann-Pick type C Disease

by

Matthew J. Elrick

A dissertation submitted in partial fulfillment
of the requirements for the degree of
Doctor of Philosophy
(Neuroscience)
in The University of Michigan
2011

Doctoral Committee:

Associate Professor Andrew P. Lieberman, Chair
Professor John K. Fink
Professor Daniel J. Klionsky
Professor Miriam H. Meisler
Associate Professor Kristen J. Verhey

In loving memory of my grandparents, Solomon and Rebecca Feinblum, who handed down their values of scholarship and love of family.

Acknowledgements

I would like to thank all of the members of the Lieberman lab, both for helping me to grow as a scientist and for providing a truly enjoyable atmosphere to come to work in every day. In particular, I thank Chris Pacheco, who welcomed me into the lab and showed me the ropes as a brand new student, and whose work formed the foundation for my own. I thank Adrienne Wang, who was always there when I needed to vent about the latest frustration or just wanted to chat, who was always willing to offer advice, and who was an endless source of those all-important lab tricks. I thank Nahid Dadgar, who was always available to lend a hand to keep my experiments running smoothly, and made sure I was well fed and well-supplied with product show freebies. And finally a very special thank you to Andy Lieberman, for being the best mentor I could have possibly hoped for. He taught me how to design a project and how to write about it well. He always looked out for my best interest first. Most importantly, he has served as a superb role model, who can run a productive lab with a friendly, collaborative environment, while being the exemplar of thoughtfulness and kindness.

I am very grateful to the members of my thesis committee, John Fink, Dan Klionsky, Miriam Meisler, and Kristen Verhey for dedicating their time, expertise, and personal concern. Each brought a different perspective to my project, and I have greatly valued their input. It was a privilege to have such a superb group of scientists as my committee. I truly enjoyed the opportunity to discuss my data with them.

Thanks to the MSTP office, especially Ron Koenig, Penny Morris, and Ellen Elkin, for their continuous support and genuine interest in not only my training but also my personal well-being. Thanks likewise to the Neuroscience Program for their support, in particular Steve Maren and Valerie Smith. I am also greatly indebted to the many faculty, students, postdocs and lab staff who generously gave of their own time and expertise to give me advice or teach me new methods, often inviting me into their own labs and asking nothing in return: Roger Albin, Sara Tallaksen-Greene, Mary Heng, Vikram Shakkottai, Arul Chinnaiyan, Shanker Kalyana-Sundaram, Steve Qin, Nick Lukacs, Sue O'Shea, Jim Shayman, Liming Shu, Kristen Verhey, John Dishinger, Joel Swanson, and Mike Davis. Thanks also to everyone at the Microscopy and Imaging Laboratory, especially Chris Edwards and Bruce Donohoe, for their guidance and expertise.

I thank my family for being so supportive of me. In particular, my parents who always encouraged me to follow my interests whatever they may be, and who taught me the value of honesty, compassion, and a strong work ethic. Thank you to my wife, Heather, who has proven to be the best reason of all for coming to Michigan. I couldn't imagine a better partner for undertaking the challenges of grad school, and with whom to savor every happy little moment life has to offer.

Finally, I thank all of the tremendous friends I've made through both the medical and graduate schools at Michigan. They have been a source of diversion when I need it, and of support and camaraderie always.

Table of Contents

List of Figures

Abstract

Niemann-Pick type C disease (NPC) is an autosomal recessive lysosomal storage disorder characterized by liver dysfunction and neurodegeneration causing diverse neurologic symptoms such as ataxia, cognitive decline, and seizures, and finally leading to premature death. It is caused by mutations in the *NPC1* or *NPC2* genes, leading to accumulation of cholesterol and glycosphingolipids in late endosomes and lysosomes of all tissues. At present, the link between lipid storage and neurodegeneration is unknown, representing a major impediment to the development of effective therapies for NPC disease.

In chapter 2, I characterize a novel conditional knockout mouse model for NPC disease and use it to determine the extent to which the degeneration of cerebellar Purkinje cells is cell autonomous. Deletion of *Npc1* only in Purkinje cells was sufficient to cause their degeneration, and lead to symptoms of ataxia and tremors. However, these mice did not demonstrate the weight loss or premature death that is characteristic of global *Npc1* mutants, demonstrating that these phenotypes arise from other cell types. I also noted a marked differential vulnerability to degeneration among Purkinje cell subpopulations. In chapter 3, I use bioinformatic methods to identify 16 genes whose expression patterns correlated strongly with this pattern of Purkinje cell death. One of these genes, *Hsp27*, promotes the survival of neurons in an *in vitro* model of NPC neurodegeneration.

In chapter 4, I identify autophagy as a contributor to neurodegeneration in NPC. Autophagy is a pathway for delivering cytoplasmic cargoes to the lysosome via double-membrane bound organelles known as autophagosomes. It has been closely linked to the process of neurodegeneration, and the induction of autophagy along with accumulation of autophagosomes has been documented in NPC disease. Here I show that autophagy induction lies downstream of Toll-like receptor signaling through the adapter protein TRIF. Further, autophagy is a major source for stored cholesterol in NPC lysosomes. Finally, lipid storage impairs the maturation of autolysosomes via inhibition of lysosomal cathepsin activity. Inhibition of autophagy by wortmannin reduced cholesterol storage, restored lysosomal proteolysis, and rescued neurodegeneration *in vitro*, thus demonstrating that autophagy plays a detrimental role in NPC pathogenesis.

Chapter 1

Introduction

Niemann-Pick disease type C (NPC) is a neurodegenerative disorder of childhood. It belongs to the family of more than 50 lysosomal diseases, which collectively represent the most common cause of neurodegeneration in childhood, with an incidence of 1:8000 births. Lysosomal diseases are characterized by accumulation of lysosomal substrates, due to genetic mutations that disrupt hydrolytic or transport activities of the lysosome (Wilcox, 2004). NPC disease arises from mutations in the *NPC1* or *NPC2* genes (Carstea et al., 1997; Naureckiene et al., 2000), which are involved in the export of cholesterol from late endosomes and lysosomes (Kwon et al., 2009). As a result of these mutations, a broad collection of lipids including cholesterol and glycosphingolipids accumulate in late endosomes and lysosomes of nearly all cells in the body (Vanier and Millat, 2003).

Typically, the earliest symptoms of NPC disease are visceral, including neonatal jaundice and hepatosplenomegaly. Following several years of normal development, patients begin to display cognitive decline, progressively worsening ataxia, dystonia, vertical supranuclear gaze paresis, and often seizures or cataplexy. Death typically

occurs in the teen years (Higgins et al., 1992). However, there is a remarkable amount of variability. Late onset forms of NPC disease may present primarily as psychiatric illness such as depression or schizophrenia in adulthood, only later progressing to motor symptoms and dementia (Josephs et al., 2003). At the other end of the spectrum, NPC disease may present in infancy and rapidly proceed to death within months to years (Vanier and Millat, 2003). Current treatments for NPC are primarily supportive in nature; no treatments are available that substantially modify the course of this devastating disease (Wraith et al., 2009).

At present, the link between impaired lipid trafficking and neurodegeneration is not known. It will be important to fill this knowledge gap in order to promote the design of targeted therapies capable of reversing the course of NPC disease. Further, insights gained from the study of NPC disease may prove valuable in understanding other lysosomal diseases, as well as related adult-onset disorders such as Alzheimer disease and Parkinson disease, two common forms of neurodegeneration whose origins are far less understood. Therefore, a major goal of this dissertation is to improve our understanding of the causes of neurodegeneration in NPC disease.

1.1 Pathophysiology

1.1.1 Genetics

NPC disease is inherited in an autosomal recessive fashion. Mutations in the *NPC1* gene are responsible for approximately 95% of cases, while *NPC2* mutations account for the remainder (Carstea et al., 1997; Naureckiene et al., 2000). NPC1 encodes a thirteen transmembrane spanning protein with homology to Patched that localizes to late endosomes and lysosomes (LE/LY) (Ioannou, 2001). It contains a sterol sensing

domain in the transmembrane region, similar to that found in cholesterol biosynthetic genes HMG-CoA reductase, SCAP, and 7DHCR; an amino terminal cholesterol binding domain on the luminal side of the membrane; and several luminal loops of unknown function (Scott and Ioannou, 2004; Infante et al., 2008). The domain structure of NPC1 I s diagrammed in **Figure 1.1**. NPC2 is a soluble protein primarily localized to the LE/LY lumen (Naureckiene et al., 2000). It binds cholesterol in an orientation opposite that of the NPC1 N-terminal domain. It is capable of extracting cholesterol from lipid bilayers, and then transferring it to another, or to the NPC1 N-terminal domain (Infante et al., 2008; Xu et al., 2008). NPC1 and NPC2 are thought to act cooperatively via a "hand-off" mechanism to export unesterified cholesterol from the LE/LY compartment (Wang et al., 2010).

Figure 1.1 NPC1 domain structure

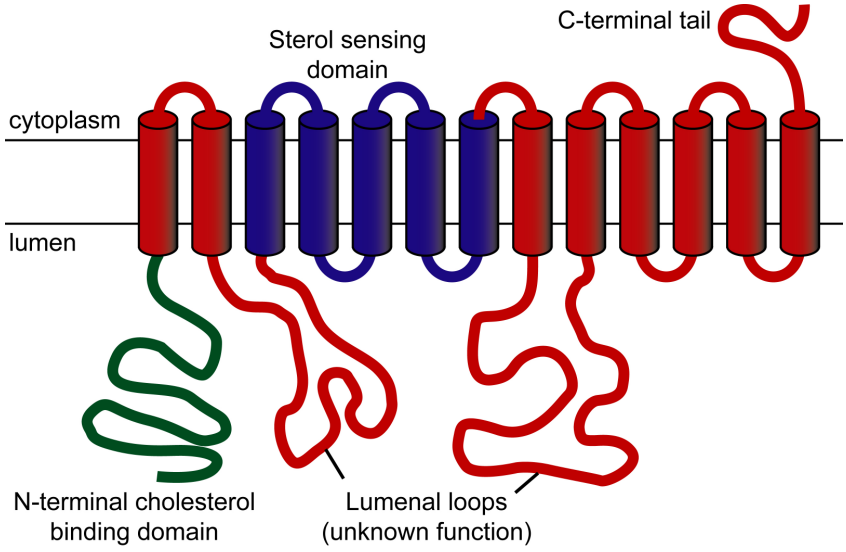

Over 200 disease-causing mutations in *NPC1* have been described, plus an additional 10 mutations in *NPC2* (Vanier and Millat, 2003). Surprisingly, there is very little genotype-phenotype correlation in NPC disease, and even siblings with the same

disease-causing mutations have demonstrated markedly different clinical courses (Fink et al., 1989). Several of these mutations are true null mutations. However, many encode a functional NPC1 protein that is detected as misfolded by endoplasmic reticulum (ER) chaperones and thus targeted for proteasomal degradation. As a result, almost no functional NPC1 reaches the late endosome and lysosome (Gelsthorpe et al., 2008). Disease-causing mutations therefore all act through a loss-of-function mechanism.

1.1.2 Lipid Trafficking and Storage

Cholesterol metabolism is tightly regulated at the whole organism level. For non-CNS tissues, the primary site of cholesterol synthesis is the liver, where cholesteryl esters are packaged into low-density lipoprotein (LDL) particles that also contain triglycerides and apolipoproteins, and are released into the blood circulation. Cells then take up these LDL particles via receptor-mediated endocytosis. Similarly, excess cholesterol can be secreted from the cell and carried back to the liver on high density lipoprotein (HDL) particles for recycling or excretion (Dietschy et al., 1993). However, LDL does not cross the blood brain barrier, and therefore a different system for metabolizing cholesterol is required in the brain. There is ample evidence that neurons are capable of synthesizing their own cholesterol *de novo*. Additionally, astrocytes can synthesize cholesterol and package it into an HDL-like particle containing ApoE and ApoJ for secretion into the extracellular space. This cholesterol can be taken up by neurons via receptor-mediated endocytosis, using a mechanism that is analogous to LDL-cholesterol uptake in the periphery. The relative importance of endogenous cholesterol synthesis versus uptake of exogenous cholesterol for neurons is unknown and may vary between neuronal populations or during development. Cholesterol excretion also varies markedly between

the brain and the periphery, again a requirement imposed by the fact that lipoprotein particles cannot cross the blood-brain barrier. The only means of removing cholesterol from the brain is by enzymatic conversion to 24S-hydroxycholesterol, which is capable of crossing the blood-brain barrier to enter the plasma circulation, from which it is presumably excreted or metabolized (Dietschy and Turley, 2001; Vance et al., 2005).

Once inside the cell, cholesterol arrives at the lysosome by two distinct mechanisms. The first, and best characterized, lies immediately downstream of receptor-mediated endocytosis of cholesteryl ester containing lipoproteins. Upon reaching the late endosome, cholesteryl esters dissociate from the lipoprotein particle and are hydrolyzed by lysosomal acid lipase (Goldstein and Brown, 2009). This unesterified cholesterol then exits late endosomes and lysosomes in an NPC1- and NPC2-dependent manner (Pentchev et al., 1985). The topology of the lysosome presents a particular challenge for lipid degradation and efflux. The lysosome is defined at its perimeter by a limiting membrane, protected from degradative enzymes on its lumenal side by a thick glycocalyx, formed by heavily glycosylated transmembrane proteins known as lysosomal associated membrane proteins (LAMPs) and lysosomal integral membrane proteins (LIMPs). Within the lysosome are a number of vesicular structures, known as the inner lysosomal membranes. Lipids arriving at the lysosome partition into these structures, which form the platform for the degradation of complex lipids. To remove cholesterol from the lysosome, therefore, it must first be extracted from the inner membranes, in which it is highly soluble, and then be carried across the aqueous environment of the lysosomal lumen and through the hydrophilic glycocalyx, in which it is relatively insoluble (Schulze et al., 2009). In the leading model for this process, NPC2 extracts cholesterol from the inner

membranes of the lysosome and then transfers it to the amino-terminal cholesterol binding domain of NPC1 (Infante et al., 2008). NPC1 likely then carries cholesterol across the glycocalyx lining the inner surface of the lysosomal membrane (Gallala et al., 2011). From here, it is unknown whether NPC1 simply inserts cholesterol into the limiting membrane of the lysosome or pumps it across the membrane. Next, cholesterol is transferred to the ER through a process that may involve the oxysterol binding protein related protein ORP5 (Du et al., 2011). Finally, cholesterol is redistributed by vesicular trafficking to various cellular membranes, where it plays an important role in membrane fluidity and microdomain formation, or it is re-esterified and stored in lipid droplets for later use (Maxfield and van Meer, 2010). This model of NPC1/NPC2 function is illustrated in **Figure 1.2**.

Figure 1.2 Model for NPC1/NPC2 function

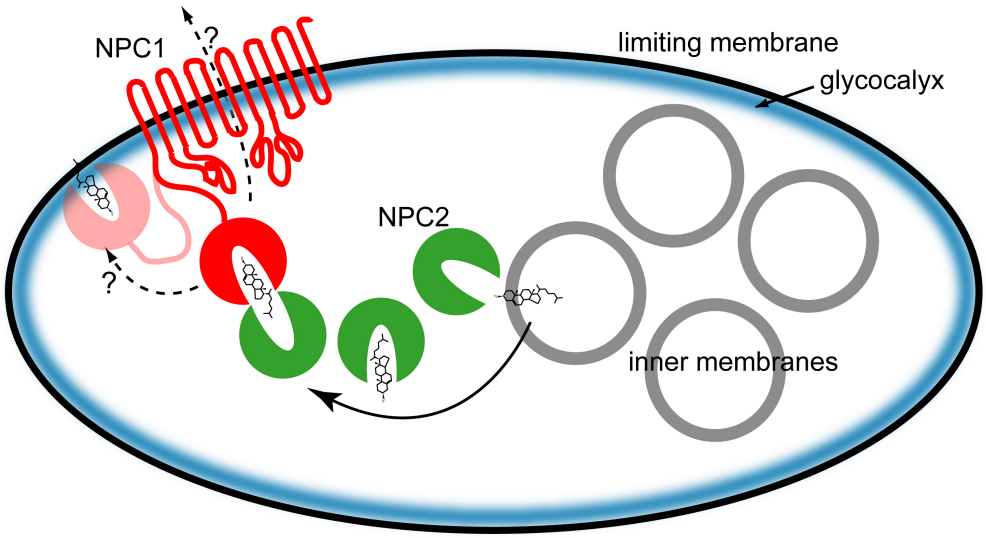

A second, more recently described, pathway that moves cholesterol through the lysosome is macrolipophagy (Singh et al., 2009). This pathway is involved in the liberation of cholesterol esters and triglycerides from lipid droplets, specialized

organelles containing a core of neutral lipids surrounded by a lipid monolayer and a number of associated proteins. The major role of this organelle is to store excess triglycerides and cholesterol, derived either from receptor-mediated endocytosis or endogenous *de novo* synthesis, for their later use in membrane structure or energy metabolism (Goodman, 2008). In macrolipophagy, lipid droplets are dismantled in a piecemeal fashion via enclosure in an autophagic vesicle, which goes on to fuse with the lysosome (Singh et al., 2009). Cholesteryl esters from the lipid droplet are hydrolyzed and exported from the lysosome in a manner that is presumably identical to that for LDL-derived cholesterol. It is important to note that additional modes of autophagy can also deliver various lipids to the lysosome, found in the membranes of organelles which are sequestered for autophagic degradation. One critical feature that all cholesterol trafficking pathways have in common is the absolute dependence upon NPC1 and NPC2 for efflux of cholesterol from the LE/LY compartment. A model of the two pathways proposed to contribute to cholesterol storage in NPC disease is presented in **Figure 1.3**.

Figure 1.3 Two routes for arrival of cholesterol at the lysosome, and storage in NPC disease

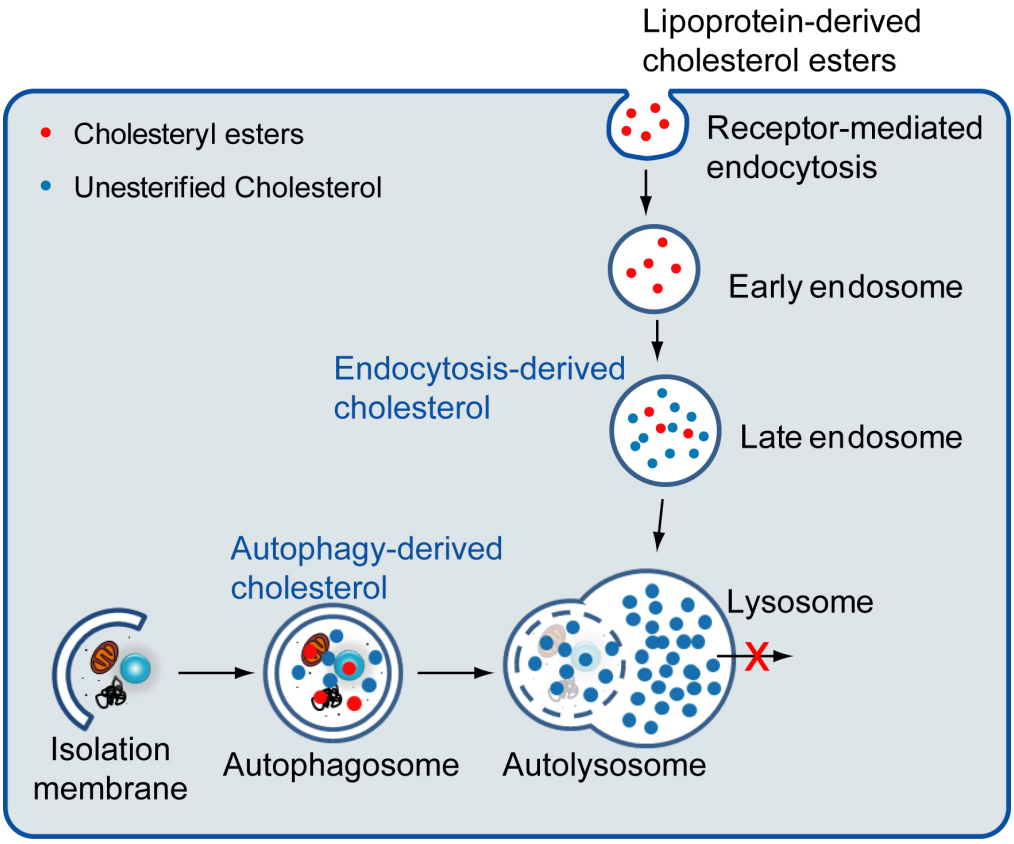

The most striking cellular consequence of NPC disease is the dramatic accumulation of lipids in late endosomes and lysosomes, and subsequent paucity of these lipids in membranes elsewhere in the cell. Primary among these lipid trafficking defects is unesterified cholesterol, which is readily stained in cultured cells and tissues by filipin. However, numerous glycosphingolipids (GSL) also accumulate, including sphingomyelin, glucosylceramide, lactosylceramide, globotriaosylceramide, sphingosine, and gangliosides G_M2 and G_M3 (Karten et al., 2009). The accumulation of cholesterol is easily explained by the direct role of NPC1 and NPC2 in cholesterol efflux. GSL storage, on the other hand, appears to be secondary to cholesterol accumulation. This

may arise from the altered ability of lipid hydrolases to access the internal membranes of the lysosome in the presence of excess cholesterol, or from a direct inhibition of hydrolysis or transport activity in the altered lysosomal environment (Schulze et al., 2009). Alternatively, a direct role for NPC1 and NPC2 in transporting GSLs cannot be ruled out. Classically, stored cholesterol in NPC lysosomes has been considered to be derived exclusively from the endocytic pathway via receptor-mediated endocytosis of lipoproteins (Mukherjee and Maxfield, 2004). However, it is important to consider that autophagy could also serve as an additional source of stored cholesterol. This novel mechanism of cholesterol storage will be investigated in Chapter 4.

1.1.3 Altered Cell Biology

As a result of impaired lipid trafficking, NPC1- or NPC2-deficient cells demonstrate a broad array of cell biological defects, including numerous abnormal phenotypes in the endosome-lysosome system. Large numbers of vesicular structures, observable by electron microscopy, accumulate in the cytoplasm. These include multilamellar vesicles, likely derived from lysosomes containing undigested lipids; increased numbers of normal-appearing endosomes and lysosomes; and double-membrane bound autophagic vesicles containing cargoes in various stages of degradation (Higashi et al., 1993; Pacheco et al., 2007). Rab7 and Rab9 are sequestered on vesicle membranes, and subsequently the intracellular trafficking of late endosomes is impaired (Choudhury et al., 2002; Ganley and Pfeffer, 2006). Defects in lysosomal calcium homeostasis have been described as well (Lloyd-Evans et al., 2008). Finally, NPC cells show marked alterations in autophagy (see section 1.5).

Several additional cellular and histopathological phenotypes have been demonstrated that are unique to the brain. Surprisingly, most of these phenotypes have no obvious connection to the endosome-lysosome system. Many neurons develop meganeurites, axonal spheroids, ectopic dendrites, Golgi fragmentation, demyelination, and altered recycling of synaptic vesicles (Elleder et al., 1985; Weintraub et al., 1987; Walkley and Suzuki, 2004; Xu et al., 2010). NPC neurons accumulate hyperphosphorylated tau, often coalescing into neurofibrillary tangles indistinguishable from those that are one of the pathological hallmarks of Alzheimer Disease (Auer et al., 1995; Love et al., 1995). Likewise, NPC neurons overproduce beta amyloid peptides, and on rare occasion NPC patients develop amyloid plaques similar to those seen in Alzheimer Disease (Mattsson et al., 2011). Lewy bodies, inclusions consisting of the α-synuclein protein that are typically characteristic of Parksinson Disease or Dementia with Lewy Bodies, have also been demonstrated in NPC patients at autopsy (Saito et al., 2004). Finally, NPC brains are deficient in the production of neurosteroids, cholesterol-derived molecules that play important roles in the development of neurons and modulation of neuronal excitability (Griffin et al., 2004). The widespread and numerous defects in neuronal biology help to explain the severity of neurologic involvement in NPC disease. However, the link between impaired cholesterol trafficking and neuronal pathology remains unknown.

1.1.4 Cell Death

Perhaps the most striking feature of NPC brain pathology is the widespread death of neurons. This is particularly notable in the Purkinje cells of the cerebellum, which degenerate in a characteristic anterior-to-posterior gradient, and are almost completely

lost by end stage. Additional neurodegeneration is present in the cortex, the thalamus, and the brainstem (German et al., 2001; Walkley and Suzuki, 2004). It remains to be established the extent to which neurological symptoms of NPC disease owe to neuron death versus neuronal dysfunction. However, as shown in Chapter 2, neurological manifestations in NPC mouse models appear only after a considerable number of neurons have been lost, suggesting that it is the death of neurons that leads to the neurological symptoms of NPC disease.

In order to effectively target neurodegeneration as a therapeutic strategy, it is important to understand the mechanism of cell death. Across various neurodegenerative diseases, multiple mechanisms have been proposed to explain neuron loss, including classical apoptosis (Mattson, 2000), other more chronic caspase-associated forms of cell death (Spires-Jones et al., 2009), autophagic programmed cell death (Yue et al., 2002), or necrosis (Syntichaki and Tavernarakis, 2003). What little evidence exists for NPC disease suggests that neuron death is a caspase-3 dependent apoptotic process, perhaps downstream of p73 activation (Cheung et al., 2004; Alvarez et al., 2008). However, whether apoptosis is the sole contributor to neurodegeneration in NPC disease remains unclear, as do the mechanisms that may link NPC1/NPC2 deficiency to the apoptotic pathway.

1.2 Models of NPC disease

A number of models for the study of NPC disease in the laboratory have been developed that have informed our current understanding of NPC pathogenesis. Common cell culture models include dermal fibroblasts donated by NPC patients with a variety of different mutations in NPC1 or NPC2, and a stable CHO cell line that is null for NPC1

(Pentchev et al., 1985; Cruz et al., 2000). Additionally, the small molecule U18666A, which is both a sterol and an amphiphilic amine, has been a popular tool due to its ability to rapidly induce a lipid storage phenotype identical to that of NPC1 or NPC2 deficient cells (Liscum and Faust, 1989). However, it remains to be determined whether U18666A acts as an antagonist of either of the NPC proteins, or induces lipid storage through some other mechanism.

Animal models have been a particularly popular tool in the study of NPC disease. Chief among these is the *npc*^{nih} mouse, a spontaneous null mutant of the *Npc1* gene occurring on the *Balb/c* background. *npc*^{nih} mice demonstrate many pathologic features resembling human NPC disease, including lipid storage, neurodegeneration, motor discoordination, cognitive deficits, weight loss, and premature death (Loftus et al., 1997; Voikar et al., 2002). An NPC cat model has also been a valuable tool for defining NPC pathology and testing therapeutic candidates (Lowenthal et al., 1990). These models have been invaluable in advancing our understanding of NPC disease and providing a platform for preclinical drug tests. However, animal models are lacking that would allow a more fine tuned and mechanistic dissection of NPC pathology, for example by manipulating the timing or location of NPC1 expression. To address this need, Chapter 2 will introduce of a novel conditional knockout mouse model of NPC disease.

1.3 Cell-Autonomous Neurodegeneration

A critical step in understanding the mechanisms underlying neurodegeneration in NPC disease, or any neurodegenerative disorder, is to define which cell types are driving the process. It is easy to imagine that neuron death may arise from an intrinsic ("cell-autonomous") defect that triggers programmed cell death or causes a failure of normal

metabolism and homeostasis. However, neuronal survival is also critically dependent on the support of glial cells, both to provide neurotrophic factors and to remove excess neurotransmitters and metabolites from the extracellular space (Barres, 2008). Further, survival of neurons often requires an intact connection to their pre- or post-synaptic partners.

Non-cell-autonomous forms of neurodegeneration have been recognized increasingly for their roles in diverse neurodegenerative diseases. The most well studied examples have been mouse models of familial SOD1-linked amyotrophic lateral sclerosis (ALS). Expression of disease-causing mutant SOD1 in any one cell type of transgenic mice has been insufficient to cause the motor neuron degeneration that is the hallmark of the disease (Gong et al., 2000; Lino et al., 2002). On the other hand, varying degrees of phenotypic rescue have been achieved in mice ubiquitously expressing a floxed SOD1 transgene that is excised by a tissue-specific Cre recombinase. Using this approach, direct roles in neurodegeneration have been demonstrated for motor neurons, microglia, and astrocytes (Boillee et al., 2006; Yamanaka et al., 2008). These data reveal a complex interplay between many cell types to drive motor neuron death, rather than a simple cell-autonomous mode of neurodegeneration.

Spinocerebellar ataxia type 7 (SCA7), on the other hand, demonstrates a purely non-autonomous mechanism of neurodegeneration. In SCA7 mouse models, expression of the disease causing polyglutamine expanded *ataxin-7* in Bergmann glia is sufficient to cause Purkinje cell degeneration identical to that caused by ubiquitous expression (Custer et al., 2006). In Huntington Disease, a similar approach has demonstrated that expression of pathogenic polyglutamine expanded huntingtin is only toxic to cortical pyramidal

neurons when additionally expressed in other neuronal populations, thus demonstrating a pathological interaction between neurons (Gu et al., 2005). Taken together, these studies demonstrate that cell-autonomous versus non-autonomous cell death is not a universal feature of neurodegenerative disease. Instead, a full spectrum exists between purely autonomous and purely non-autonomous neurodegeneration.

To fully define the pathogenesis of NPC disease, it will be important to first determine where it lies on this spectrum. Many individual observations have pointed to a role for glial involvement in the disease process. Microgliosis and astrocytosis are prominent features of NPC neuropathology (German et al., 2002). Further, NPC1-deficient astrocytes show defects in neurosteroid production (Griffin et al., 2004) and co-culture of *Npc1*$^{-/-}$ astrocytes with wild type neurons impairs neurite outgrowth (Chen et al., 2007). Mouse and fly models of NPC disease in which an NPC1 transgene under control of GFAP or glial promoters, presumed to drive expression in mouse astrocytes or fly glia, have been able to slow neurodegeneration and partially rescue the phenotype of these animals (Phillips et al., 2008; Zhang et al., 2008). Contrary to the above, the generation of chimeric mice demonstrated that wild type Purkinje neurons can survive in an environment containing *Npc1*$^{-/-}$ neurons and glia (Ko et al., 2005). Clearly, more work is needed to quantitatively define the contributions of cell-autonomous and non-cell-autonomous processes to neurodegeneration in NPC disease. In Chapter 2, I introduce a novel conditional knockout mouse model of NPC disease, and use it to determine the extent to which Purkinje cell degeneration is cell-autonomous.

1.4 Selective vulnerability

A prominent feature of nearly all neurodegenerative diseases is the selective vulnerability to degeneration of specific neuronal subpopulations, and the partial or complete resistance of others (Double et al., 2010). This is particularly surprising in the case of genetic neurodegenerative disorders, wherein the disease-causing gene is often ubiquitously expressed. However, toxicity from the mutation may be found only in the brain, and then is further limited only to a specific subset of neurons. In the case of NPC disease, neurodegeneration, while widespread, is limited to distinct subpopulations of neurons within the cerebellum, cortex, thalamus, and brainstem (German et al., 2001; Walkley and Suzuki, 2004). Further, among cerebellar Purkinje cells there is a characteristic pattern of cell loss along an anterior-to-posterior gradient, as well as a parasagittal "striping" pattern of Purkinje cell survival (Sarna et al., 2003). Understanding the cellular pathways that define the differences between vulnerable and resistant populations will yield significant insight into the mechanisms of pathogenesis of NPC and other neurodegenerative diseases. Further, the pathways responsible for selective vulnerability are likely to be valuable therapeutic targets. In Chapter 3, I explore the mechanisms by which Purkinje cells in the posterior cerebellar lobules resist neurodegeneration in NPC disease.

1.5 Autophagy

Autophagy, or "self eating," is the delivery of the cell's cytoplasmic constituents to the lysosome for degradation and recycling (Klionsky, 2005). It consists of three forms. Chaperone-mediated autophagy is a mechanism by which individual proteins containing a KFERQ motif are unfolded and fed through the lysosomal membrane

through a process mediated by the chaperone hsc70 and the lysosomal integral membrane protein LAMP-2A (Orenstein and Cuervo, 2010). Microautophagy involves the direct invagination of a small portion of cytoplasm into the lysosome (Uttenweiler and Mayer, 2008). Finally, macroautophagy is the sequestration of a large portion of cytoplasm in a double-membrane bound vesicle which fuses with late endosomes or lysosomes to deliver its contents into the degradative pathway (Yang and Klionsky, 2010). Of the various forms of autophagy, macroautophagy is the focus of this dissertation, and will here forth simply be referred to as "autophagy."

At the molecular level, autophagy is a tightly regulated process. The formation of the autophagosomal membrane requires two distinct ubiquitin-like conjugation cascades. In the first, the ubiquitin-like molecule Atg12 is conjugated to the E1-like ligase Atg7, then the E2-like Atg10, and finally the E3-like Atg5. In the second cascade, microtubule associated protein light chain 3 (LC3) is first cleaved by Atg4 to yield LC3-I. In this cascade, LC3-I is the ubiquitin-like protein, and Atg7 and Atg3 play the role of E1 and E2 ligases, respectively. Atg3 is capable of acting as its own E3-like enzyme to exchange itself for the diacyl group of phosphatidylethanolamine, thus forming the lipidated LC3-II. However, this step is markedly accelerated by a protein complex formed by the association of Atg5-Atg12 with Atg16 which also has E3-like activity. LC3-II is inserted into the autophagosomal membrane, and appears to be required for its formation, enclosure and proper trafficking (Ravikumar et al., 2010).

Upstream of the conjugation cascades, the major regulators of autophagy are mTOR and Beclin-1. mTOR receives numerous signals relating to the cell's nutrient and energy status and thus represses autophagy in times of nutrient excess. This is achieved

through inhibitory phosphorylation of the ULK1/2-Atg13-FIP200 complex, which is involved in recruitment of members of the Atg conjugation cascade to the autophagosomal membrane (Ravikumar et al., 2010). Beclin-1 is a part of the class III phosphatidylinositol-3-kinase (PI3K) complex, which generates PI(3)P, a lipid that is required for autophagosome formation. The association of Beclin-1 with the PI3K complex stimulates its activity (Kihara et al., 2001). However, Beclin-1 may be sequestered away from this complex by proteins of the Bcl-2 family, thus inhibiting autophagy (Pattingre et al., 2005). Therefore, Beclin-1 may stimulate autophagy via its transcriptional upregulation or by dissociation from Bcl-2. This disinhibition is achieved through phosphorylation of either protein, and possibly through additional as-yet uncharacterized mechanisms. These events lie downstream of diverse signaling pathways, including JNK1, lipid second messengers, calcium-dependent kinases, and toll-like receptors (He and Levine, 2010). Together, the various proteins involved in autophagosome biogenesis, structure, and trafficking provide valuable tools for monitoring the status of the autophagic pathway in living cells and tissues.

The process of autophagy can be broken down into multiple steps. First, an isolation membrane is formed, consisting of a flattened vesicular structure. The isolation membrane then extends around its cytoplasmic cargo and encloses it, forming a double-membrane bound vesicle known as the autophagosome. These early steps, leading to the creation of a cargo-containing autophagosome, are often referred to as "induction" of autophagy. Next, the autophagosome must be transported in a retrograde manner along microtubules and fuse with a lysosome. Alternatively, the autophagosome may first fuse with a late endosome to form an amphisome, which then goes on to fuse with a lysosome.

The resulting structure, known as the autolysosome, undergoes maturation consisting of degradation of the internal membrane and its cargoes into their constituent amino acids, saccharides, lipids, and nucleic acids; efflux of these materials into the cytosol for reuse; and finally regeneration of a functional lysosome. Collectively, the steps following autophagy induction are known as "completion" of autophagy. Importantly, autophagy induction and completion are dissociable events and may be regulated independently (Ravikumar et al., 2010). The combined process of induction and completion of autophagy is known as "autophagic flux." This term represents the sum total of material moving through the autophagic pathway (Klionsky et al., 2007).

Autophagy has long been thought of as a mediator of non-specific bulk degradation of cytoplasmic constituents, including proteins and organelles. However, recent evidence has revealed specific mechanisms for the recognition of substrates such as mitochondria, peroxisomes, protein aggregates, and others (Komatsu and Ichimura, 2010). Accumulation of damage appears to be a particularly significant signal for targeting to the autophagic pathway, indicating a role of autophagy not only in bulk degradation, but also in quality control of proteins and organelles. Accordingly, inactivation of autophagy causes the accumulation of ubiquitinated protein aggregates and dysfunctional organelles. In the nervous system, loss of autophagy alone is sufficient to trigger neurodegeneration, thus indicating a very important role for basal autophagy in neuronal homeostasis (Hara et al., 2006; Komatsu et al., 2006). However, excessive autophagy could also be harmful to the neuron. Degradation of cellular components at a rate in excess of new protein synthesis and organelle biogenesis is a form of cellular stress in its own right, and autophagy may even be involved in its own form of

programmed cell death (Yu et al., 2004). Proper control of autophagy, therefore, is critical to neuronal homeostasis and survival. It is perhaps not surprising that altered autophagy has been demonstrated in many of the well-studied neurodegenerative diseases, including Alzheimer disease, Parkinson disease, Huntington disease, and several lysosomal diseases (Settembre et al., 2008; Banerjee et al., 2010).

Alterations of autophagy are a particularly common and striking feature of lysosomal diseases. Large accumulations of autophagosomes have been demonstrated in many of these diseases, including Mucolipidosis type IV(Jennings et al., 2006), the neuronal ceroid lipofuscinoses (Koike et al., 2005), Danon disease (Tanaka et al., 2000), Pompe disease (Fukuda et al., 2006), and several mucopolysaccharidoses (Settembre et al., 2008). Importantly, while multiple studies have documented increased numbers of autophagosomes in lysosomal disease, few have demonstrated whether this represents an increase in autophagosome production or a decrease in autophagosome degradation. In other words, an increased quantity of autophagosomes could be an indicator of either increased or decreased autophagic flux. Making this distinction is important, as the two interpretations would suggest opposite strategies for therapeutic intervention. In the case of Multiple Sulfatase Deficiency and Mucopolysaccharidoses type IIIA, autophagosome accumulation is the result of impaired autophagosome-to-lysosome fusion, and therefore represents a block in the autophagic pathway. The authors of this study suggest that impaired autophagy may be the more proximal cause of neurodegeneration in these diseases, and suggest that autophagic dysfunction may be a unifying theme linking lysosomal diseases to neurodegeneration (Settembre et al., 2008).

In NPC disease, the first observation of altered autophagy came from the examination of Purkinje cells in chimeric *Npc1*$^{-/-}$ mice by electron microscopy, demonstrating markedly increased numbers of autophagosomes (Ko et al., 2005). Further work by our lab extended this observation to the remainder of the *npc* mouse brain and liver, as well as cultured skin fibroblasts from human NPC patients (Pacheco et al., 2007). Further, this study demonstrated that, in contrast with the mucopolysaccharidoses, autophagic flux is increased in NPC1- and NPC2-deficient cells. It was also shown that the up-regulation of autophagy is mediated by Beclin-1. This study of course begs the question: what is the significance of autophagy induction for NPC disease? Autophagy induction may represent a cytoprotective response to the pathology, or could itself be a pathologic event. As discussed above, the autophagic pathway represents a second route by which cholesterol can reach the lysosome, however it remains undetermined whether this contributes to lipid storage in NPC disease. To determine the extent to which autophagy represents a viable therapeutic target in NPC disease, it will be necessary to answer these questions and to characterize alterations of the autophagic pathway in much greater detail. These are the aims of Chapter 4.

1.6 Research Objectives

Despite recent progress in our understanding of the normal function of the NPC genes and characterization of NPC pathogenesis, the link between NPC1/NPC2 deficiency and neurodegeneration remains unknown. This knowledge gap is significant, as it impedes progress towards effective therapies. The work presented in this dissertation pursues parallel approaches towards defining the mechanisms underlying neurodegeneration in NPC disease. The first objective is to determine the extent to which

Purkinje cell degeneration in NPC disease is cell autonomous. This work demonstrated that Purkinje cell death arises from a purely autonomous defect, and is presented in Chapter 2. As an extension of this data, Chapter 3 explores the factors underlying the selective resistance to neurodegeneration of a subpopulation of Purkinje cells, and identifies a gene, *Hsp27*, that contributes to this resistance. The second objective of this dissertation is to define the role of autophagy in NPC pathogenesis. In Chapter 4, I show that NPC cells have a defect in lysosomal proteolysis that, in combination with autophagy induction, is responsible for the considerable accumulation of autophagosomes. Further, the autophagic pathway is a significant source of stored cholesterol in NPC disease and therefore contributes to pathogenesis, leading to the conclusion that autophagy inhibition may be a successful therapeutic strategy in NPC disease.

Chapter 2

Conditional Niemann-Pick C mice demonstrate cell autonomous Purkinje cell neurodegeneration[1]

2.1 Abstract

Pathways regulating neuronal vulnerability are poorly understood, yet are central to identifying therapeutic targets for degenerative neurological diseases. Here, we characterize mechanisms underlying neurodegeneration in Niemann-Pick type C (NPC) disease, a lysosomal storage disorder characterized by impaired cholesterol trafficking. To date, the relative contributions of neuronal and glial defects to neuron loss are poorly defined. Using gene targeting, we generate Npc1 conditional null mutant mice. Deletion of *Npc1* in mature cerebellar Purkinje cells leads to an age-dependent impairment in motor tasks, including rotarod and balance beam performance. Surprisingly, these mice did not show the early death or weight loss that are characteristic of global *Npc1* null mice, suggesting that Purkinje cell degeneration does not underlie these phenotypes.

---

[1] This chapter was published as:
Elrick MJ, Pacheco CD, Yu T, Dadgar N, Shakkottai VG, Ware C, Paulson HL and Lieberman AP. 2010. Conditional Niemann-Pick C mice demonstrate cell autonomous Purkinje cell neurodegeneration. Hum Mol Genet 19(5): 837-847.

Histological examination revealed the progressive loss of Purkinje cells in an anterior-to-posterior gradient. This cell autonomous neurodegeneration occurs in a spatiotemporal pattern similar to that of global knockout mice. A subpopulation of Purkinje cells in the posterior cerebellum exhibits marked resistance to cell death despite Npc1 deletion. To explore this selective response, we investigated the electrophysiological properties of vulnerable and susceptible Purkinje cell subpopulations. Unexpectedly, Purkinje cells in both subpopulations displayed no electrophysiological abnormalities prior to degeneration. Our data establish that Npc1 deficiency leads to cell autonomous, selective neurodegeneration, and suggest that the ataxic symptoms of NPC disease arise from Purkinje cell death rather than cellular dysfunction.

2.2 Introduction

Niemann-Pick type C (NPC) disease is an autosomal recessive neurovisceral lipid storage disorder of childhood, characterized by liver dysfunction and neurodegeneration resulting in progressive cognitive impairment, ataxia, seizures, dystonia and early mortality (Higgins et al., 1992). NPC disease is caused by loss-of-function mutations in the *NPC1* or *NPC2* genes, members of an intracellular lipid trafficking pathway that act cooperatively to facilitate the efflux of exogenously-derived cholesterol from endosomes and lysosomes (Carstea et al., 1997; Naureckiene et al., 2000; Kwon et al., 2009). As a result of these mutations, intracellular lipid trafficking is deficient, and unesterified cholesterol and glycosphingolipids accumulate in late endosomes and lysosomes (Vanier and Millat, 2003). Currently, the link between lipid storage and the neurodegeneration that mediates patient mortality is unknown, and the mechanisms leading to selective neuronal vulnerability in NPC disease are not understood.

From studies of animal models of NPC, including mice in which an insertional mutation disrupts the *Npc1* gene (Loftus et al., 1997), several general principles have emerged that guide our understanding of disease pathogenesis (Pacheco and Lieberman, 2008). In Npc1 deficient mice, as in patients with this disorder, neurons accumulate lipids, abnormally swollen axons are frequent, and demyelination is present (Paul et al., 2004). These features are associated with impaired motor function and early death that model the degenerative phenotype of patients with this disease (Morris et al., 1982). While systemic manifestations also occur in both NPC disease patients and mice, progressive neurological impairment is due to loss of functional Npc1 protein in the nervous system (Loftus et al., 2002). Neurotoxicity is associated with the appearance of abnormal dendrites (Walkley, 1995), the accumulation of hyperphosphorylated tau (Auer et al., 1995; Bu et al., 2002), a dysregulation of lysosomal calcium homeostasis (Lloyd-Evans et al., 2008), and the activation of autophagy (Ko et al., 2005; Pacheco and Lieberman, 2007), thereby implicating a host of mechanisms that may act as mediators of neuronal dysfunction or serve as compensatory responses elicited to promote neuronal survival. Many of these pathways are predicted to act within neurons to influence cell survival, consistent with an analysis of chimeric mice that suggested Npc1 deficiency triggers cell autonomous Purkinje cell loss (Ko et al., 2005). In contrast, transgenic rescue experiments in NPC mouse and drosophila models (Phillips et al., 2008; Zhang et al., 2008), and co-culture experiments with neurons and astrocytes (Chen et al., 2007), indicate that glia are critical contributors to neurotoxicity and question the extent to which neuronal loss is cell autonomous.

Our understanding of disease mechanisms is also guided by recent therapeutic insights from studies of NPC mice. Most striking are data demonstrating that a single dose of the neurosteroid allopregnanolone delivered with cyclodextrin (Griffin et al., 2004) or cyclodextrin alone (Liu et al., 2009) at postnatal day 7 ameliorates Purkinje cell loss and motor deficits while prolonging overall survival. In contrast, similar intervention at postnatal weeks 2 – 3 has significantly diminished affects (Griffin et al., 2004). These data raise the possibility that there exists a critical period for Purkinje cell loss in Npc1 deficient mice during development or early postnatal life. This notion, however, has not been rigorously tested.

To resolve these questions, we generated a conditional null mutant of the mouse *Npc1* gene, and used it to study effects of Purkinje cell-specific gene deletion. Of all neuronal populations affected by NPC disease, Purkinje cells degenerate earliest and to the greatest extent (Vanier and Millat, 2003). As the sole output of the cerebellar cortex, their loss is thought to underlie the ataxic symptoms of NPC patients. In NPC mice, Purkinje cell loss progresses through a well-characterized anterior-to-posterior gradient, with the majority of Purkinje cells lost by end stage (Sarna et al., 2003). Here we demonstrate that cell-specific deletion of *Npc1* in Purkinje cells at postnatal weeks 2 – 3 is sufficient to cause Purkinje cell degeneration in a spatiotemporal pattern similar to that seen in global null mice, thus demonstrating cell autonomous neuronal loss that is independent of effects during embryonic development or the first postnatal week. Further, we show that a subpopulation of Purkinje cells in the posterior cerebellum survives despite *Npc1* deletion. Finally, we investigate the electrophysiologic properties

of degenerating Purkinje cells and show that electrophysiological dysfunction does not precede Purkinje cell death.

2.3 Results

2.3.1 Generation and characterization of *Npc1^{flox}* mice

To generate a conditional null mutant of the mouse *Npc1* gene (*Npc1^{flox}* mice), we used gene targeting to insert *loxP* sites on either side of exon 9 **(Figure 2.1A)**. Cre-mediated excision of exon 9 is predicted to cause the splicing of exon 8 directly to exon 10, leading to a frameshift and the incorporation of multiple stop codons. This strategy was chosen since an analogous spontaneous mutation is found in the widely used *npc^{nih}* (*Npc1$^{-/-}$*) mouse, in which a retrotransposon insertion into exon 9 introduces multiple stop codons (Loftus et al., 1997) and yields a functional null allele.

Following production of *Npc1^{flox}* mice **(Figure 2.1B, C)**, we verified that the targeted allele produces normal amounts of Npc1 protein, and that Cre-mediated deletion of exon 9 yields a functional null that is equivalent to the *Npc1^{-}* allele of *npc^{nih}* mice. To delete the floxed allele in the germline, we used mice expressing Cre recombinase under the control of the ubiquitous EIIa promoter (Lakso et al., 1996). The resulting mosaic offspring were bred with *Npc1$^{+/-}$* mice to generate *Npc1$^{\Delta/-}$* compound heterozygotes, where Δ indicates the germline-deleted version of the floxed Npc1 allele. Similar to *Npc1$^{-/-}$* mice, *Npc1$^{\Delta/-}$* compound heterozygotes expressed no detectable Npc1 protein **(Figure 2.1D)** and decreased amounts of *Npc1* mRNA **(Figure 2.1E)**. In contrast, *Npc1$^{flox/flox}$* mice expressed wild type levels of Npc1 protein and slightly elevated levels of *Npc1* mRNA.

Figure 2.1 Generation of *Npc1*^{flox} mice

(A) Schematic representation of the endogenous *Npc1* locus (a), targeting construct (b), locus following homologous recombination (c), FLP-mediated deletion of the neomycin resistance cassette (d), and Cre-mediated deletion of exon 9. FRT sites are shown as circles, loxP sites are represented by diamonds. **(B)** Genomic Southern blot of tail biopsy derived DNA from a black pup sired by one of two independently derived male chimeras. Genomic DNA was digested with EcoRV and Southern blots analyzed using probes that fall outside the targeting vector. The 5' exon 5 (on left) and 3' exon 18 (on right) probes both hybridize to a 19.2 kb band from the non-recombined allele. The recombined *Npc1* allele generates a 5.2 kb band with the 5' probe and a 14 kb band with the 3' probe. **(C)** PCR genotyping of *Npc1* mutant mice. (Left panel) Schematic representation of primers used. (Right panel) PCR products visualized by agarose gel electrophoresis. **(D)** Western blot for NPC1 protein in mouse liver lysates. **(E)** Quantitative RT-PCR for *Npc1* mRNA as detected by probes recognizing the junction between exons 1 and 2 (white bars) or exons 9 and 10 (black bars). N = 3 mice per genotype. Data are mean +/- SEM. *Panels A and B were performed by Christopher D. Pacheco.*

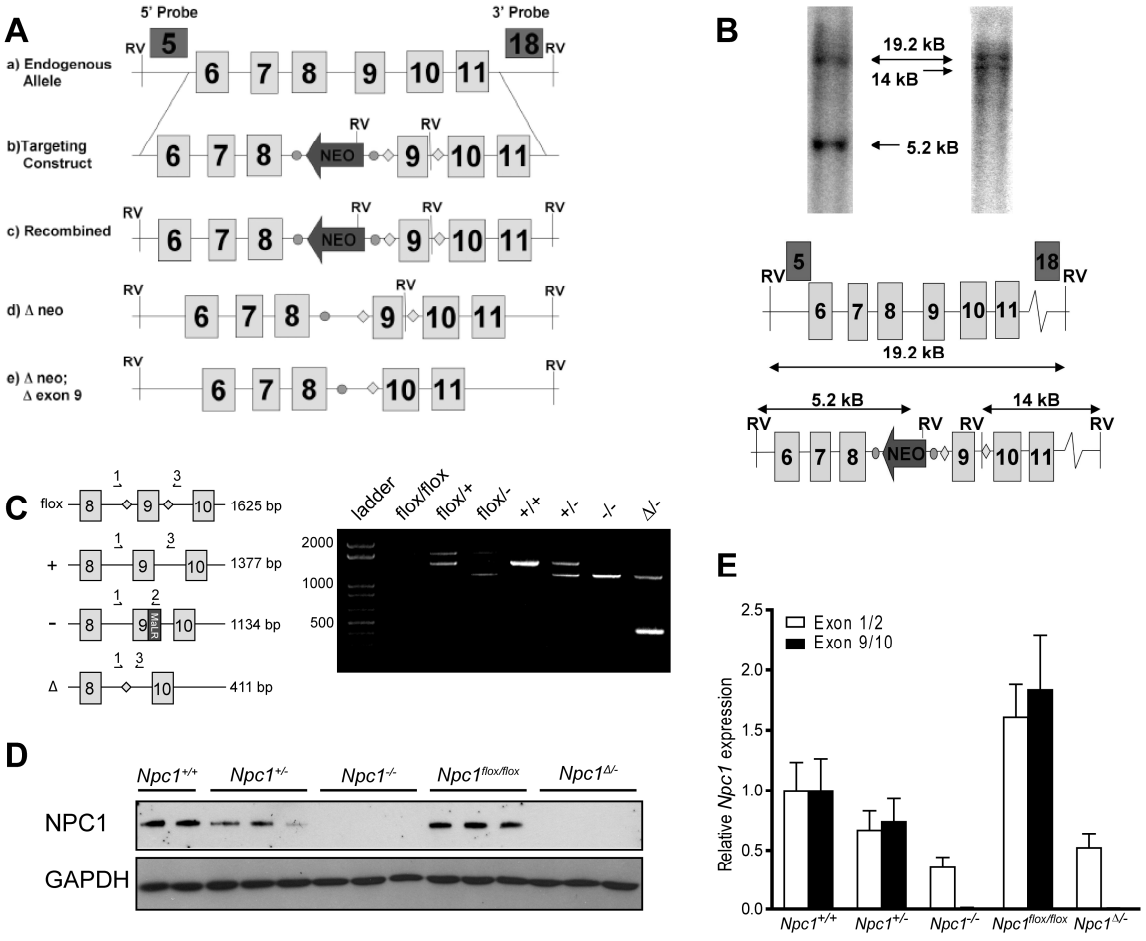

The functional consequences of germline deletion of the floxed allele were weight loss, motor deficits, and premature death, similar to the phenotype of *Npc1*$^{-/-}$ mice (Morris et al., 1982; Voikar et al., 2002). *Npc1*$^{\Delta/-}$ mice, but not *Npc1*$^{flox/-}$ controls, showed small size at weaning, followed by weight loss initiating at ~7 weeks **(Figure 2.2A, B)**, impaired rotarod performance **(Figure 2.2C)**, and early death at an average of 48.1±5.1 days **(Figure 2.2D)**. This phenotype was verified on a second, independently derived line of gene targeted mice (data not shown). While this time course of disease is more accelerated than what is typically reported for *Npc1*$^{-/-}$ mice on the *Balb/c* background (Morris et al., 1982), we observed a similarly severe phenotype in *Npc1*$^{-/-}$ mice backcrossed ten generations onto C57BL6/J (data not shown). This finding is consistent a prior report demonstrating the influence of strain background on the severity of the phenotype of *Npc1*$^{-/-}$ mice (Liu et al., 2008). Pathological examination of cerebellar tissue demonstrated Purkinje cell loss by seven weeks **(Figure 2.2E)**. This was associated with marked microgliosis and astrogliosis throughout the brain, and the proliferation of foamy macrophages in the liver **(Figure 2.3)**, all of which are prominent features of NPC disease and are identical to the pathology of *Npc1*$^{-/-}$ mice. Furthermore, staining with filipin identified accumulations of unesterified cholesterol in *Npc1*$^{\Delta/-}$ and *Npc1*$^{-/-}$ mice, but not in *Npc1*$^{flox/-}$ controls **(Figure 2.2E)**. We conclude that *in vivo* deletion of *Npc1*^{flox} inactivates the *Npc1* gene and reproduces the NPC phenotype.

Figure 2.2 Phenotype and pathology following germline deletion of *Npc1*
(A, B) Weight curves for male (A) and female (B) mice. **(C)** Rotarod performance at 7 weeks. Data are mean +/- SEM. ***p<0.001. **(D)** Kaplan-Meyer survival curve. p=0.0001. **(E)** Cerebellar pathology at 7 weeks. (Row 1) Calbindin immunofluorescence demonstrates patchy Purkinje cell loss in the anterior zone of the cerebellum in *Npc1*$^{-/-}$ and *Npc1*$^{\Delta/-}$ mice. (Rows 2-4) Calbindin and filipin co-stain highlight filipin-positive lipid accumulations in *Npc1*$^{-/-}$ and *Npc1*$^{\Delta/-}$ cerebellum. (Original magnification 100x)

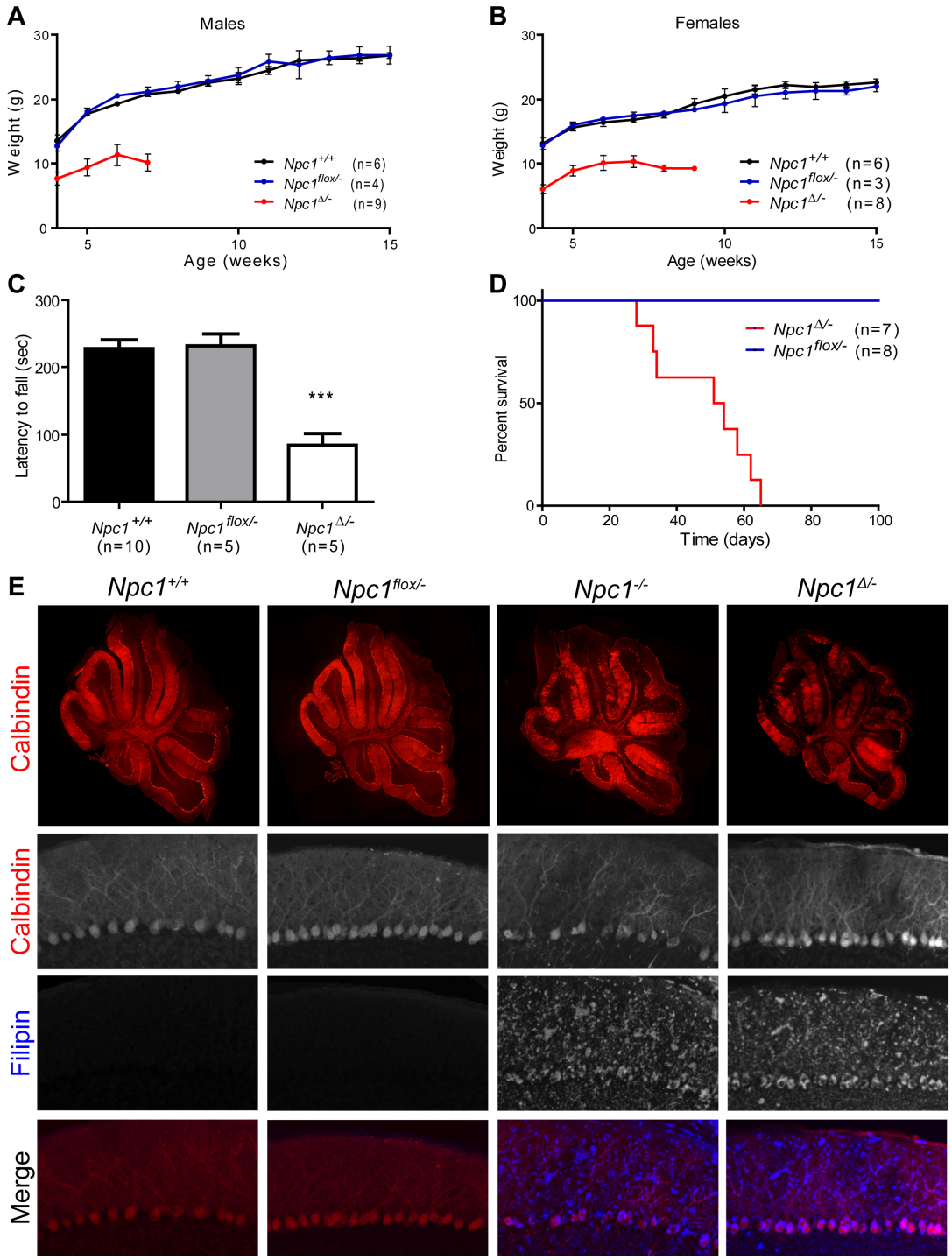

Figure 2.3 Glial and liver pathology following germline deletion of Npc1
Immunohistochemical staining for markers of microglia (Iba1, top row) and astrocytes (GFAP, middle row) demonstrate gliosis in Npc1-/- and Npc1Δ/-, but not control cerebella. (Bottom row) H&E staining of liver tissue demonstrates foamy macrophages in Npc1-/- and Npc1Δ/- mice, but not controls.

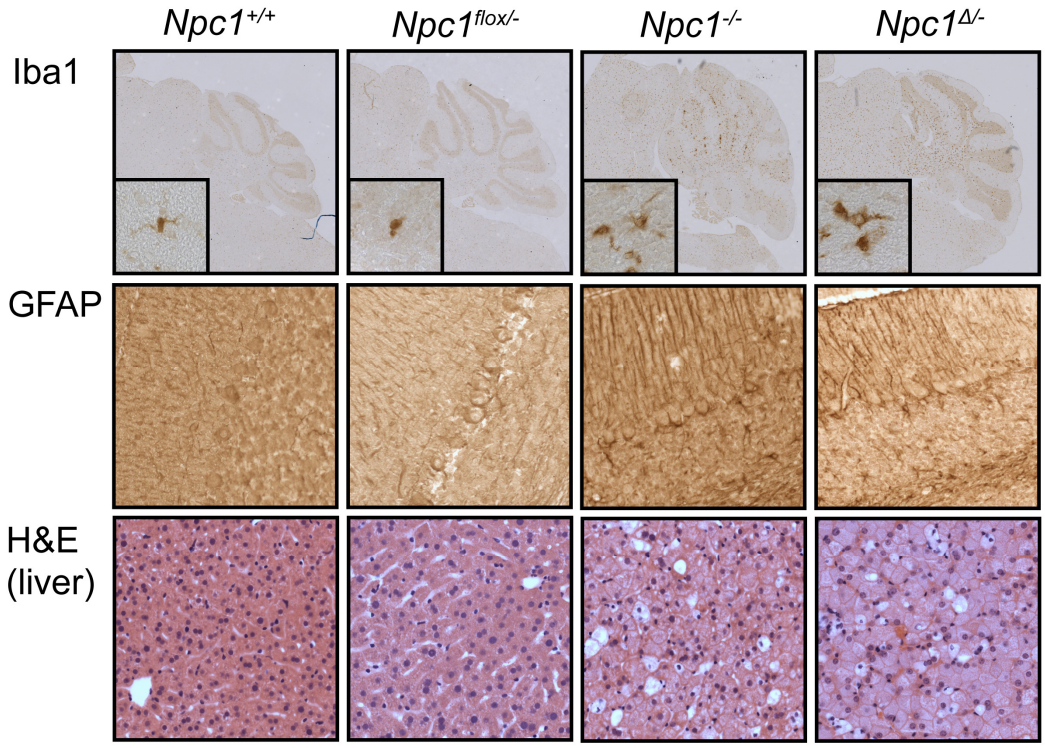

2.3.2 Purkinje cell specific deletion of *Npc1* causes ataxia, but not weight loss or early mortality

We next sought to determine the extent to which cell autonomous toxicity mediates Purkinje cell loss in Npc1 deficient mice. To achieve Purkinje cell specific deletion of *Npc1*, we used *Pcp2-Cre* mice (Barski et al., 2000), in which expression of Cre recombinase is limited to cerebellar Purkinje cells and retinal bipolar neurons. Expression in Purkinje cells is initiated when these neurons acquire their adult pattern of gene expression, beginning as early as postnatal day six in some cells, and present in all

Purkinje cells by postnatal weeks two to three. Deletion of *Npc1* by this strategy is therefore not only cell-type restricted, but also post-developmental. Purkinje cell specific null mutants (*Npc1$^{flox/-}$;Pcp2-Cre^{+})*, but not littermate controls (*Npc1$^{flox/+}$;Pcp2-Cre^{+})*, displayed age-dependent motor deficits detectable by impaired rotarod performance by 15 weeks **(Figure 2.4A)**, decreased ability to traverse a balance beam by 10 weeks **(Figure 2.4B),** and tremors by 13 weeks (data not shown). However, Purkinje cell null mutants gained weight normally **(Figure 2.4C, D).** Further, of 36 *Npc1$^{flox/-}$;Pcp2-Cre^{+}* mice generated, none died prematurely, including seven followed for 20 weeks **(Figure 2.4C, D insets)** and a small number followed as long as 40 weeks. By contrast, global null mutants never survived longer than nine weeks **(Figure 2.4D)**. We conclude that Npc1 deficiency in Purkinje cells is sufficient to cause motor impairment but not other features of the disease phenotype in mice.

Figure 2.4 Purkinje cell specific deletion of *Npc1* impairs rotarod and balance beam performance
(A, B) Age-dependent performance on rotarod (A) and balance beam (B). Data are mean +/- SEM. n.s. not significant, **p*<0.05, ***p*<0.01, ****p*<0.001. **(C, D)** Weight curves for male (A) and female (B) mice. **Insets** depict 100% survival of mice followed for 20 weeks.

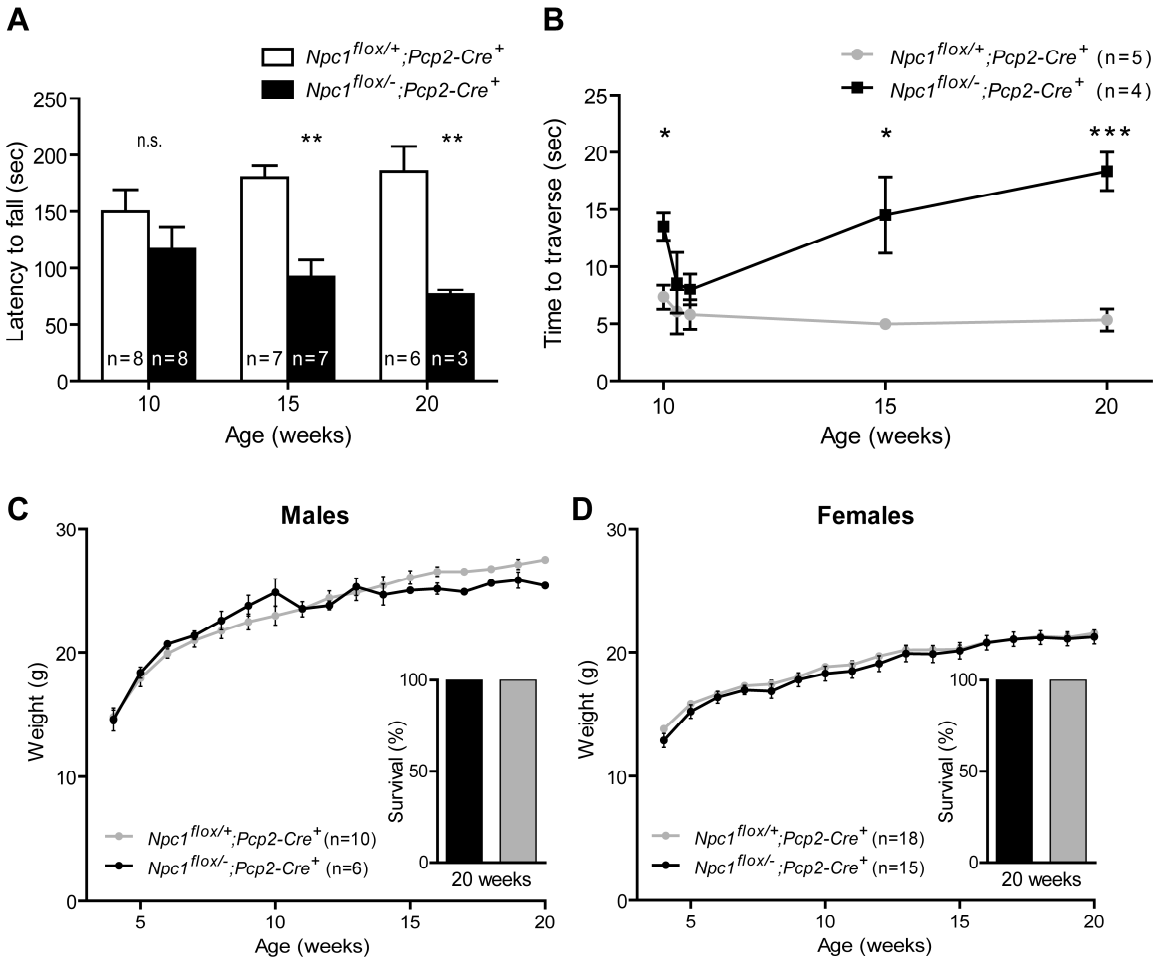

2.3.3 Cell specific deletion of *Npc1* causes Purkinje cell loss in a spatial and temporal pattern similar to that of global null mice

Following phenotype analysis of Purkinje cell specific null mice, we used histological examination of cerebellar tissue to determine effects on Purkinje cell survival. Sagittal midline cerebellar sections stained for calbindin revealed loss of

Purkinje cells by 7 weeks of age, starting in the anterior zone (lobules II-V) and progressing posteriorly **(Figure 2.5A)**. This same pattern of Purkinje cell loss has been documented previously in *Npc1* global null mutants (Sarna et al., 2003). Activation and proliferation of microglia and astrocytes were also detected in Purkinje cell null mutants as early as seven weeks, advancing in a pattern that mirrored Purkinje cell loss **(Figure 2.6)**. Quantification of Purkinje cells in midline cerebellar sections demonstrated that the rate of loss fit tightly to a model incorporating a plateau followed by exponential decay **(Figure 2.5B)**. That cell loss began after a plateau was supported by quantifying Purkinje cells in conditional null mutants and controls at 4 weeks, prior to the onset of exponential loss **(Figure 2.5C)**. These data are consistent with a model that a single hit underlies neuronal loss in NPC, and are similar to observations in other neurodegenerative disorders (Clarke et al., 2000).

Our findings establish that deletion of *Npc1* only in Purkinje cells is sufficient to cause cell autonomous degeneration. However, we considered the possibility that dysfunction of *Npc1*-null glia may additionally enhance neurodegeneration in NPC disease. If this were the case, it would be expected that Purkinje cell loss would occur more slowly in Purkinje cell specific null mutants than in global null mutants. Ideally, this would be determined by comparing half-lives of Purkinje cells in $Npc1^{flox/-}$;*Pcp2-*Cre^{+} and $Npc1^{\Delta/-}$ mice. However, due to the early death of *Npc1* global null mutants on the C57BL6/J background, we were unable to reliably determine the half life of Purkinje cell loss in these animals. To gain an approximation, we compared the initial rate of Purkinje cell loss in $Npc1^{flox/-}$;*Pcp2-*Cre^{+} and $Npc1^{\Delta/-}$ mice between 5.5 and 7 weeks **(Figure 2.5D)**. No significant difference was observed between the slopes of these lines

(-2.37 ± 0.98 vs. -3.93 ± 2.53, p=0.59). A small, but significant, right-shift of the curve for *Npc1*$^{flox/-}$;*Pcp2-Cre*$^{+}$ mice was observed, suggesting that the onset of Purkinje cell loss was slightly delayed in these mice, likely owing to the timing of *Npc1* deletion. We conclude that cell death occurs at approximately the same rate regardless of whether *Npc1* is deleted in all cells or only in Purkinje cells, and that the rate is independent of the developmental timing of *Npc1* deletion.

Figure 2.5 Cell autonomous Purkinje cell loss
(A) Calbindin immunofluorescence demonstrates progressive anterior-to-posterior Purkinje cell loss in *Npc1*$^{flox/-}$;*Pcp2-Cre*$^{+}$ mice (top row), but not *Npc1*$^{flox/+}$;*Pcp2-Cre*$^{+}$ controls (bottom row). Roman numerals label cerebellar lobules. **(B)** Quantification of Purkinje cell loss over time in the cerebellar midline, expressed as Purkinje cell density. Slope of the exponential decay phase indicates a half-life for Purkinje cells of 16.3 days. **(C)** Purkinje cell density at 4 weeks, demonstrating no cell loss at this age in *Npc1*$^{flox/-}$;*Pcp2-Cre*$^{+}$ mice versus *Npc1*$^{flox/+}$;*Pcp2-Cre*$^{+}$ controls. **(D)** Initial rate of Purkinje cell loss, calculated from density at 5.5 and 7 weeks, for *Npc1*$^{flox/-}$;*Pcp2-Cre*$^{+}$ mice and *Npc1*$^{\Delta/-}$ global null mice (mean +/- SEM).

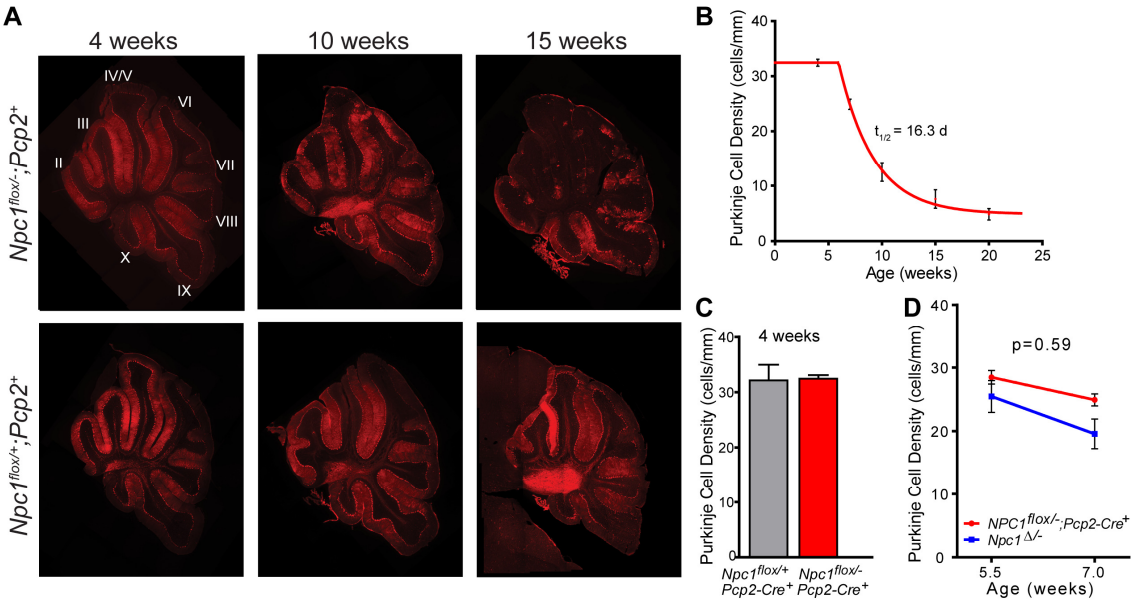

Figure 2.6 Reactive gliosis in Purkinje cell specific *Npc1* null mutants.
(A) Staining for Iba1 reveals proliferation of microglia with activated morphology in *Npc1*$^{flox/-}$;*Pcp2-Cre*$^{+}$ mice, but not controls. **(B)** Staining for GFAP reveals proliferation of astrocytes in the molecular layer of *Npc1*$^{flox/-}$;*Pcp2-Cre*$^{+}$ mice, but not controls.

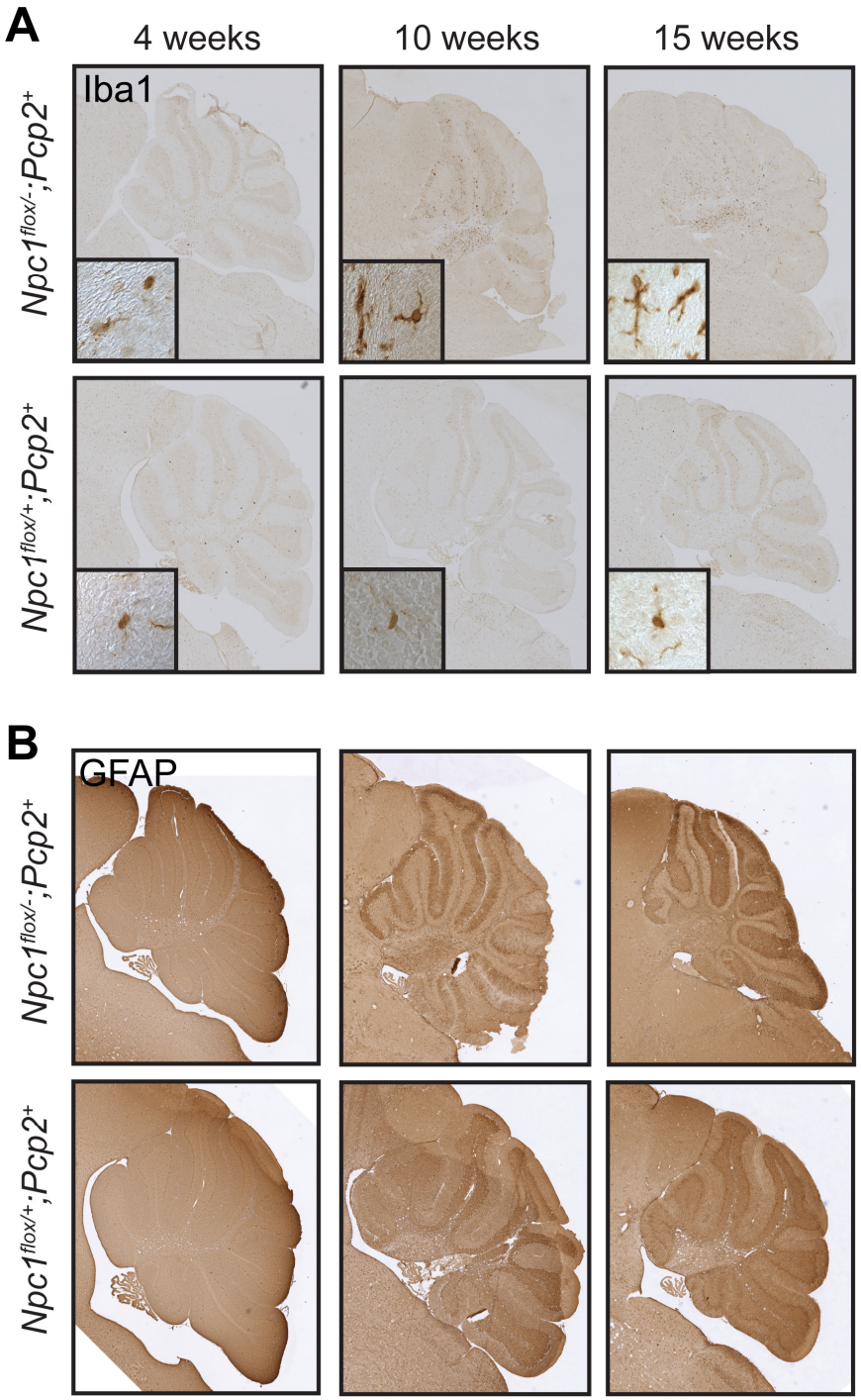

2.3.4 Differential survival of Purkinje cell subpopulations

Our initial analysis suggested that Purkinje cell specific deletion of *Npc1* recapitulated the anterior – posterior gradient of cell loss that has been demonstrated to occur in global null mutants (Sarna et al., 2003). To verify this observation, we quantified Purkinje cell survival by lobule **(Figure 2.7A)**, and established that conditional null mutants exhibited this same pattern of cell loss. Aging of $Npc1^{flox/-}$;$Pcp2\text{-}Cre^{+}$ mice beyond the typical lifespan of $Npc1^{-/-}$ mice, however, allowed a striking observation to emerge. In lobule X, although the anterior-most ~15% of Purkinje cells were lost by 10 weeks, there was no further cell loss between 10 and 20 weeks. This was in stark contrast with lobules II-V, where Purkinje cell loss was greater than 75% at 10 weeks and approached 100% by 15 weeks. This observation suggested that a marked difference exists between these two ostensibly similar neuronal populations in their susceptibility to cell death following Npc1 deficiency. The resistance of lobule X Purkinje cells was associated with delayed accumulation of unesterified cholesterol as detected by staining with the fluorescent dye filipin **(Figure 2.7B)**. Nearly all Purkinje cells in lobules II-V were filipin positive by 4 weeks. In the remainder of the cerebellum, there was roughly ~60% filipin positivity at this age, progressing to 80-90% by 7 weeks, and nearly 100% by 10 weeks. This differential rate of unesterified cholesterol accumulation and Purkinje cell loss was not explained by delayed deletion of *Npc1* exon 9, as crossing *Pcp2-Cre* mice with ROSA reporter mice demonstrated that nearly all Purkinje cells stained for β-galactosidase at 4 weeks **(Figure 2.7C)**. Our data establish that patterned Purkinje cell loss is a manifestation of cell autonomous toxicity mediated by *Npc1* deletion. While lobule X Purkinje cells also display delayed cholesterol accumulation, we believe that

this is unlikely to be a sufficient explanation of their resistance since they continued to survive long after the acquisition of filipin staining.

Figure 2.7 Differential survival of Purkinje cell subpopulations.
(A) Purkinje cell loss by lobule in midline sections of *Npc1*$^{flox/-}$;*Pcp2-Cre*$^{+}$ mice (mean +/- SEM). **(B)** Lipid accumulation in *Npc1*$^{flox/-}$;*Pcp2-Cre*$^{+}$ mice. Calbindin-positive Purkinje cells were scored as filipin-positive or filipin-negative in midline cerebellar sections from mice at 4, 7, and 10 weeks (n = 3 mice at each age). Data are mean +/- SEM. **(C)** *Pcp2-Cre* expression at 4 weeks, as determined by crossing with ROSA reporter mice. Calbindin-positive Purkinje cells were scored for X-gal staining in midline cerebellar sections. Data are mean +/- SEM.

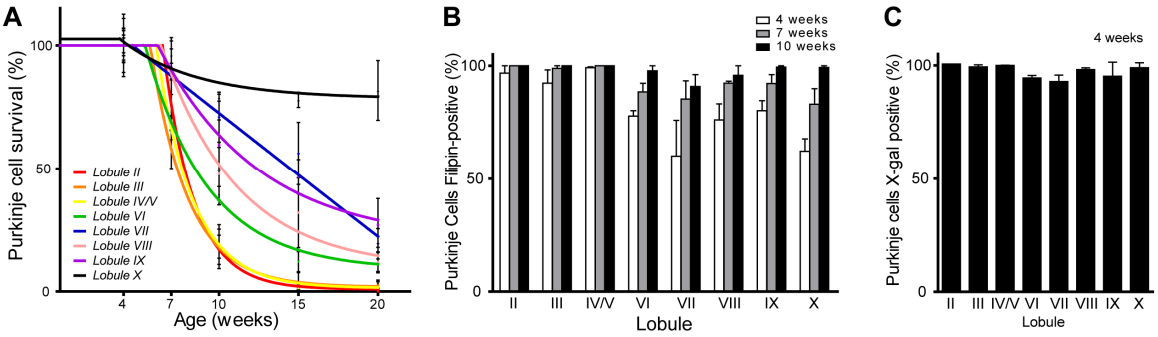

2.3.5 Absence of electrophysiological abnormalities in degenerating Purkinje cells

To further investigate the mechanism of neurodegeneration in NPC, we considered the possibility that electrophysiological dysfunction contributed to Purkinje cell death in NPC. Ion channel mutations are a known cause of inherited neurodegenerative ataxias in humans and mice (Zhuchenko et al., 1997; Trudeau et al., 2006), and channel function is influenced by membrane lipid composition (Tillman and Cascio, 2003), leading to a potential mechanism by which lipid trafficking defects could influence neuronal function. We therefore investigated the extent to which electrophysiological properties differed between vulnerable and resistant Purkinje cell

subpopulations. We also sought to determine whether lobule X Purkinje neurons, which appear histologically intact despite the presence of filipin-positive lipid storage material, are able to support normal physiology. Normal Purkinje neurons exhibit characteristic spontaneous repetitive firing (Raman and Bean, 1999). The spontaneous firing of these neurons depends on the presence of the correct composition of plasma membrane ion channels and normal cellular energy homeostasis (Genet and Kado, 1997). Therefore, assessment of electrophysiological function provided a means to evaluate several pathways that could influence the function and survival of Purkinje cells in NPC mice.

We measured the spontaneous activity of Purkinje cells in acute cerebellar slices from ten-week *Npc1*$^{flox/-}$*;Pcp2-Cre*$^{+}$ mice **(Figure 2.8)**. Purkinje cells in lobule X **(Figure 2.8A)**, which are resistant to the toxicity of Npc1 deficiency, demonstrated normal spontaneous firing (n=5, not shown), indicating that these cells are both morphologically and electrophysiologically intact at this age. Surviving Purkinje cells in the anterior zone (lobules II-V) were infrequent, and those that remained had shrunken soma and dystrophic dendrites **(Figure 2.8B)**. Unexpectedly, these cells also showed normal spontaneous activity as measured by whole-cell recordings (n=6, **Figure 2.8C**). To confirm that supplying energy substrates in the internal solution was not restoring firing in these neurons, we also assessed spontaneous activity through extracellular recordings. Extracellularly recorded spike frequency was similar to recordings obtained in the whole cell mode (n = 4, **Figure 2.8D**). The pattern of repetitive firing in lobule II-V neurons was indistinguishable from that of lobule X Purkinje cells. We also determined if the spike width, a measure of potassium current-dependant action potential repolarization (McMahon et al., 2004), differed between Purkinje cells in the anterior and

posterior cerebellum. Spike width was indistinguishable between lobule II-V and lobule X neurons (0.37 ± 0.02 and 0.44 ± 0.05, p = 0.2, **Figure 2.8E**). Although the surviving lobule II-IV neurons were smaller and had abnormal dendrites, their passive membrane properties including total cellular capacitance were similar to those of lobule X neurons **(Figure 2.8F).** These findings indicate that Purkinje neurons in NPC mice retain plasma membrane integrity even as morphological changes are occurring. Altogether, our observations indicate that electrophysiological dysfunction is unlikely to precede the death of Npc1 deficient Purkinje cells, and suggest that defects in ion homeostasis and energy metabolism do not underlie the vulnerability of Purkinje cells in the anterior zone of the cerebellum. Further, our data demonstrate that Purkinje cells maintain normal electrophysiological behavior despite NPC-induced lipid trafficking defects.

Figure 2.8 Electrophysiology of Purkinje cell subpopulations.
(A-B) Infrared differential interference contrast (IR-DIC) microscopy of representative Purkinje cells from which recordings were performed, in lobules X (A) and III (B). Scale bar = 10 □M (**C)** Whole cell recording from a lobule III Purkinje cell. **(D)** Extracellular recording from a lobule IV/V Purkinje cell. **(E)** Overlay of action potentials from a lobule X (black) and lobule III (grey) Purkinje cell. **(F)** Passive membrane properties of anterior zone vs. lobule X Purkinje cells, including capacitance (left) and input resistance (right). *These experiments were performed by Vikram G. Shakkottai.*

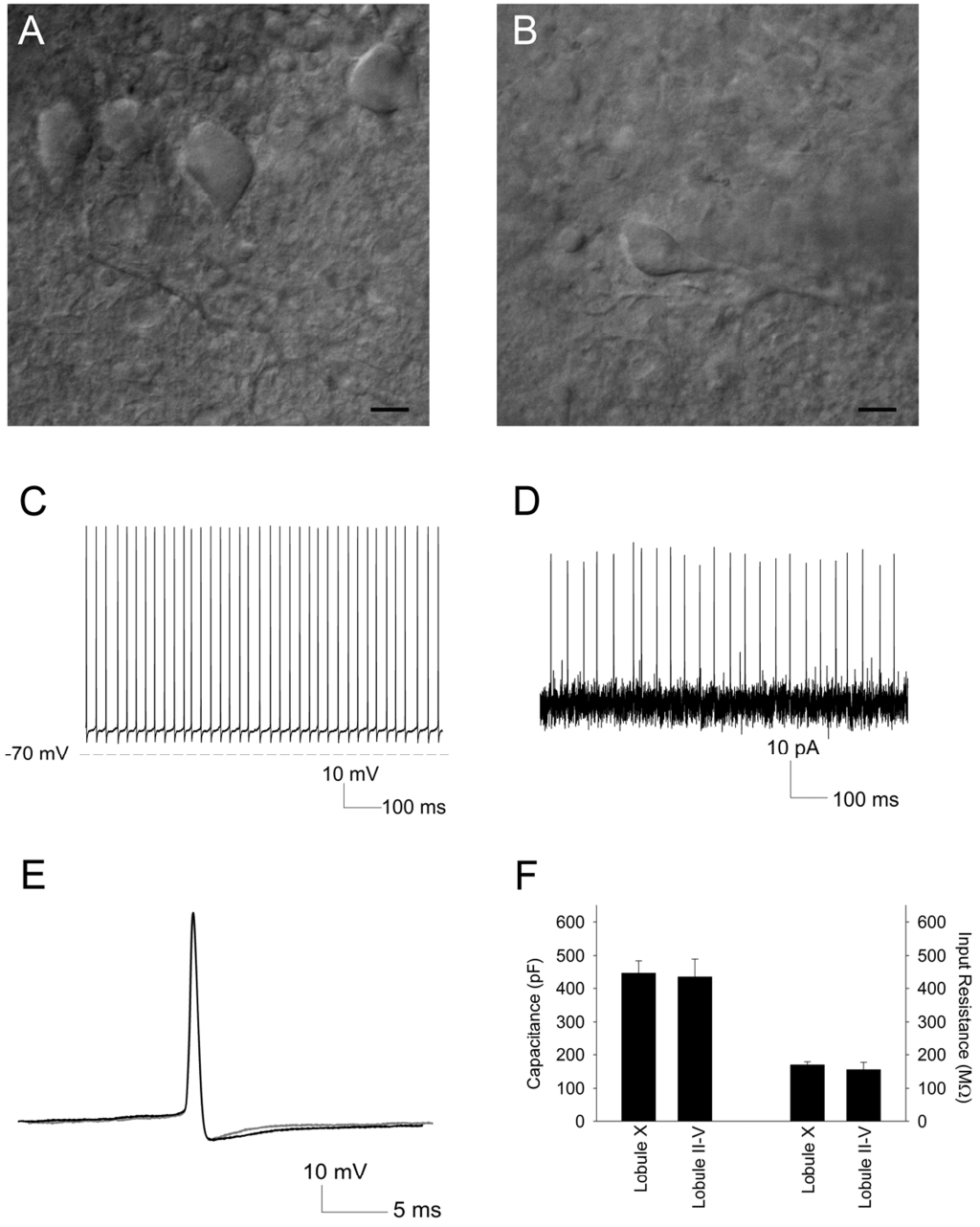

2.4 Discussion

Here we characterize a conditional null mutant of the mouse *Npc1* gene, and demonstrate that gene deletion restricted to Purkinje cells is sufficient to cause cell autonomous neuronal loss. Purkinje cell specific null mutants display impaired motor function, but not weight loss or early death, indicating that cerebellar degeneration accounts for limited aspects of the NPC phenotype in mice. Our data also establish that Purkinje cells in the anterior cerebellar lobules exhibit vulnerability to the toxicity of Npc1 deficiency, whereas those in the posterior lobules unexpectedly show remarkable resistance. Finally, we demonstrate that Npc1-deficient Purkinje cells in both susceptible and resistant lobules display normal electrophysiological activity prior to their degeneration, indicating that defects in ion homeostasis and energy metabolism do not underlie their loss. Our findings demonstrate that Npc1 deficiency leads to cell autonomous, selective neuronal vulnerability, and suggest that the ataxic symptoms of NPC disease arise from Purkinje cell death rather than cellular dysfunction.

Studies of a diverse array of neurodegenerative disorders have yielded increasing evidence that neuronal dysfunction and death can arise from defects extrinsic to the neurons that are lost. Among the most compelling evidence in support of this conclusion comes from studies in animal models. For example, expression of polyglutamine-expanded ataxin-7, the cause of spinocerebellar ataxia type 7, only in Bergmann glia is sufficient to trigger Purkinje cell degeneration in mice (Custer et al., 2006). Similarly, the deletion of mutant SOD1 from microglia (Boillee et al., 2006) or astrocytes (Yamanaka et al., 2008) slows disease progression in a mouse model of familial amyotrophic lateral sclerosis. Additionally, studies in a transgenic mouse model of

Huntington disease indicate that pathological interactions between neurons are important for cortical pathology (Gu et al., 2005). These observations and others have lead to a model in which neurodegeneration can be caused by cell autonomous mechanisms, defects in supporting glia, aberrant interactions between neurons, or a combination of these (Lobsiger and Cleveland, 2007).

The data reported here establish that Purkinje cell degeneration in NPC mice is cell autonomous. Our findings support conclusions from the analysis of a chimeric mouse model of NPC disease (Ko et al., 2005), and extend this work by showing the extent of selective vulnerability of Purkinje cell subpopulations. As *Npc1* deletion mediated by the *Pcp2-Cre* transgene occurs in post-developmental Purkinje cells (Barski et al., 2000), we also conclude that this neuronal loss is independent of events during embryonic or early postnatal development. Prior studies raised the possibility that degeneration of Purkinje cells in NPC mice may arise from developmental defects, perhaps mediated by decreased production of neurosteroids to guide neuronal maturation (Griffin et al., 2004). Our findings do not support this conclusion. Whereas *Npc1* is deleted weeks later in $Npc1^{flox/-};Pcp2\text{-}Cre^{+}$ mice than in $Npc1^{\Delta/-}$ mice, the rate of Purkinje cell degeneration is similar in both sets of animals. Cell loss is therefore independent of the cumulative time following *Npc1* deletion, and instead likely reflects a requirement for Npc1 only after Purkinje cells reach maturity.

It is notable that $Npc1^{flox/-};Pcp2\text{-}Cre^{+}$ mice do not exhibit weight loss or early death. Although there has been some speculation that cerebellar ataxia impairs feeding ability of NPC mice, in turn causing weight loss and death, our data are inconsistent with this notion. Prior work established that weight loss and death are due to Npc1 deficiency

in the nervous system (Loftus et al., 2002), yet the identity of the specific cellular population(s) responsible for these aspects of the phenotype remains enigmatic. It is possible that weight loss stems from dysfunction of feeding centers in the hypothalamus, and that early death results from degeneration of distinct brain regions required for support life, such as the brainstem (Luan et al., 2008). Our data suggest that therapies targeted to Purkinje cells would be expected to rescue limited aspects of the neurological phenotype, particularly those reflecting ataxia. Weight loss and early death are likely mediated by impairment of other cell types, and further studies are needed to clarify their identity.

Our observation that Purkinje cells in posterior cerebellar lobules exhibit resistance to the toxicity of Npc1 deficiency prompted us to consider the possibility that electrophysiological dysfunction contributed to the differential survival of Purkinje cell subpopulations in NPC. To test this notion, we examined the spontaneous firing of Purkinje cells in acute cerebellar slices from ten-week *Npc1*$^{flox/-}$*;Pcp2-Cre*$^{+}$ mice. Surprisingly, Purkinje cells from both anterior and posterior cerebellar lobules exhibited normal spontaneous firing activity. These data indicate that electrophysiological defects do not underlie neuronal vulnerability, and that Purkinje cells can function despite the presence of filipin-positive lipid storage material. Based on these findings, we suggest that the cerebellar ataxia that develops in these mice is largely dependent upon Purkinje cell death rather than cellular dysfunction. Consistent with this interpretation, *Npc1*$^{flox/-}$*;Pcp2-Cre*$^{+}$ mice develop symptoms only after the loss of a substantial proportion of their Purkinje cells. This is in marked contrast with other cerebellar disorders, including many of the spinocerebellar ataxias, episodic ataxias, and paraneoplastic ataxia, wherein

symptoms become evident prior to, or even in the absence of, frank Purkinje cell loss (Shakkottai and Paulson, 2009). This observation raises the possibility that therapies directed at preventing neuron death (Alvarez et al., 2008) may be as valuable as those aimed at relieving the primary lipid trafficking defect (Davidson et al., 2009; Liu et al., 2009) for treating aspects of the neurological symptoms in NPC disease.

2.5 Materials and Methods

2.5.1 Mice.

The targeting vector was constructed using a BAC containing the C57BL/6J *Npc1* genomic clone, which was digested with BamH1 to obtain a 9.3 kb fragment of the *Npc1* gene that includes exon 9. This fragment was subcloned into pcDNA3, and then digested with Ssp1 and EcoRV to generate a 3.0 kb 5' arm, and with Asp718 to generate a 5.2 kb 3' arm. These arms were cloned into ploxPFlpneo, a vector that contains the neomycin resistance gene and the PGK promoter flanked by *FRT* sites (gift of Dr. James Shayman, University of Michigan). Included within the neomycin resistance gene is an EcoRV site that was used during screening for recombinants by Southern blot by probing for exons 5 and 18, both of which fall outside the targeting vector. *Npc1* exon 9 and flanking intronic sequence were amplified from C57BL/6J genomic DNA by high fidelity PCR, sequenced, and inserted between *loxP* sites. The targeting vector was electroporated into Bruce4 mouse embryonic stem cells, a line derived from C57BL6 mice that shares 85% genetic identity with this strain (Hughes et al., 2007). Euploid clones that had undergone homologous recombination were injected into albino C57BL6/J blastocysts. Germline transmission of the floxed allele in offspring of two independently derived chimeras was confirmed by the appearance of black fur, Southern blotting and PCR. Resulting mice

were crossed with mice expressing FLP recombinase (Jackson Laboratories, #003800, backcrossed to C57BL6/J for 10 generations) to remove the Neo cassette. These offspring were then backcrossed to C57BL6/J for seven generations and interbred to generate floxed homozygotes. *Pcp2-Cre* mice were obtained from Jackson Laboratories (#004146) and backcrossed to C57BL6/J for seven generations. $npc1^{nih}$ mice were obtained from Jackson Laboratories (#003092) and backcrossed to C57BL6/J for ten generations. $Npc1^{\Delta/+}$ mice were generated by mating $Npc1^{flox/+}$ mice with *EIIa-Cre* mice (Jackson #003724, backcrossed to C57BL/6J for 10 generations) and breeding the resulting mosaics with wild type C57BL6/J mice. All animal procedures were approved by the University of Michigan Committee on the Use and Care of Animals.

2.5.2 Genotyping.

Genotyping was performed on DNA isolated from tail biopsy at the time of weaning. PCR primers for $Npc1^{flox}$ mice were primer 1, 5'-TACTTGGTAGTTGTCAGGTAGGCTTATGCT-3'; primer 2, 5'-GTCCACAGAACGGGTCATCT-3'; and primer 3, 5'-ACACTGCAACGGGCTCCTTTG-3'. PCR was performed for 30 cycles, with denaturation at 95° for 30 sec, annealing at 62° for 30 sec, and extension at 72° for 2 min. Predicted PCR products are demonstrated in Figure 1C. Genotyping of *Cre* mice was as described by Jackson Laboratories.

2.5.3 Western blotting.

Liver lysates were homogenized in RIPA buffer (Thermo Scientific) with c*O*mplete Protease Inhibitor Cocktail (Roche) plus 50 mM sodium fluoride and 5 mM

sodium orthovanadate (Sigma). Samples were electrophoresed through a 10% SDS-polyacrylamide gel and transferred to nitrocellulose membranes (BioRad) on a semidry transfer apparatus. Immunoreactivity was detected by Immobilon chemilluminescent substrate (Millipore). Antibodies used were rabbit anti-NPC1 (1:1000, Abcam) and GAPDH (1:20,000 Abcam).

2.5.4 Gene expression analysis.

Total RNA was isolated from liver using TRIzol (Invitrogen) per the manufacturer's protocol. cDNA was synthesized using the High Capacity cDNA Archive Kit (Applied Biosystems). Quantitative real time PCR (RT-PCR) was performed on 5 ng cDNA per reaction, in duplicate. Primers and probes for *Npc1* exon 1-2, *Npc1* exon 9-10, and 18S rRNA were purchased from Applied Biosystems. Threshold cycle (Ct) values were determined on an ABI Prism 7900HT Sequence Detection System. Relative expression values were calculated by the standard curve method and normalized to 18S rRNA.

2.5.5 Histology.

Mice were anesthetized with isofluorane and perfused transcardially with 0.9% normal saline followed by 4% paraformaldehyde. Brain and liver were removed and post-fixed in 4% paraformaldehyde overnight. Brains were bisected, with the right half processed for paraffin embedding and the left half processed for frozen sections. Prior to freezing, brain tissue was cryoprotected in 30% sucrose for 48 hr at 4°C. Brains were frozen in isopentane chilled by dry ice and embedded in OCT (Tissue-Tek). Free floating sections were prepared with a cryostat at 30 μm and used for immunofluorescent staining

for calbindin (1:1000, Sigma), using secondary antibodies conjugated to Alexa Fluor 594 (Molecular Probes) for visualization. Sections were subsequently stained for unesterified cholesterol by incubating tissue for 90 min in PBS with 10% fetal bovine serum plus 25 μg/ml filipin (Sigma). Images were captured on a Zeiss Axioplan 2 imaging system. Paraffin-embedded sections were prepared at 5 μm and used for H&E staining, Iba1 (1:5000, Wako), and GFAP (1:1000, Dako) immunohistochemistry. Quantification of Purkinje cell loss was performed on H&E stained sections. Purkinje cells were recognized as large cells with amphophilic cytoplasm, large nuclei with open chromatin and prominent nucleoli that were located in the Purkinje layer. Counts were normalized to the length of the Purkinje layer, as measured by NIH ImageJ software, and reported as Purkinje cell density.

2.5.6 Phenotype analysis.

All mice were weighed weekly. Motor function was measured by the balance beam and rotarod tests. The balance beam consists of a 5 mm wide square beam suspended at 50 cm. Mice were trained at 10 weeks of age to cross the beam quickly and without stopping. Mice were then tested in triplicate on three consecutive days, followed by retesting at 15 and 20 weeks. Data were reported as time to traverse the beam, allowing a maximum of 20 seconds, and scoring falls as 20 seconds (Heng et al., 2007). For rotarod analysis, mice were trained for five minutes on a rod rotating at 5 rpm. Four additional trials were performed on each of two days at 1 hr intervals on a rod accelerating linearly from 5 rpm to 40 rpm over 5 min. Data reported for each mouse is the average latency to fall from the rod for the four trials on the second day of testing. Clinging to the rod for a full rotation was scored as a fall. Mice were allowed to stay on

the rotarod for a maximum of 5 min. All behavioral tests were performed in the latter half of the light phase of a 12-hr light-dark cycle. The endpoint used for survival analysis was when mice appeared moribund according to the guidelines of the University of Michigan Committee on the Use and Care of Animals.

2.5.7 Electrophysiology.

Whole-cell recordings were obtained from Purkinje neurons in 300 μm parasagittal cerebellar slices prepared from 10 week old mice. Vibratome sections were cut in ice-cold solution containing (in mM): 87 NaCl, 2.5 KCl, 25 $NaHCO_3$, 1 NaH_2PO_4, 0.5 $CaCl_2$, 7 $MgCl_2$, 75 sucrose and 10 glucose, bubbled with 5% CO_2/95% O_2. Slices were incubated at 33 ^oC in artificial CSF (ACSF) containing (in mM): 125 NaCl, 3.5 KCl, 26 $NaHCO_3$, 1.25 NaH_2PO_4, 2 $CaCl_2$, 1 $MgCl_2$ and 10 glucose, bubbled with 5% CO_2/95% O_2 for 45 minutes. Purkinje neurons were visualized with infrared differential interference contrast (IR-DIC) optics on a Nikon upright microscope. Borosilicate glass patch pipettes (with resistances of 4–6 MΩ) were filled with internal recording solution containing (in mM): 119 K Gluconate, 2 Na Gluconate, 6 NaCl, 2 $MgCl_2$, 10 EGTA, 10 HEPES, 14 Tris-Phosphocreatine, 4 MgATP, 0.3 tris-GTP. Whole-cell recordings were made in ACSF at room temperature 1–5 h after slice preparation using an Axopatch 200B amplifier, Digidata 1440A interface and pClamp-10 software (Molecular Devices). Voltage data was acquired in the fast current clamp mode of the amplifier and filtered at 2 kHz. The fast current-clamp mode is necessary to reduce distortion of action potentials observed when patch-clamp amplifiers are used in current-clamp mode (Magistretti et al., 1996). We could obtain stable recordings without oscillations in fast current-clamp mode with electrode resistances above 3 MΩ, as has been previously reported (Swensen and

Bean, 2003). Series resistance was monitored but not compensated; cells were rejected if the series resistance exceeded 20 MΩ. Total cell capacitance was calculated from measurement of the area under current transients evoked from a 10 mV depolarizing step from -80 mV. Input resistance was calculated from the change in the leak current from an applied 10 mV voltage step from -80 mV. Data were digitized at >10 kHz. Voltage traces were corrected for a 10 mV liquid junction potential.

2.5.8 Statistics.

Statistical significance was assessed by unpaired Student's *t* test (for comparison of two means) or ANOVA (for comparison of more than two mean). The Newman-Keuls post hoc test was performed to carry out pairwise comparisons of group means if ANOVA rejected the null hypothesis. Statistics were performed using the software package Prism 4 (GraphPad Software). *P* values less than 0.05 were considered significant.

Chapter 3

Heat shock protein 27 is neuroprotective in Niemann-Pick type C disease[2]

3.1 Abstract

Many neurodegenerative diseases are characterized by the selective vulnerability of certain neuronal populations. Identification of the mechanisms underlying this phenomenon is an important problem that will improve our understanding of the neurodegenerative process and offer therapeutic targets for these devastating disorders. Purkinje cell degeneration in an anterior-to-posterior gradient is a common feature of many cerebellar disorders, including Niemann-Pick type C disease (NPC), a lysosomal storage disorder characterized by childhood onset of multiple progressive neurologic deficits. Here, we describe an approach to identify candidate genes underlying selective vulnerability of Purkinje cells using data freely available in the Allen Brain Atlas. Further, we demonstrate that one of these genes, *HSP27,* promotes neuronal survival in

[2] This chapter will be included in a larger publication with the following authors:
Elrick MJ*, Chung C*, Qin ZS, Kalyana-Sundaram S, Chinnaiyan AM, and Lieberman AP.
(*these authors will have contributed equally to the final publication)

an *in vitro* model of NPC disease, through a mechanism that likely involves inhibition of apoptosis. These results highlight the novel use of bioinformatic tools to uncover pathways leading to neuronal protection in neurodegenerative disorders.

3.2 Introduction

Selective vulnerability of specific neuronal populations is a well characterized, though often perplexing feature of many neurodegenerative diseases (Double et al., 2010). Most commonly, these disorders are initiated by a uniform stress to the entire CNS, such as a genetic mutation, toxic insult, or aging. However, only some neurons respond to these stressors by degenerating, while others remain resistant and apparently maintain their normal function. Although this phenomenon is widely observed, the underlying mechanisms remain poorly understood. Notably, the factors regulating neuronal vulnerability represent attractive therapeutic targets, with the potential to convert susceptible neuronal populations into disease resistant ones.

One particularly striking example of selective vulnerability is the degeneration of cerebellar Purkinje cells (Sarna and Hawkes, 2003). Purkinje cells represent the sole output of the cerebellar cortex. Loss of Purkinje cells, therefore, leads to significant deficits of motor coordination, including ataxia and tremors. Despite the apparent uniformity of Purkinje cells in their morphology, connectivity, and electrophysiological properties, most cerebellar disorders affect Purkinje cells in a non-uniform way, leading to a distinct spatiotemporal pattern of loss that is reproducible not only between cases of a single disease, but across many otherwise unrelated diseases and injuries. One common pattern reveals a strong resistance of Purkinje cells in lobule X to degeneration, contrasted with the exquisite sensitivity of the anterior zone (lobules II-V), and moderate

susceptibility of the intermediate (lobules VI-VII) and posterior zones (lobule VIII and rostral aspect of lobule IX). Superimposed onto this anterior-to-posterior gradient is often a pattern of parasagittal stripes in which differential vulnerability is also observed (Sarna and Hawkes, 2003). Diseases displaying the classic anterior-to-posterior gradient may arise from genetic mutations, including spinocerebellar ataxias type 1 (Clark et al., 1997) and 6 (Takahashi et al., 1998), late infantile neuronal ceroid lipofuscinosis (Sleat et al., 2004), saposin C deficiency, a rare cause of Gaucher Disease (Yoneshige et al., 2010), ataxia telangiectasia (Tavani et al., 2003), and Niemann-Pick disease types A/B (Sarna et al., 2001) and C (Sarna et al., 2003); sporadic disorders, including multiple system atrophy (Kume et al., 1991) and chronic epilepsy (Crooks et al., 2000); toxins, including alcohol (Torvik and Torp, 1986), cytosine arabinoside (Winkelman and Hines, 1983), and methotrexate (Ciesielski et al., 1994); hypoxia/ischemia (Welsh et al., 2002; Biran et al., 2011); paraneoplastic syndromes (Mizutani et al., 1988); and even normal aging (Andersen et al., 2003). This pattern is also seen in many spontaneous mouse mutants, including *pcd* (Wang and Morgan, 2007), *leaner* (Heckroth and Abbott, 1994), *toppler* (Duchala et al., 2004), *robotic* (Isaacs et al., 2003), *shaker* (Tolbert et al., 1995), and *lurcher* (Armstrong et al., 2010); or targeted mutants, such as *saposin D* knockout (Matsuda et al., 2004), prion protein knockout (Rossi et al., 2001), and overexpression of the prion protein related gene *doppel* (Anderson et al., 2004). The fact that such a diverse array of insults leads to the same pattern of Purkinje cell death suggests that selective vulnerability of Purkinje cell subpopulations arises not from the initiating event of the disease process, but instead from differential regulation of cellular survival or death pathways in *response* to these injuries. We expect that the identification of pathways

responsible for this phenomenon will yield therapeutic targets broadly applicable to this large class of cerebellar disorders.

As a model for patterned Purkinje cell loss, we have studied murine Niemann-Pick type C disease (NPC). NPC is caused by mutations in the genes encoding NPC1 or NPC2 proteins, which are thought to act cooperatively in the efflux of cholesterol from late endosomes (LE) and lysosomes (LY) (Carstea et al., 1997; Naureckiene et al., 2000; Kwon et al., 2009). The consequence of these mutations is the accumulation of cholesterol and glycosphingolipids in the LE/LY compartment, leading to neurodegeneration by mechanisms that are not yet understood (Vanier and Millat, 2003). We recently demonstrated that conditional deletion of *Npc1* in Purkinje cells leads to a purely cell autonomous degeneration that recapitulates the spatiotemporal pattern of cell loss observed in mice with germline *Npc1* deletion (Elrick et al., 2010). Further, because Purkinje cell death does not cause early mortality in these mice, we were able to follow Purkinje cell survival beyond the typical lifespan of NPC mice. During this period, the population of surviving Purkinje cells in lobule X remained stable, while neurodegeneration continued to progress in lobules II-IX, thus highlighting the strong resistance of these cells to degeneration. Given the cell autonomous nature of Purkinje cell loss in NPC, we hypothesized that this selective vulnerability arises from intrinsic biological differences that are driven by differential gene expression. To test this notion, here we used a bioinformatic approach to identify genes that are differentially expressed between disease-resistant and vulnerable Purkinje cell populations. To test the biological function of these differentially expressed genes, we used an *in vitro* model of NPC and

characterized the ability of one of these candidate genes to protect neurons from degeneration.

3.3 Results

3.3.1 Identification of candidate genes underlying selective vulnerability of Purkinje cells

To search for genes differentially expressed between Purkinje cell subpopulations, we utilized the Allen Brain Atlas (**Figure 3.1**). This resource contains quantitative three-dimensional expression data derived from *in situ* hybridizations for greater than 20,000 genes in the adult C57BL6/J mouse brain (Lein et al., 2007). The complete gene expression dataset was downloaded and used to construct a single expression matrix with spatial coordinates and gene identifiers arrayed on separate axes. This strategy allowed us to treat the data for each location in the brain analogously to a single microarray experiment. The coordinates corresponding to cerebellar lobule X, the location of the most resistant Purkinje cells, and lobules II and III, the most highly vulnerable, were defined as regions of interest. For analysis, all coordinates falling within one region of interest were treated as replicate microarray experiments. This approach allowed us to use bioinformatics tools developed for microarray analysis to query the Allen Brain Atlas dataset. Differential gene expression between lobules was determined by *t*-test and Significance Analysis of Microarrays (SAM) (Tusher et al., 2001), followed by manual curation of *in situ* hybridization images. Manual curation was required to remove false positives created by expression in non-Purkinje cell types and technical artifacts in the archived images.

Figure 3.1 Schematic of gene expression analysis. (A) Summary of differential vulnerability of Purkinje cell subpopulations. Regions of interest were selected to include the population that experiences the most rapid neurodegeneration (lobules II and III, ROI #1) or the population that does not degenerate (lobule X, ROI #2). **(B)** Approach to gene expression analysis. Allen Brain Atlas data was downloaded and consolidated into a single gene expression matrix. Each row represents gene expression data from a single series of *in situ* hybridization data, while each column represents a single voxel within the mouse brain. The data set was then narrowed to include only voxels lying within the defined regions of interest. To identify genes differentially expressed between regions of interest, expression data was treated analogously to replicate microarrays and subjected to standard statistical tests (*t*-test and Significance Analysis for Microarrays). The top 1000 most significant genes were accepted for manual curation to verify expression in Purkinje cells. The gene list was further narrowed to include only genes with absolute expression differences between regions of interest, and expression matching the pattern of Purkinje cell survival or death throughout the entire cerebellum. *Construction of the gene expression matrix was performed by Shanker Kalyana-Sundaram.*

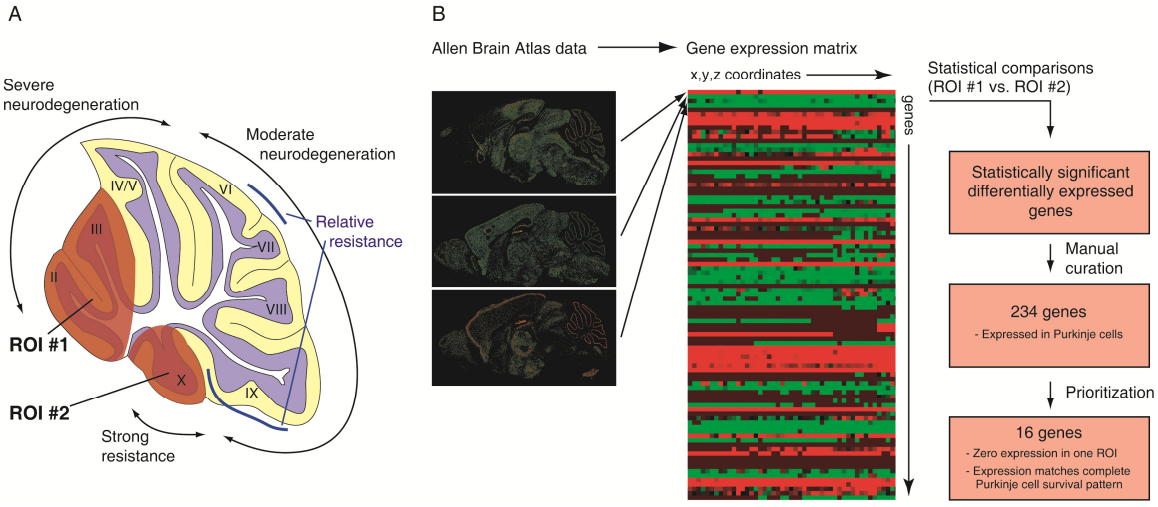

Initial analysis revealed 234 differentially expressed genes, of which 185 were overexpressed in lobules II and III and 49 were overexpressed in lobule X. We next sought to prioritize this list to identify testable candidates with putative roles in promoting or preventing neurodegeneration. The Allen Brain Atlas data, being derived from *in situ* hybridizations, presented a challenge in this regard, as expression levels were regarded as semi-quantitative. Further, because expression data within each *z* plane came from the same hybridization experiment, they were not considered statistically

independent samples. For these reasons, we were unable to rank the gene list by either the magnitude of differential expression or the degree of significance. Instead, we prioritized genes whose expression differences were absolute and tightly correlated with Purkinje cell survival in midline cerebellar sections. To accomplish this, we only included genes whose expression was undetectable in one region of interest, and whose expression matched or was the inverse of the survival pattern in 20 week old *Npc1*$^{flox/-}$*;Pcp2-Cre*$^{+}$ mice: strong in lobule X, patchy throughout the intermediate and posterior zones, with additional sparing in the caudal aspect of lobule IX and a region spanning the caudal aspect of lobule VI and rostral lobule VII (**Figure 3.2D**). This yielded six candidate neuroprotective genes and ten candidate susceptibility genes (**Figure 3.2A**, **Table 3.1**); *in situ* hybridization images from the Allen Brain Atlas for the candidate neuroprotective genes are shown in **Figure 3.2C**.

We analyzed the functions of these candidate genes and their human orthologues by querying their gene ontology (GO) annotations using AmiGO (Carbon et al., 2009). The GO Term Enrichment tool revealed significant over-representation (p<0.01) for GO terms containing *Prkca, Prkcd*, and *Plcxd2*, members of the phospholipase C – protein kinase C signal transduction cascade, suggesting that this pathway is differentially regulated between regions of interest. AmiGO was also used to query the complete list of GO Biological Process terms associated with candidate genes. In support of our hypothesis that the differentially expressed genes would include regulators of cellular

Table 3.1 Differentially expressed genes

Gene Symbol	Gene Name	Entrez Gene ID	Overexpressed in
B3galt5	UDP-Gal:betaGlcNAc beta 1,3-galactosyltransferase, polypeptide 5	93961	posterior
Hspb1	heat shock protein 1	15507	posterior
Pde1b	phosphodiesterase 1B, Ca2+-calmodulin dependent	18574	posterior
Plcxd2	phosphatidylinositol-specific phospholipase C, X domain containing 2	433022	posterior
Prkcd	protein kinase C, delta	18753	posterior
Th	tyrosine hydroxylase	21823	posterior
Alpk2	alpha-kinase 2	225638	anterior
Bace1	beta-site APP cleaving enzyme 1	23821	anterior
Chml	choroideremia-like	12663	anterior
Chst8	carbohydrate (N-acetylgalactosamine 4-0) sulfotransferase 8	68947	anterior
Dbc1	deleted in bladder cancer 1	56710	anterior
Kcnh7	potassium voltage-gated channel, subfamily H (eag-related), member 7	170738	anterior
Lgr5	leucine rich repeat containing G protein coupled receptor 5	14160	anterior
Opn3	opsin (encephalopsin)	13603	anterior
Prkca	protein kinase C, alpha	18750	anterior
Sgpp2	sphingosine-1-phosphate phosphotase 2	433323	anterior

survival and death decisions, 5 genes were associated with cell death related annotations, including "cell death" (GO:0008219, *Dbc1* and *Hspb1*), "apoptosis" (GO:0006915, *Pde1b* and *Prkcd*), "negative regulation of apoptosis" (GO:0043066, *Hspb1*), and "induction of apoptosis by intracellular signals" (GO:0008629, *Prkca*). Further, the gene product of *Sgpp2*, sphingosine 1-phosphate phosphatase 2, is likely involved in the regulation of apoptosis as well, due to its hydrolysis of sphingosine 1-phosphate (Ogawa et al., 2003), a lipid second messenger that is a negative regulator of apoptosis (Spiegel and Milstien, 2003). Finally, we performed an analysis of Cellular Component annotations to determine the subcellular localization of the protein products of candidate genes (**Figure 3.2B**). The vast majority of gene products are localized outside of the

endosome-lysosome system, further suggesting that selective vulnerability of Purkinje cell populations arises not from the primary site of pathogenesis in NPC disease, but from responses to cellular stress that take place elsewhere.

Figure 3.2 Candidate neuroprotective or pro-degenerative genes. (A) Hierarchical clustering of candidate genes, demonstrating strong differential expression between regions of interest. Rows are genes. Columns are individual voxels within the regions of interest. **(B)** Subcellular localization of candidate gene products, based on GO Cellular Component terms. Proteins with more than one localization were listed multiply. **(C)** *In situ* hybridization images from Allen Brain Atlas for candidate neuroprotective genes. **(D)** Calbindin stain of cerebellum from 20-week old *Npc1*$^{flox/-}$;*Pcp2-Cre*$^{+}$ mouse, demonstrating survival pattern of Purkinje cells.

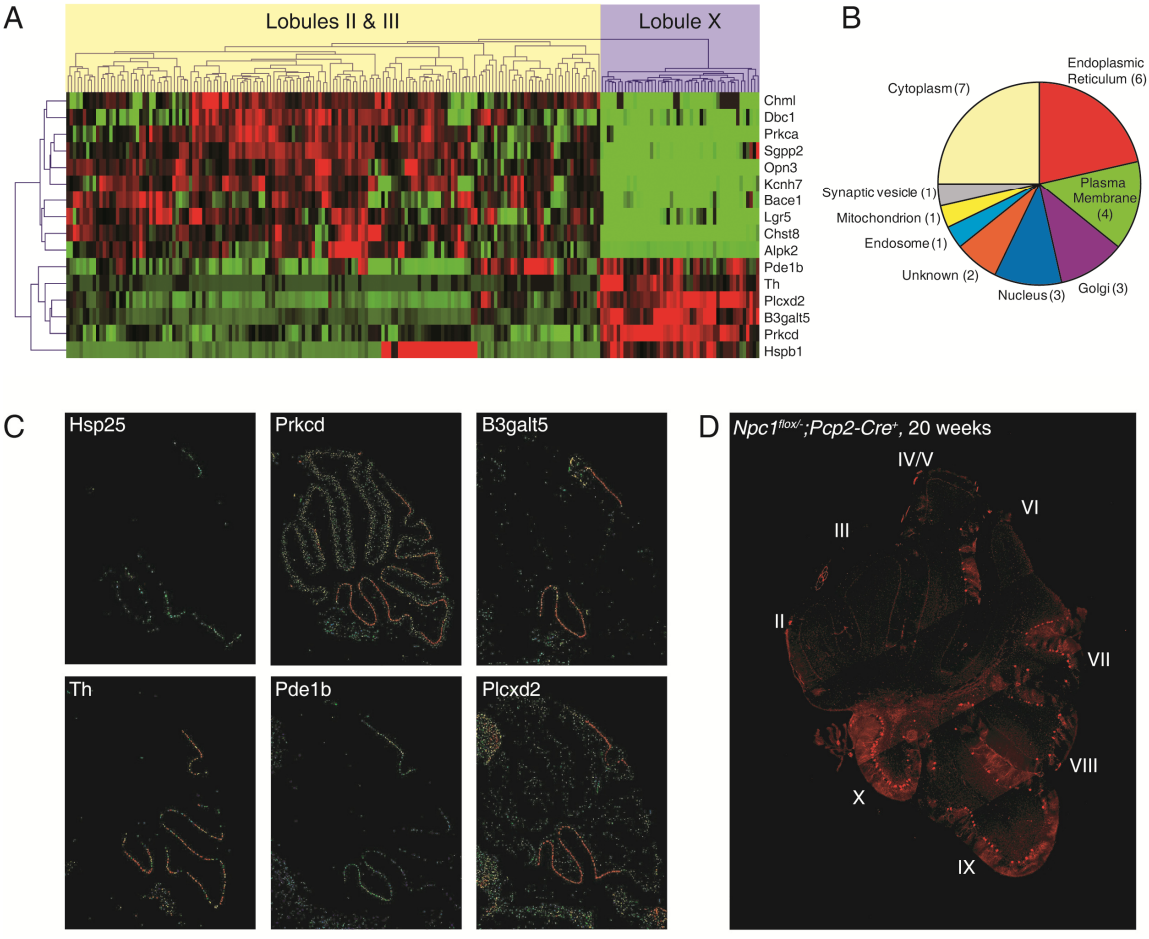

3.3.2 *HSP27* promotes survival of *in vitro* models of NPC disease

We next sought to directly test the extent to which candidate genes influence cellular survival in models of NPC disease. We chose to study one particularly attractive candidate that was over-expressed by lobule X Purkinje cells, heat shock protein 25 (*Hsp25,* also called *HspB1*). This gene has been previously linked to neurodegeneration, as mutations in the human ortholog, *HSP27,* cause some cases of Charcot-Marie-Tooth disease and distal hereditary motor neuropathy (Evgrafov et al., 2004). Additionally, HSP27 regulates multiple events that influence neuronal viability, including stability of the actin cytoskeleton, protein folding, reactive oxygen species (ROS), and apoptosis (Arrigo, 2007), and its robust expression has been documented previously in surviving Purkinje cells from *Npc1*$^{-/-}$ mice (Sarna et al., 2003).

We initially sought to confirm that Hsp25 expression in mutant mice with active disease matched the pattern predicted by the Allen Brain Atlas. Strong expression of Hsp25 was detected in lobule X Purkinje cells of *Npc1*$^{flox/-}$*;Pcp2-Cre*$^{+}$ mice at 7 weeks of age, just after the onset of Purkinje cell degeneration (**Figure 3.3A**). In contrast, Hsp25 was undetectable in the more susceptible Purkinje cells of lobules II and III. To determine whether HSP27 functions as an inhibitor of cell death pathways in NPC cell models, we knocked down its expression using siRNA. We initially treated HeLa cells with U18666A, a small molecule which induces lipid trafficking defects identical to those seen in NPC disease (Liscum et al., 1989). Knockdown of *HSP27* in U18666A-treated cells, but not in vehicle controls, led to a significant increase of caspase activity (**Figure 3.3B**). Likewise, *HSP27* knockdown in NPC patient fibroblasts significantly increased the percentage of apoptotic cells, while *HSP27* knockdown had no effect on control

fibroblasts (**Figure 3.3**C). These results are consistent with a model in which HSP27 prevents the induction of apoptosis in response to the intracellular lipid trafficking defects caused by NPC1 deficiency.

Figure 3.3 *HSP27* promotes the survival of NPC1-deficient cells. (A) Expression of Hsp25 in *Npc1*$^{flox/-}$;*Pcp2-Cre*$^{+}$ cerebellum at 7 weeks. **(B)** (Upper panel) HeLa cells were transfected with non-targeted (lanes 1 and 3) or *HSP27* siRNA (lanes 2 and 4), then treated with vehicle (lanes 1-2) or 1 μg/ml U18666A (lanes 3-4) for 24 hr. HSP27 expression was determined by western blot. GAPDH is loading control. (Lower panel) Caspase activity in HeLa cell lysates. Data are mean ± SEM. **p*<0.05. **(C)** NPC1 null human dermal fibroblasts were transfected with non-targeted or *HSP27* siRNA. Cells were stained with Hoechst, and the percentage of cells with condensed chromatin was scored. Data are mean ± SEM. ***p*<0.01.

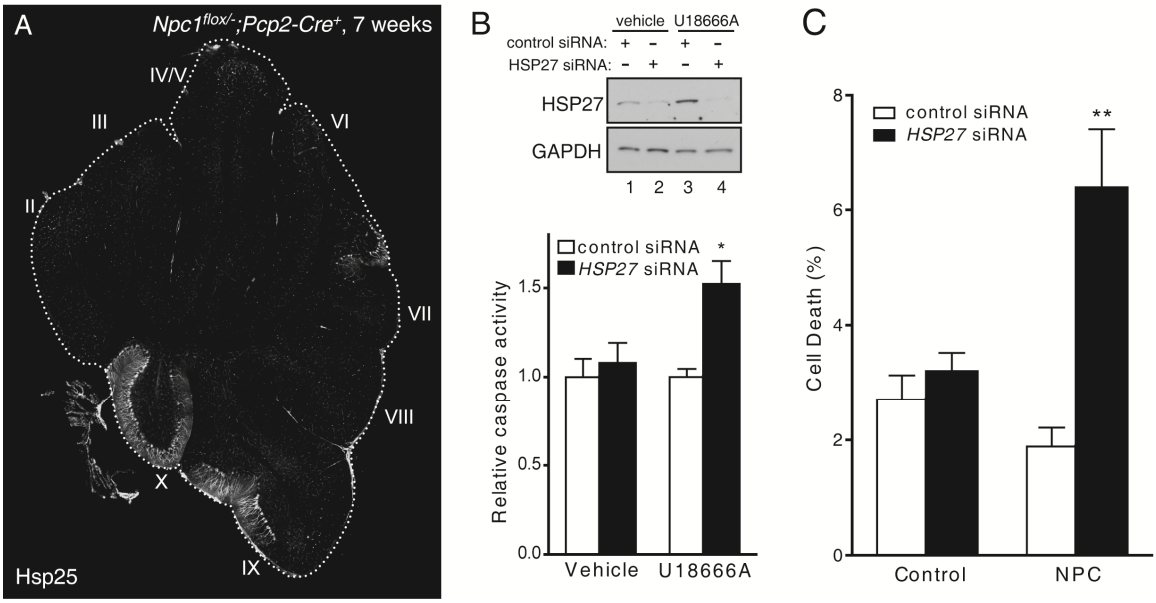

To test the role of HSP27 in the survival of neurons, the cell type critical for NPC disease neuropathology, we utilized a neuronal culture model. Primary cortical neurons treated with U18666A develop filipin-positive lipid inclusions and progressive degeneration, and have been used previously to model NPC disease (Cheung et al., 2004; Amritraj et al., 2009). As expected, neurons treated with 2.5 μg/ml U18666A

demonstrated progressive degeneration starting 48 hours after treatment (**Figure 3.4A**). These neurons expressed no detectable Hsp25 (**Figure 3.4C**), and exogenous expression of human HSP27 almost completely prevented their degeneration (**Figure 3.4A**). To probe the mechanism of this effect, we took advantage of the fact that many of HSP27's functions are attributable to different oligomerization states, regulated by phosphorylation at serine residues 15, 78 and 82. Mutation of these residues to alanine (non-phosphorylatable) or aspartate/glutamate (phosphomimetic) has been widely used to study phosphorylation state dependent properties of HSP27 (Arrigo, 2007). Transduction of U18666A-treated neurons with the phosphomimetic HSP27^{3E} recapitulated the neuroprotective affects of wild-type HSP27, while non-phosphorylatable HSP27^{3A} was inactive (**Figure 3.4B**). We conclude that the neuroprotective effects of HSP27 are mediated by the phosphorylated species.

Figure 3.4 HSP27 protects neurons from U18666A-induced neurodegeneration. **(A)** Primary cortical neurons were transduced with FIV-Hsp27^{wt} or left uninfected at 3 div. U18666A was added at 2.5 µg/ml at 7 div to induce degeneration. XTT assay for viability was performed at the indicated times. **(B)** Neurons were transduced with Hsp27 wild type and phosphomutant vectors and subjected to U18666A, as described for panel A. XTT assay was performed 72 hrs post U18666A. **(C)** Neuron lysates were probed for Hsp25 expression by western blot. Neurons treated with 100 nM geldanamycin were included to induce Hsp25 expression as a positive control.

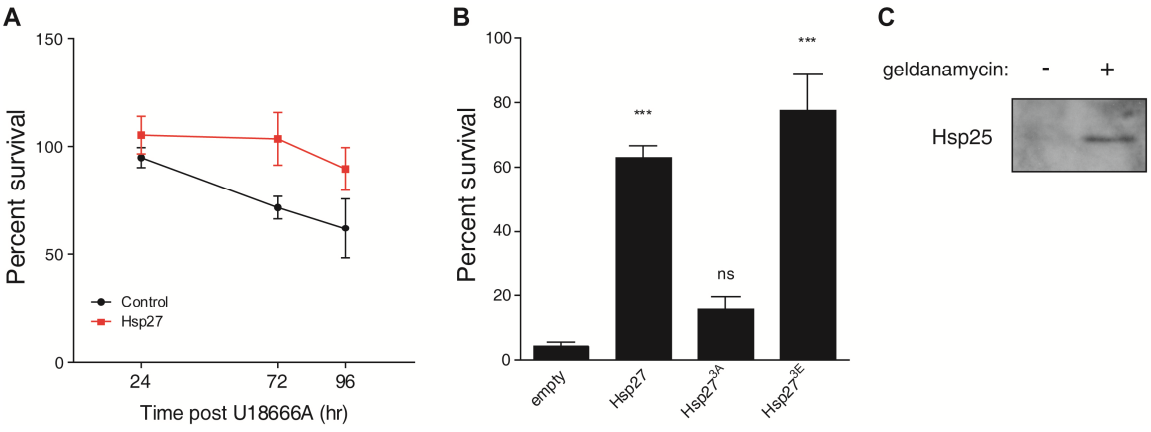

3.4 Discussion

Here, we have reported a bioinformatic approach to the identification of disease-modifying genes in neurodegenerative disorders. Using NPC disease as a model for the study of selective neuronal vulnerability, we have shown that one of our candidate genes, HSP27, was strongly protective in cultured neurons.

HSP27 is a multifunctional protein, with documented roles in actin stability, protein folding, oxidative damage, and apoptosis (Arrigo, 2007). Interestingly, defects in proteostasis (Higashi et al., 1993; Love et al., 1995) and overproduction of ROS have been documented in NPC disease (Zampieri et al., 2009; Porter et al., 2010), and the death of neurons in NPC appears to be mediated by apoptosis (Cheung et al., 2004; Alvarez et al., 2008). To determine which of these functions were critical to HSP27's neuroprotective properties, we utilized HSP27 phosphomutants. Phosphorylation of HSP27 regulates its oligomerization state, which ranges from dimers and tetramers (favored by phosphorylation) to multimers of up to 800 kDa (favored by dephosphorylation). Large complexes of dephosphorylated HSP27 have chaperone activity (Jakob et al., 1993; Ehrnsperger et al., 2000) and are capable of preventing oxidative damage (Preville et al., 1999). In contrast, smaller, phosphorylated species stabilize the actin cytoskeleton (Lavoie et al., 1995; Huot et al., 1996). Additionally, HSP27 is a direct inhibitor of apoptosis at multiple levels, through binding and sequestration of cytochrome c (Bruey et al., 2000) and caspase-3 (Pandey et al., 2000), and inhibition of Bax activation (Havasi et al., 2008) and DAXX signaling (Charette and Landry, 2000). The phosphorylation state required for most of these activities is unknown, with the exception of DAXX inhibition, which requires phosphorylated HSP27

(Charette and Landry, 2000). Recently, phosphomimetic mutants of HSP27 were shown to protect against a broad array of apoptosis-inducing stimuli, while non-phosphorylatable mutants showed no protection against some stimuli and only mild protection against others, suggesting that anti-apoptotic activities of HSP27 are primarily attributable to the phosphorylated species (Paul et al., 2010).

Because only phosphorylated HSP27 protected neurons in our assay, it is less likely that HSP27's chaperone or anti-oxidative activities prevent U18666A-induced neurodegeneration. We favor a model in which HSP27 is acting through a direct anti-apoptotic mechanism. This conclusion is further supported by the fact that *HSP27* knockdown in NPC cell models increased caspase activity and chromatin condensation. We speculate that degeneration-resistant Purkinje cells, such as those in lobule X, have a higher threshold for inducing apoptosis in response to cellular stressors. This property is attributable to the activity of *HSP27;* additional anti-apoptotic genes that are highly expressed in lobule X and pro-apoptotic genes that are expressed in more susceptible regions may also contribute to the pattern of neuronal vulnerability. This provides an opportunity for therapeutic intervention since *HSP27* expression can be induced by HSP90 inhibitors, such as geldanamycin. Unfortunately, we could not directly test the ability of geldanamycin to prevent degeneration *in vitro* due to its toxicity to cultured neurons. However, the geldanamycin analogue 17-N-allylamino-17-demethoxygeldanamycin (17-AAG) crosses the blood-brain barrier, displays no neuronal toxicity *in vivo* (Egorin et al., 2001; Waza et al., 2005), and is currently undergoing clinical trials, phases I-III, for the treatment of several cancers (www.clinicaltrials.gov).

This is a clear candidate for preclinical trials in NPC animal models. Additionally, drugs inhibiting apoptosis through other mechanisms may also have therapeutic benefit.

Our identification of candidate disease modifying genes relied on quantitative *in situ* hybridization data available in the Allen Brain Atlas. Methods had not been developed previously to use this resource for unbiased studies of differential gene expression. For guidance in designing our approach, we looked to tools developed for the analysis of microarray data, where studies of differential gene expression are commonplace. Several caveats exist when applying our strategy to Allen Brain Atlas data. First, this method is heavily dependent upon manual curation as standard statistical tests yielded high false positive rates. These were variably due to signals generated by other cell types that fell within or adjacent to the region of interest, or artifacts and noise on the *in situ* hybridization images. Second, while the majority of differentially expressed genes were identified by both *t*-test and SAM, many were found only by one method. Therefore, it was necessary to combine the use of both approaches, and it remains possible that some differentially expressed genes were not discovered by either. To streamline future studies, a more robust method for working with Allen Brain Atlas data may need to be developed. Despite these technical concerns, our study provides proof of concept for the use of Allen Brain Atlas data to identify therapeutic targets in neurodegenerative disease. This method is readily applicable to any brain region, and could be used to discover novel therapeutic targets in other neurodegenerative diseases.

3.5 Methods

3.5.1 Genome-wide expression profiling.

The Expression Energy Volume for each gene in the Allen Mouse Brain Atlas was downloaded via the Allen Brain Atlas API (Lein et al., 2007). These data were then reorganized into a single expression matrix and filtered to include locations corresponding to the regions of interest, cerebellar lobules X and II/III, and extending laterally 1400 microns from the midline. This data matrix was then loaded into TM4 MultiExperiment Viewer software (Saeed et al., 2003), in which differential expression between regions of interest was determined by Student's *t*-test and Significance Analysis of Microarrays (SAM) (Tusher et al., 2001). The top 1000 genes returned by each method were manually verified by direct inspection of *in situ* hybridization data on the Allen Brain Atlas website in midline and several adjacent sagittal sections. Criteria for validation were (1) expression present in the Purkinje cell layer in at least one region of interest, and (2) differential expression between regions of interest.

3.5.2 Apoptosis Assays.

Caspase 3 activity in HeLa cells was determined by assaying DEVDase activity in cell lysates using the ApoTarget caspase 3 / CPP32 fluorimetric protease assay kit (Biosource) according to the manufacturer's instructions. Fluorescence was measured using a SpectraMax Gemini EM plate reader (Molecular Devices). NPC fibroblasts were stained with Hoechst (Immunocytochemistry Technologies). Cells were counted in five randomly selected fields per transfection at 200x magnification and scored for chromatin condensation.

3.5.3 Cell culture.

All cell lines were cultured at 37°C with 5% CO_2. HeLa cells were maintained in DMEM (Gibco) supplemented with 10% FBS, 10μ/ml penicillin, 10μ/ml streptomycin, and 2mM glutamine. Human skin fibroblast line GM03123 from an NPC patient and GM08399 from an age and sex match control (Corriell Cell Repositories) were maintained in MEM (Gibco) supplemented with 15% FBS, 10μ/ml penicillin, 10μ/ml streptomycin, and 2mM glutamine. To manipulate HSP27 expression, cells were transfected with ON-TARGET*plus* SMART pool human HSP27 or non-targeting control (Dharmacon). HeLa cells were transfected using the DharmaFECT reagent (Dharmacon), according to the manufacturer's instructions. Fibroblasts were transfected by electroporation with the Lonza Nucleofector normal human dermal fibroblast kit.

3.5.4 Primary cortical neuron culture and viability assay.

C57BL6/J mice were obtained from Jackson Laboratories. All animal procedures were approved by the University of Michigan Committee on the Use and Care of Animals. Cortices from P0 mouse pups were dissected free of meninges, minced, and then dissociated and cultured as described previously (Jakawich et al., 2010). Neurons were plated in poly-D-lysine (Millipore) treated 96-well plates at a density of $6x10^4$ per well. Cytosine arabinoside (Sigma) was added to the culture media the following day at a final concentration of 5 μM to prevent glial growth. U18666A was added at 2.5 μg/ml at 7 div to induce lipid storage. Neuronal viability was determined by XTT assay (Cell Proliferation Kit II, Roche) following the manufacturer's instructions.

3.5.5 Viral vectors.

A lentiviral expression clone of C-terminally FLAG-tagged human *HSP27* was ordered from Genecopoeia. Serine-to-alanine and serine-to-glutamate mutations were introduced at serines 15, 78, and 82 using the QuikChange Lightning Multi Site-Driected Mutagenesis kit (Stratagene). Wild type *HSP27, HSP27*^{3A}*, HSP27*^{3E}*,* and empty vector plasmids were packaged into feline immunodeficiency virus (FIV) vectors by the Iowa Vector Core. Viral infection was performed at 10 MOI, followed by a 75% media change four hours after infection.

3.5.6 Statistics.

Statistical significance was assessed by unpaired Student's *t* test (for comparison of two means) or ANOVA (for comparison of more than two means). The Newman-Keuls post hoc test was performed to carry out pairwise comparisons of group means if ANOVA rejected the null hypothesis. Statistics were performed using the software package Prism 4 (GraphPad Software). *P* values less than 0.05 were considered significant. Statistical analysis of gene expression data was performed using TM4 MultiExperiment Viewer software (Saeed et al., 2003). For these calculations, statistical significance was determined using Student's *t*-test with Bonferroni correction for multiple comparisons and Significance Analysis for Microarrays (Tusher et al., 2001).

Chapter 4

Autophagy promotes Niemann-Pick type C disease pathogenesis by enhancing lipid storage and lysosomal dysfunction[3]

4.1 Abstract

Niemann-Pick type C disease (NPC) is a childhood onset neurodegenerative disorder arising from lipid trafficking defects caused by mutations in the *NPC1* or *NPC2* genes. Marked accumulation of autophagosomes is a prominent feature of NPC cells, yet a detailed understanding of the disease-associated alterations in autophagy and their role in pathogenesis has been lacking. We report that aberrant Toll-like receptor signaling contributes to autophagy induction in the setting of NPC1 deficiency. Further, lipid storage in NPC disease not only induces autophagy, but also impairs the clearance of autolysosomes by inhibiting lysosomal protease activity. Additionally, we demonstrate that the autophagic pathway is a major source of stored cholesterol in the NPC lysosome. Inhibition of autophagy significantly reduces cholesterol storage, restores normal lysosomal proteolysis, and enhances the survival of neurons in an *in vitro* model of NPC

[3] This chapter will be submitted for publication with the following authors:
Elrick MJ and Lieberman AP.

neurodegeneration, demonstrating that activation of the autophagic pathway contributes to disease pathogenesis.

4.2 Introduction

Macroautophagy (hereafter referred to as "autophagy") is the sequestration of cytoplasmic constituents into double-membrane bound organelles known as autophagosomes, and their subsequent delivery to lysosomes for degradation and recycling (Klionsky, 2005). Basal autophagy plays an important role in the turnover of proteins and organelles. Autophagy may also be induced in response to cellular stressors, such as nutrient depletion, endoplasmic reticulum stress, and proteostasis defects. Recent progress has revealed a significant role for autophagy in health and disease, including cancer, immunity, and neurodegeneration (Levine and Kroemer, 2008). Basal autophagy is an absolute requirement for neuronal homeostasis, as autophagy-deficient mouse mutants display neurodegeneration associated with the accumulation of ubiquitinated protein aggregates and the appearance of motor impairments (Hara et al., 2006; Komatsu et al., 2006). The promotion of autophagy has proven to be a beneficial therapeutic strategy in neurodegenerative protein aggregation disorders, presumably by facilitating turnover of the offending, misfolded protein (Ravikumar et al., 2004). Conversely, excessive autophagy has also been implicated in neurodegeneration (Yue et al., 2002), though these findings remain controversial (Levine and Yuan, 2005; Nishiyama et al., 2010). In accordance with its putative roles in neurodegeneration, alterations of the autophagic pathway have been reported in multiple disorders, including Alzheimer, Parkinson, and Huntington diseases, as well as many of the lysosomal storage diseases (Settembre et al., 2008; Banerjee et al., 2010). In most cases, the relevance of these

autophagic alterations to disease pathogenesis remains poorly defined and this represents a significant barrier to the use of autophagy as a therapeutic target.

Niemann-Pick type C disease (NPC) is a neurodegenerative lysosomal storage disorder characterized by ataxia, cognitive decline, seizures, dystonia, and cataplexy (Vanier and Millat, 2003). It is caused by mutations in the *NPC1* or *NPC2* genes (Carstea et al., 1997; Naureckiene et al., 2000), whose protein products are thought to act cooperatively in the efflux of cholesterol from late endosomes and lysosomes (Kwon et al., 2009). In NPC disease, unesterified cholesterol accumulates in late endosomes and lysosomes of all tissues, and is classically considered to be derived from receptor-mediated endocytosis of low density lipoprotein (LDL)-cholesterol (Pentchev et al., 1985). A broad array of glycosphingolipids accumulates as well (Karten et al., 2009), though it is unknown whether this latter phenomenon is attributable to a direct role for NPC1/NPC2 in glycosphingolipid trafficking or is secondary to cholesterol accumulation.

The storage of lipids in NPC disease has a number of cell biological consequences. One of the most striking among these is the marked accumulation of autophagic vesicles, which has been demonstrated in multiple tissues of NPC mice and cultured cells from human NPC patients (Ko et al., 2005; Pacheco et al., 2007). We have previously demonstrated that this elevated load of autophagic vesicles is associated with increased autophagic flux, and this autophagy induction is dependent upon Beclin-1 (Pacheco et al., 2007). In the present study, we further advance our understanding of the role of autophagy in NPC disease. We find that lipid storage causes not only autophagy induction, but also impairs the turnover of autolysosomes via inhibition of lysosomal cathepsin activity. Further, we show that autophagy is a major source of stored

cholesterol in NPC lysosomes, creating a positive feedback loop between lipid storage and autophagy induction. Breaking this feedback loop, by way of autophagy inhibition, reduced lipid storage, enhanced lysosomal protease activity, and improved neuronal survival. These data demonstrate a deleterious role for autophagy in NPC disease.

4.3 Results

4.3.1 Toll-like receptor signaling contributes to autophagy induction in NPC disease

We previously reported that autophagy induction in NPC requires Beclin-1 (Pacheco et al., 2007). While transcriptional upregulation of Beclin-1 is sufficient to induce autophagy in some instances, regulation of Beclin-1is primarily achieved through post-translational mechanisms (He and Levine; He and Levine, 2010). For instance, several pathways converge upon phosphorylation of Bcl-2 by JNK1, thereby relieving Beclin-1 of repression by Bcl-2. However, we were unable to find evidence of phosphorylation of either Bcl-2 or JNK1 in NPC patient fibroblasts or mice (data not shown). We therefore investigated Toll-like receptor (TLR) signaling as a trigger for Beclin-1-mediated autophagy activation. TLR adapter proteins MyD88 and TRIF have been shown to interact directly with Beclin-1, and this interaction promotes autophagy by mechanisms that are not well understood (Shi and Kehrl, 2008; Xu et al., 2008). Notably, TLR4 is trapped in lipid-laden endolysosomes in NPC disease, where it is persistently activated, leading to a number of inflammatory sequelae (Suzuki et al., 2007). We therefore sought to determine whether signaling through TLR4, and perhaps other TLRs, mediated autophagy induction as well. To test this hypothesis, we knocked down MyD88 and TRIF, either alone or together, in NPC patient fibroblasts. Knock down of

TRIF, but not MyD88, significantly reduced levels of the autophagosome marker LC3-II in these cells (**Figure 4.1A, B**). We next moved upstream of TRIF to determine which TLRs were responsible for the induction of autophagy. Of the many TLRs, TRIF interacts only with TLR3 and TLR4. While knock down of either of these receptors alone was insufficient to reduce autophagy induction, simultaneous knockdown of TLR3 and TLR4 did significantly reduce LC3-II levels, indicating that both are involved in the induction of autophagy in NPC disease (**Figure 4.1C, D**). Interestingly, TLR3 and TLR4 are the only TLRs found in late endosomes and lysosomes with an orientation that exposes their ligand-binding domains to lipid storage material in NPC1 deficient cells. To confirm these results, we tested the ability of TRIF-null mouse embryonic fibroblasts (MEF) to induce autophagy in response to U18666A, a drug that induces a lipid storage phenotype identical to that of NPC disease (Liscum and Faust, 1989). These cells had a reduced induction of autophagy compared to wild-type controls (**Figure 4.1E**). However, they were still capable of inducing autophagy, indicating either a genetic compensation in these cells that allows TLR signaling to induce autophagy through an adapter other than TRIF, or that additional pathways are involved in autophagy induction.

Figure 4.1 TLR signaling contributes to autophagy induction in NPC disease. (A) Human dermal fibroblasts from an NPC patient or healthy control were transfected with siRNA against MyD88 or TRIF, as indicated, and lysates were analyzed three days post-transfection for LC3 levels by western blot. **(B)** Quantification of three independent experiments, as described in A. **(C)** Human dermal fibroblasts were transfected with siRNA against TLR3 or TLR4, as indicated, and lysates were analyzed four days post transfection for LC3 levels by western blot. **(D)** Quantification of three independent experiments, as described in C. **(E)** Wild type or *Trif* knockout MEFs were treated with 2 μg/mL U18666A for 24 hr prior to determination of LC3 levels by western blot. **p* < 0.05, ****p* < 0.001 Error bars are SEM.

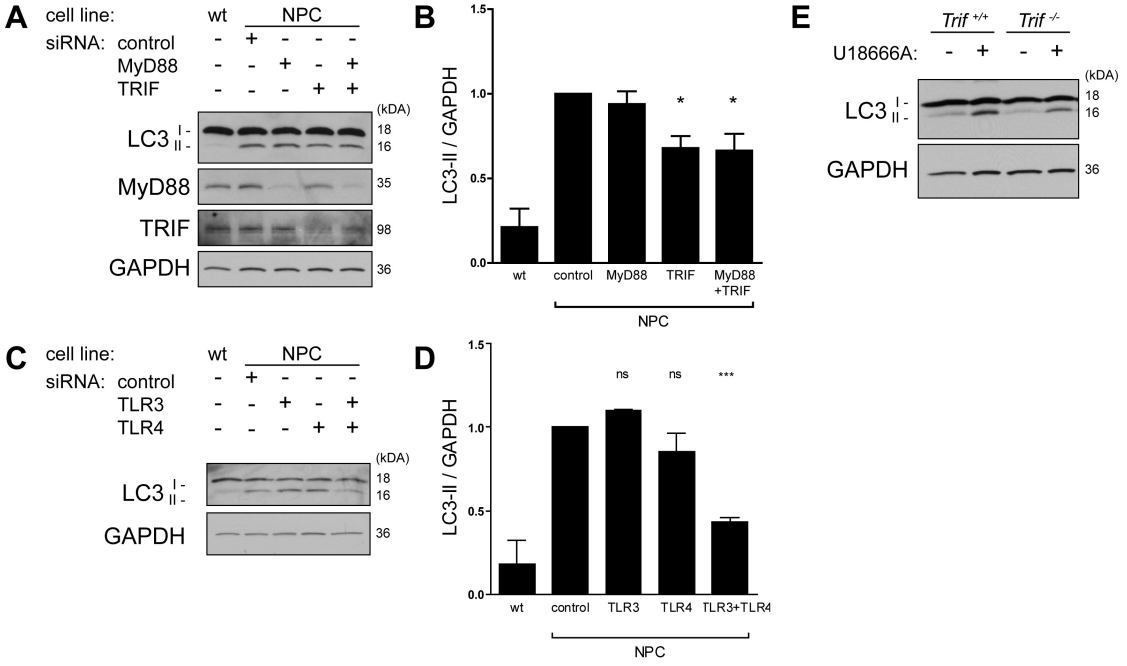

4.3.2 Autophagy is a major source of stored cholesterol in NPC disease

To understand the consequences of increased autophagy in NPC disease, we first determined whether this pathway played a role in the primary lipid storage defect. We found that further induction of autophagy by treatment with rapamycin led to a significant increase in total cholesterol levels in NPC fibroblasts, but not in normal controls (**Figure 4.2A**). We also tested the effects of rapamycin on a panel of glycosphingolipids known to be stored in NPC fibroblasts. Of these, only glucosylceramide showed a modest increase following rapamycin treatment, while

lactosylceramide and globotriaosylceramide were unaltered (**Figure 4.2B**). Sphingomyelin levels were also measured, but this lipid was not stored in NPC cells under our culture conditions (data not shown). We concluded that cholesterol was the primary lipid affected by autophagy, and thus we made it the focus of our subsequent analyses. For these studies, we utilized filipin, a dye that stains unesterified cholesterol *in situ*, allowing us to use imaging techniques to assess cholesterol levels specifically in lipid storage organelles. Rapamycin treatment enhanced filipin staining of NPC fibroblasts, whereas treatment with the autophagy inhibitor wortmannin decreased filipin staining (**Figure 4.2C**). To determine quantitatively the proportion of stored cholesterol due to autophagy, we used *Atg5* null MEFs, which are incapable of forming autophagosomes (Kuma et al., 2004). After treating these cells with U18666A, $Atg5^{-/-}$ MEFs developed half as much filipin staining as wild type MEFs (**Figure 4.2D**). This unexpected result indicated that autophagic delivery of endogenous cholesterol and endocytosis of exogenous LDL-cholesterol contributed similarly to cholesterol storage in NPC1 deficient fibroblasts.

Figure 4.2 Autophagy contributes to lipid storage in NPC cells. **(A)** Human dermal fibroblasts were treated with 1 μM rapamycin or vehicle (DMSO) for 24 hrs. Lipids were then extracted and cholesterol content was measured by HPTLC. **(B)** Summary of HPTLC data for cholesterol, glucosylceramide, lactosylceramide, and globotriaosylceramide. "Storage" is defined as [NPC] – [wt]. **(C)** Human dermal fibroblasts were treated with DMSO, 1 μM rapamycin, or 250 nM wortmannin. Cholesterol storage was analyzed by filipin staining. **(D)** Wild type or Atg5$^{-/-}$ MEFs were treated with 1 μg/ml U18666A for 24 hrs and then stained with filipin to demonstrate cholesterol storage (left panel). Quantification of filipin intensity across three independent experiments (right panel). Scale bar, 50 μm. *$p < 0.05$, ***$p < 0.001$. Error bars are SEM.

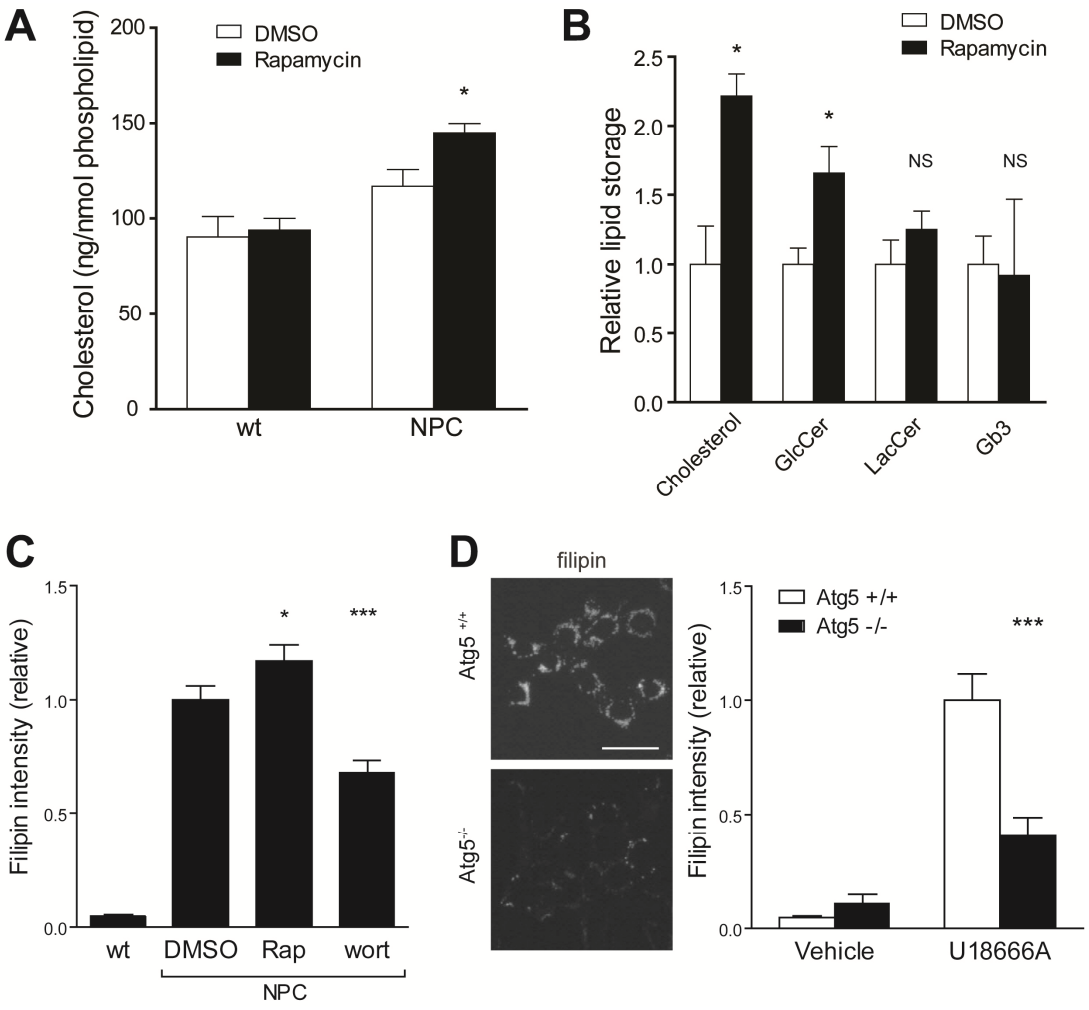

4.3.3 Autolysosome cargo degradation is impaired in NPC cells due to decreased cathepsin activity

The process of autophagy consists of multiple independently regulated components, and we considered that NPC1 deficiency may have separate effects on its induction and completion. Induction of autophagy is a multistep process that includes stimulation of the LC3 conjugation cascade, the formation of an isolation membrane and envelopment of cytoplasmic cargoes to form an autophagosome. Completion of autophagy requires microtubule-based trafficking of the autophagosome into the proximity of a lysosome, autophagosome-to-lysosome fusion to form an autolysosome, and maturation of the autolysosome, consisting of cargo degradation, efflux of degradation products, and regeneration of the lysosome. The sum total of these steps is known as autophagic flux (Klionsky et al., 2007). Previous experiments have indicated that the flux of protein substrates through the autophagic pathway in NPC disease is increased approximately 25% (Pacheco et al., 2007). However, autophagosome numbers in NPC cells are markedly higher than those from healthy controls (Pacheco et al., 2007). An accumulation of autophagosomes to this magnitude in the context of such a modest increase in autophagic flux suggests that, in addition to autophagy induction, there is an impairment in the completion of autophagy. This defect could arise from disruption of autophagosome trafficking, autophagosome-to-lysosome fusion, or degradation of autolysosomes following fusion.

To distinguish between these possibilities, we used a tandem-tagged LC3, consisting of LC3 fused to both GFP and mCherry (Pankiv et al., 2007). In acidic environments, GFP loses its fluorescence while mCherry retains it, enabling the

discrimination between relatively neutral autophagosomes (both green and red) and acidic autolysosomes (red only) (Pankiv et al., 2007). If NPC cells had defects in trafficking or fusion of autophagosomes, one would expect a build-up of autophagosomes and a paucity of autolysosomes. However, NPC cells displayed a similar percentage of autolysosomes as control cells (**Figure 4.3A, B**). Further, when challenged with an increased load of autophagosomes by treatment with rapamycin, control cells were capable of handling this challenge without increasing their percentage of autolysosomes. In contrast, NPC cells displayed a marked increase in the proportion of autolysosomes (**Figure 4.3A,B**). Our results demonstrated that autophagosome-to-lysosome fusion was intact in NPC cells, and suggested that the degradation of autolysosome contents was impaired.

To directly test this notion, we utilized time lapse imaging of cells transfected with mCherry-GFP-LC3. We followed autophagosomes until they lost their green fluorescence, indicating a lysosomal fusion event. Following this event, we measured elapsed time until the red fluorescence disappeared, indicating degradation of LC3 within the autolysosome. Using this system, cargoes in control autolysosomes had a mean lifetime of 1.2 minutes. In contrast, the lifetime of cargoes in NPC autolysosomes was markedly elevated at 3.6 minutes (**Figure 4.3C, D**). Interestingly, the distribution of cargo degradation times in NPC cells was much broader than that of wild-type cells, including many that were in the normal range, but others that took as long as 18 minutes (**Figure 4.3E**).

Figure 4.3 Impaired cargo degradation within NPC autolysosomes. (A) Representative images of human dermal fibroblasts transfected with mCherry-GFP-LC3, followed by 24 hr treatment with vehicle (DMSO), 1 μM rapamycin, or 100nM bafilomycin A1. Bafilomycin A1 treatment was included as a negative control, as it neutralizes the pH of lysosomes. Scale bar, 10 μm. **(B)** Quantification of the percent of total puncta that are autolysosomes (i.e. red only). *n* = 8-10 cells per group, pooled from two independent experiments. **(C)** Representative live cell time lapse images from human dermal fibroblasts demonstrating the fusion of an autophagosome (yellow) with a lysosome to form an autolysosome (red), followed by maturation of the autolysosome, as indicated by loss of red signal. Scale bar, 2 μm. **(D)** Average lifetime of autolysosomes. *n* = 27 (wt) or 29 (NPC) fusion events from four independent experiments. **(E)** Histogram of data presented in D. Error bars are SEM.

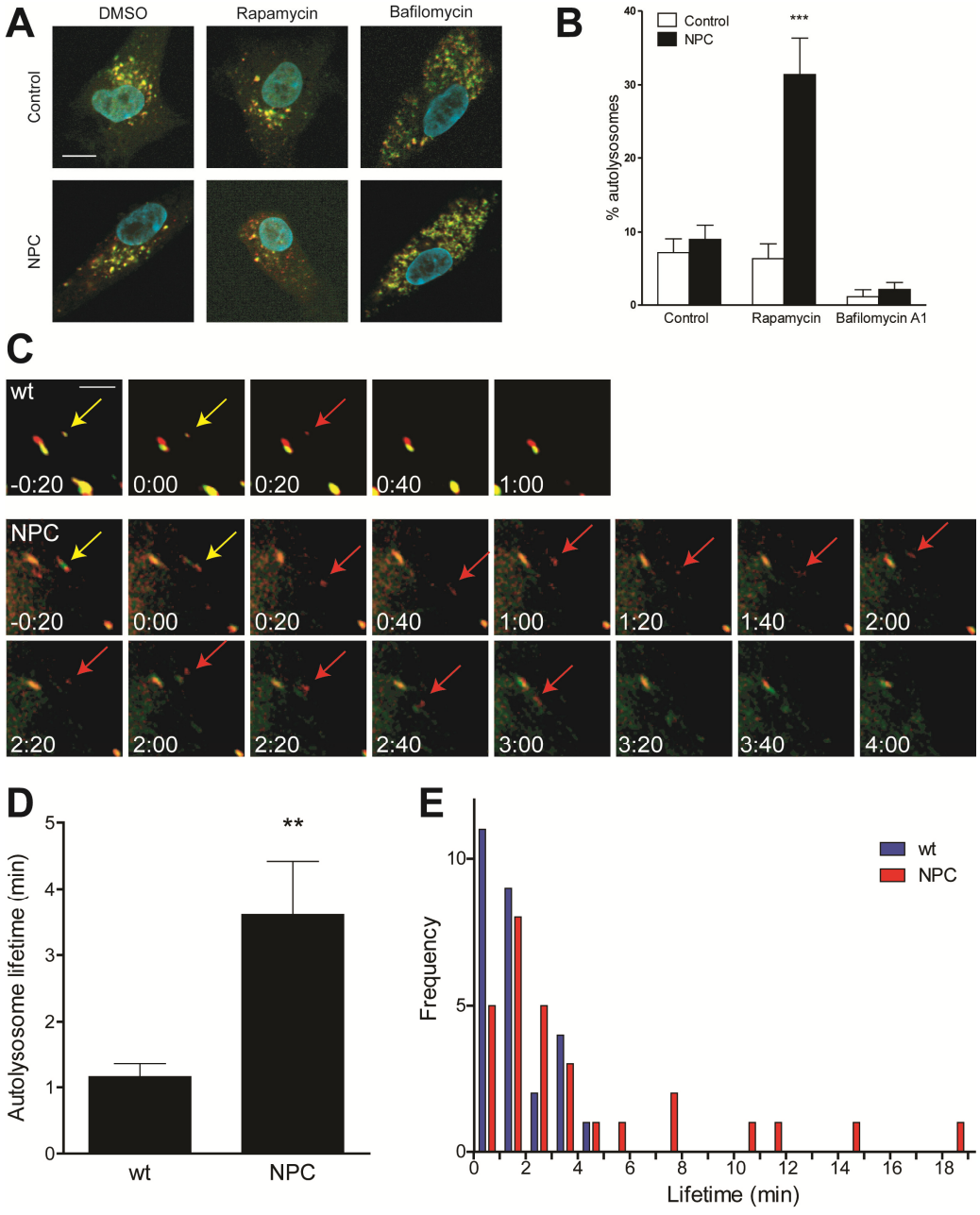

To further confirm this finding, we sought to use a non-LC3 dependent readout for lysosome function. We hypothesized that impaired maturation of autolysosomes was due to inhibition of lysosomal cathepsin activity. To test this, we used Magic Red, a commercial reagent that couples a fluorophore to a di-arginine peptide motif that quenches the fluorophore and targets the molecule for cleavage by cathepsin B. Prior to cleavage, Magic Red is cell permeable and non-fluorescent. Following cleavage, it becomes trapped in lysosomes and fluoresces red. The rate of accumulation of red fluorescence in lysosomes was used to estimate cathepsin activity *in situ*. To confirm the specificity of this reagent, we treated cells with bafilomycin A1 and found that this completely abolished the appearance of red fluorescence (data not shown). This assay revealed that cathepsin B activity in NPC1 null lysosomes was half that of lysosomes in control cells (**Figure 4.4A-C**). This defect was not a result of impaired processing of cathepsin B, which matures normally in NPC1 null cells (**Figure 4.4D**). Prior studies have linked diminished lysosomal proteolysis in some lipid storage disorders to increased lysosomal pH (Bach et al., 1999; Holopainen et al., 2001). This, however, was not the case in NPC lysosomes, as their pH was very similar to that of control lysosomes (**Figure 4.4E**). To test the role of stored lipids in inhibiting cathepsin activity, we treated NPC cells with cyclodextrin, a compound that circumvents NPC1/NPC2 to clear lipid storage from NPC lysosomes (Liu et al., 2009; Rosenbaum et al., 2010). This treatment not only rescued cathepsin activity, but lead to a rebound above wild type levels, reflective of the mild overexpression of cathepsin B in these cells (**Figure 4.4F**). We conclude that lipid storage due to NPC1 deficiency impaired lysosomal cathepsin activity and therefore slowed the degradation of cargoes within autolysosomes.

Figure 4.4 Lipid storage inhibits lysosomal proteolysis. (A) Representative time lapse images of human dermal fibroblasts treated with Magic Red Cathepsin B substrate. **(B)** Fluorescence intensity, normalized to total lysosomal area, from one representative experiment. **(C)** Relative cathepsin B activity, as determined by the slope of the fluorescence intensity plots. *n* = 7-9 fields of cells per group, from three independent experiments. **(D)** Western blot for cathepsin B in human dermal fibroblast lysates, following 24 hr treatment with 300 μM cyclodextrin or vehicle. **(E)** Lysosomal pH, measured by ratiometric imaging following uptake of Oregon Green dextran. *n*=34-92 cells for points on standard curve, 181 cells for wt, 141 cells for NPC. **(F)** Relative cathepsin B activity measured following 24 hr treatment with 300 μM cyclodextrin or vehicle. *n* = 9 fields of cells per group, from three independent experiments. Error bars are SEM.

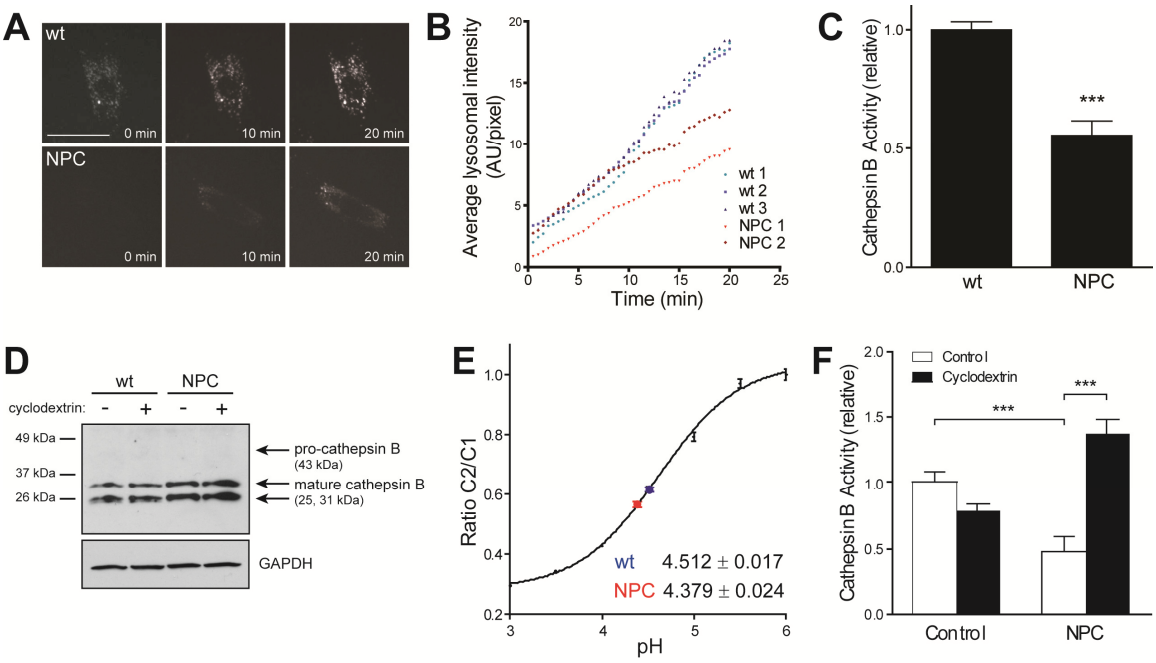

4.3.4 p62 accumulates in NPC neurons

To assess the function of the autophagic pathway in NPC mice, we stained brain tissue for p62/Sequestosome1, a multifunctional protein that seeds aggregates of ubiquitinated proteins and functions as an adapter for their recognition by the isolation membrane (Komatsu et al., 2007; Pankiv et al., 2007). As a substrate for the autophagic pathway, p62 levels tend to be inversely correlated with autophagic flux (Klionsky et al., 2007). p62 staining was found in small punctuate structures throughout multiple brain regions (**Figure 4.5A**). Strikingly, this staining pattern correlated tightly with the regions

in which neuron death and severe pathology have been documented in NPC disease: cerebellum, prefrontal cortex, deep layers of the remainder of the cortex, and multiple nuclei within the thalamus and brainstem (Suzuki et al., 1995; German et al., 2001; Walkley and Suzuki, 2004). p62 puncta were present in cells with nuclei positive for the neuronal marker NeuN in the cortex and calbindin-positive Purkinje cells in the cerebellum (**Figure 4.5B**). In contrast, p62 puncta were not identified in cells expressing the astrocyte marker GFAP or microglial marker Iba1 (Figure 5B). Within neurons, p62 puncta partially colocalized with ubiquitin, but not with LC3 or Lamp1 (**Figure 4.5C**). These data demonstrate that p62 did not accumulate within autophagosomes or lysosomes, but instead suggest its localization to cytoplasmic aggregates containing ubiquitinated proteins. These aggregates did not colocalize with typical aggresome markers such as proteasomal subunits or heat shock proteins, nor with signaling proteins that are known to interact with p62, including TRAF6, caspase-8, or ALFY (data not shown). While these p62 puncta may indicate impaired autophagic flux, we also considered that p62 accumulation could reflect increased synthesis, a phenomenon recently demonstrated in the setting of TLR signaling (Fujita et al., 2011). p62 mRNA levels were markedly increased in human NPC fibroblasts (**Figure 4.6A**), indicating that increased protein expression may have also contributed to the observed pathology. To determine the extent to which TLR signaling through TRIF contributed to this phenomenon, we treated wild type and *Trif*$^{-/-}$ MEFs with U18666A. While wild type cells showed a significant induction of p62 mRNA, *Trif* null cells exhibited a muted response (**Figure 4.6B**). These data indicate that TLR signaling contributes to both autophagy induction and p62 pathology in NPC disease.

Figure 4.5 p62 accumulates *in vivo*. (A) Immunofluorescent staining for p62 in *Npc1*$^{-/-}$ or wild type mouse brain. Scale bar, 2 mm. **(B)** Co-immunofluorescent staining for p62 (red) or markers (green) of neurons (NeuN, neuronal nuclei; or calbindin, Purkinje cells), astrocytes (GFAP), or microglia (Iba1). Scale bar, 50 um. **(C)** Confocal microscopy for colocalization of p62 (red) and autophagosomes (LC3), late endosomes and lysosomes (Lamp1), or ubiquitinated proteins (green). Scale bars, 10 μm.

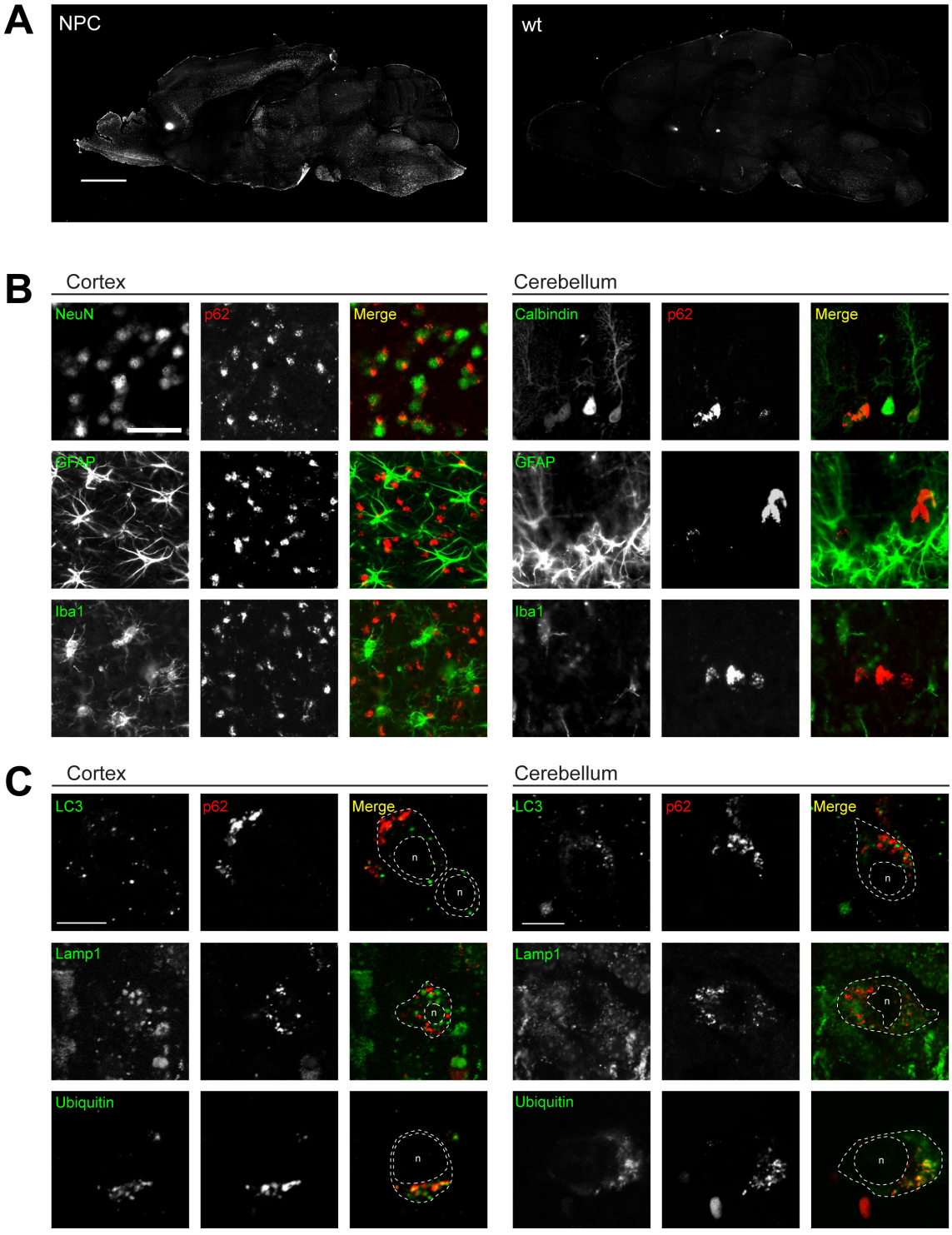

Figure 4.6 TLR signaling contributes to p62 overexpression. (A) p62 mRNA from human dermal fibroblasts was measured by quantitative real-time PCR. **(B)** Wild type and *Trif* null MEFs were treated with 1 µg/ml U18666A or vehicle (ethanol) for 24 hrs. p62 mRNA levels in lysates were measured by quantitative real-time PCR. ***p<0.001. Error bars are SEM.

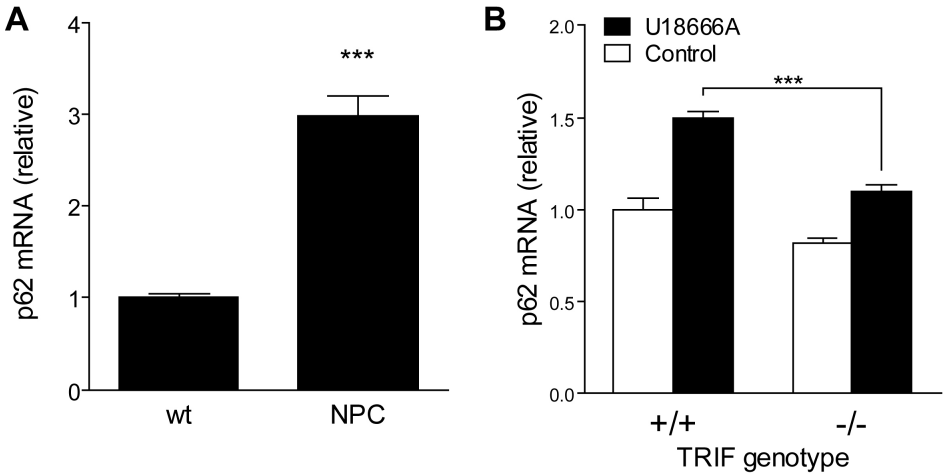

4.3.5 Autophagy inhibition reverses NPC phenotypes and enhances neuronal viability

The data presented here demonstrate that autophagy is a source of stored lipid in NPC disease, and that lipid storage impairs lysosome function by diminishing cathepsin activity. We therefore sought to determine whether autophagy inhibition would have beneficial effects on NPC phenotypes. Treatment of NPC fibroblasts with the autophagy inhibitor wortmannin for 72 hrs was sufficient to reduce filipin staining by more than 50%, while having no effect on control fibroblasts (**Figure 4.7A**). Similarly, wortmannin completely rescued the cathepsin activity defect in NPC patient fibroblasts while leaving cathepsin activity in control fibroblasts unchanged (**Figure 4.7B**). To test whether the rescue of lipid storage and lysosome function affected neuron survival, we treated primary cortical neurons with U18666A to establish an *in vitro* model of NPC-associated neurodegeneration. Autophagy inhibition by wortmannin significantly improved the

viability of these neurons (**Figure 4.7C**). These data demonstrate that inhibition of autophagy diminishes lipid storage, lysosome dysfunction and neuronal death in models of NPC disease.

Figure 4.7 Autophagy inhibition rescues NPC phenotypes. (A) Human dermal fibroblasts were treated with 250 nM wortmannin or vehicle (DMSO) for 72 hrs. Cholesterol storage was analyzed by filipin staining. *n*=6 fields of cells from two independent experiments. **(B)** Relative cathepsin B activity following 72 hr treatment with 250 nM wortmannin or DMSO. *n* = 9 fields of cells per group, from three independent experiments. **(C)** Primary cortical neuron cultures were treated with 2.5 µg/ml U18666A at 7 div to induce degeneration. Simultaneously, they were treated with 100 nM wortmannin or given no additional treatment. XTT assay for viability was performed at 10 div. **p*<0.05, ****p*<0.001. Error bars are SEM.

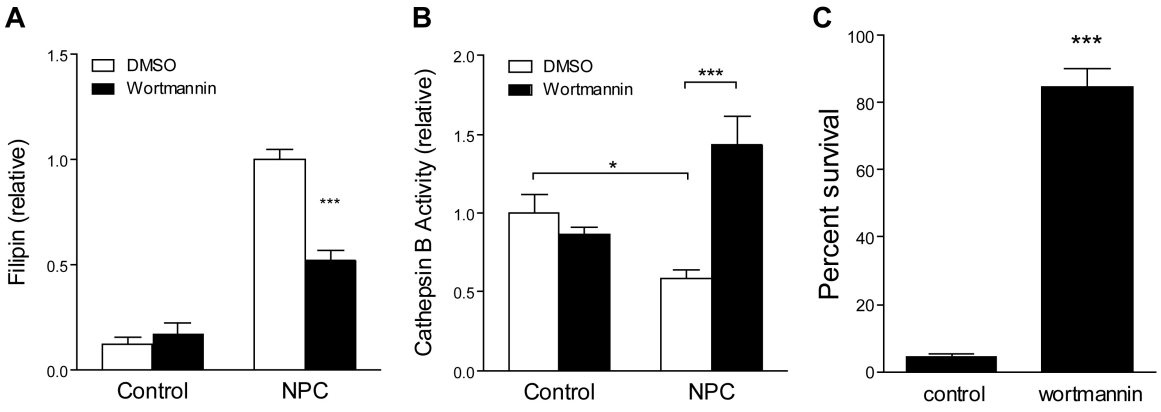

4.4 Discussion

The data presented here demonstrate that autophagy is activated by TLR signaling and increases both lipid storage and lysosome dysfunction in NPC disease. We propose a model (**Figure 4.8**) in which endolysosomal lipid storage contributes to the activation of TLR signaling to promote the induction of autophagy. We have shown that acute knock down of TLR3 and TLR4, or of their downstream adapter protein TRIF, largely reverses the induction of autophagy in NPC1-deficient cells. Our data and published findings suggest that TLR signaling is not a direct result of NPC1 deficiency, but instead lies downstream of lipid storage as cyclodextrin is sufficient to reverse autophagy induction

(Davidson et al., 2009). Endogenous glycosphingolipids, fatty acids, and oxidized sterols have been implicated in activating TLRs (Fischer et al., 2007; Miller et al., 2009; Chait and Kim, 2010) and accumulate in NPC lysosomes (Chen et al., 2005; Karten et al., 2009; Porter et al., 2010). In this location, they would have access to the ligand-binding domains of TLR3 and TLR4, or could act by altering the lipid composition of the lysosomal membrane.

Figure 4.8 Model for the role of autophagy in NPC disease. Lipid storage has two simultaneous effects on the autophagic pathway. First, it induces autophagy through a mechanism that involves TLR3 and TLR4 signaling through TRIF. Second, it inhibits lysosomal cathepsins, leading to impaired maturation of lysosomes. The results of these events are increased rate of autophagosome generation, but only mildly increased autophagic flux and an accumulation of autophagic intermediates. Further, autophagy delivers cholesterol to the lysosome, thus creating a positive feedback loop between lipid storage and autophagy induction that promotes disease pathogenesis.

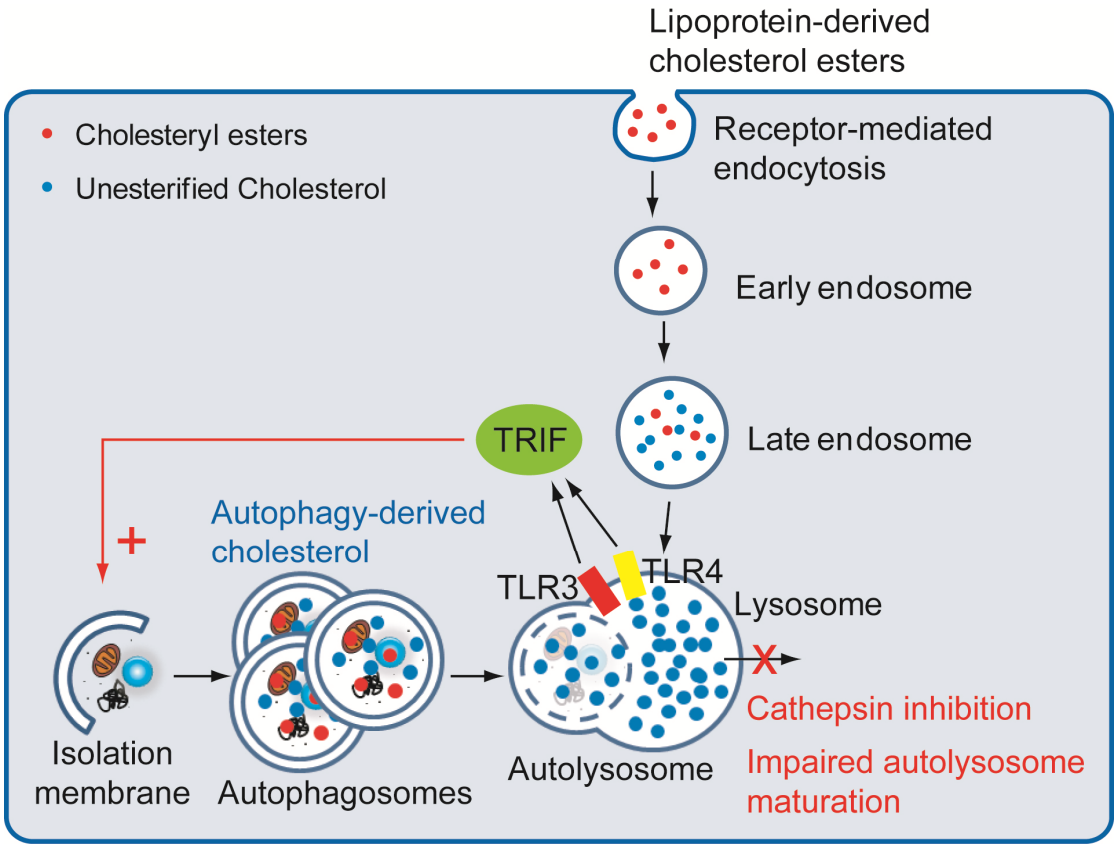

We show that increased autophagy promotes lipid storage and contributes to lysosome dysfunction. Critical to this finding was the measurement of cathepsin activity *in situ* rather than in cell lysates, where overexpressed cathepsins outside of the environment of the lipid-loaded lysosome exhibit elevated activity (Amritraj et al., 2009). Our data demonstrate that the inhibition of cathepsin activity in the NPC lysosome is due to the presence of cyclodextrin-sensitive lipid storage material rather than the result of alterations in cathepsin maturation or lysosomal pH, or due to a direct requirement for NPC1 itself. Interestingly, a recent study demonstrated that loading cells with glycosphingolipids, simply by adding a them to the culture media, leads to similar alterations of the autophagic pathway as those reported here: autophagy induction, decreased clearance of autophagosomes, and accumulation of autophagy intermediates (Tamboli et al., 2011). This raises the possibility that one or more glycosphingolipids, rather than cholesterol, may be responsible for alterations of the autophagic pathway in NPC disease. Therefore the primary storage lipid, cholesterol, and the pathogenic storage lipid in NPC disease may not be one and the same.

Classically, stored cholesterol in NPC lysosomes has been considered to be derived exclusively from the endocytic pathway via receptor-mediated endocytosis of LDL-cholesterol (Pentchev et al., 1985; Mukherjee and Maxfield, 2004). However, we demonstrate here that deletion of the critical autophagy gene *Atg5* or treatment with the autophagy inhibitor wortmannin reduces cholesterol storage in NPC cellular models by approximately 50%. In addition to the delivery of membrane-bound organelles, autophagy can mediate the delivery of cholesterol esters from lipid droplets (Singh et al., 2009), thus providing the lysosome with cholesterol and glycosphingolipids from several

sources. This pathway is likely particularly important in the brain, as LDL particles are excluded by the blood brain barrier and endogenous synthesis of cholesterol by neurons is thought to play an important role in cholesterol metabolism (Dietschy and Turley, 2001; Vance et al., 2005).

The identification of decreased proteolytic activity in the NPC lysosome raises the possibility that all pathways delivering protein cargoes to the diseased lysosome could be impaired, leading to a broader proteostasis defect. Compounding this problem is the overexpression of p62, which appears to sequester ubiquitinated proteins that may otherwise have undergone proteasomal degradation (Korolchuk et al., 2009). Alterations in the proteostasis network are a common feature of neurodegenerative diseases (Balch et al., 2008; Douglas and Dillin, 2010), and we expect that similar defects occur in the NPC brain. Parallels between the neuropathology of NPC and several age-dependent protein aggregation neurodegenerative disorders have been noted, and include the accumulation of hyperphosphorylated tau and α-synuclein (Auer et al., 1995; Spillantini et al., 1999; Bu et al., 2002; Saito et al., 2004), and in some cases beta amyloid (Saito et al., 2002). Further, it has been suggested that a prolonged half-life of autophagosomes may be detrimental through several mechanisms, including increased generation of beta amyloid aggregates (Yu et al., 2005) and production of reactive oxygen species (Kubota et al., 2010). We suggest that impaired protein quality control due to lysosome dysfunction leads to many of these changes in the NPC brain, and that proteostasis defects and the accumulation of autophagy intermediates contribute to the development of NPC neuropathology.

4.5 Materials and methods

4.5.1 Reagents

Hydroxy-β-propyl-cyclodextrin was from Cyclodextrin Technologies. Magic Red Cathepsin B substrate was from ImmunoChemistry Technologies. Oregon Green Dextran was from Invitrogen. All other chemicals were from Sigma. The mCherry-GFP-LC3 plasmid was a gift from Terje Johansen (University of Tromsø). ON-TARGET*plus* SMARTpool siRNA's for indicated genes and non-targeted control were from Dharmacon. Antibodies used were: LC3 (Novus NB600-1384), MyD88 (Stressgen CSA-510), TRIF (Cell Signaling 4596), GAPDH (Abcam ab8245), cathepsin B (Abcam ab33538), p62 (Novus H00008878-M01), NeuN (Millipore MAB-377), GFAP (Dako Z0334), Iba1 (Wako 019-19741), Lamp1 (Iowa Hybridoma Bank 1D4B), and ubiquitin (Dako Z0458).

4.5.2 Mice

npc1^{nih} mice were obtained from Jackson Laboratories (#003092) and backcrossed to C57BL6/J for more than 10 generations. Genotyping was performed as previously described (Elrick et al., 2010). *Npc1*$^{-/-}$ mice were generated as F1 hybrids between *Npc1*$^{+/-}$ mice on the C57BL6/J and Balb/cJ backgrounds, respectively. This method was found to restore Mendelian frequency of the *Npc1*$^{-/-}$ genotype, and therefore yielded experimental animals more efficiently than on either inbred background. *Trif*$^{-/-}$ mice (Yamamoto et al., 2003) were a gift of Nicholas Lukacs (University of Michigan). *Npc1/Trif* crosses were performed on the C57BL6/J background. All animal procedures

were approved by the University of Michigan Committee on the Use and Care of Animals.

4.5.3 Cell culture and transfection

Human dermal fibroblast lines GM08399 (healthy control) and GM03123 (NPC disease) were obtained from Coriell Cell Repositories, and were maintained in MEM (Gibco), supplemented with 15% FBS (Atlanta Biologicals), 10 µg/ml penicillin, 10 µg/ml streptomycin and 2 mM glutamine (Gibco). Atg5 MEF cell lines RCB2710 and RCB2711 were obtained from the RIKEN BRC Cell Bank, and where maintained in DMEM (Gibco) containing 10% FBS, 10 µg/ml penicillin, 10 µg/ml streptomycin and 2 mM glutamine. Plasmid or siRNA transfection was performed by electroporation using a Nucleofector II (Lonza) per manufacturer's instructions.

4.5.4 Western blotting

Cells were lysed in RIPA buffer (Thermo Scientific) including c*O*mplete protease inhibitor tablets (Roche) and Halt phosphatase inhibitor (Thermo Scientific). Samples were electrophoresed through a 4-20% gradient gel (Lonza) when blotting for LC3, or a 10% SDS-PAGE gel for all other genes. Samples were then transferred to nitrocellulose membranes (BioRad) using a semidry transfer apparatus. HRP-conjugated secondary antibodies were from BioRad. Blots were developed using ECL (Thermo Scientific) or TMA-6 (Lumigen) chemilluminescent reagents, following manufacturers' protocols. For quantification, blots were digitized using an Epson Perfection 2480 scanner and densitometry was performed using NIH ImageJ software.

4.5.5 Lipid analysis

Lipids were isolated from cultured human skin fibroblasts and analyzed by high performance thin layer chromatography (HPTLC) as previously described (Shu et al., 2002; Shu et al., 2005). Total phospholipid concentration was determined by lipid phosphate assay to ensure equal sample loading (Ames, 1966). Cholesterol was analyzed on HPTLC plates (EMD Chemicals) using a solvent system consisting of chloroform/glacial acetic acid (9:1). For analysis of glycosphingolipids, including glucosylceramide, lactosylceramide, globotriaosylceramide, and sphingomyelin, samples were first subjected to further purification by alkaline methanolysis and acid hydrolysis (Abe et al., 2000). For HPTLC analysis of glycosphingolipids, samples were first resolved in chloroform/methanol (98:2). The plate was then dried, and subjected to an additional resolution step in chloroforom/methanol/water/glacial acetic acid/concentrated ammonium hydroxide (64:31:3:2:0.5). HPTLC plates were developed by charring at 150°C following incubation with 8% $CuSO_4$ in methanol/water/H_3PO_4 (60:32:8). Lipid levels were quantified by densitometry using NIH ImageJ software, by extrapolation from a standard curve constructed from standards (cholesterol: Sigma, all others: Matreya) that were run on the same plate.

4.5.6 Filipin staining

Cells were grown on glass chamber slides (Lab-Tek) and stained with filipin as previously described (Pacheco et al., 2007). Images were captured on a Zeiss Axioplan 2 imaging system equipped with a Zeiss AxioCam HRc cameria, with a 10x Zeiss EC Plan-NEOFLUAR objective, NA of 0.3, using AxioVision 4.8 software. Quantitative analysis

of filipin images was performed using NIH ImageJ software, following the "LSO compartment ratio assay" method (Pipalia et al., 2006).

4.5.7 Histology

Mice were anesthetized with isofluorane and perfused transcardially with 0.9% normal saline followed by 4% paraformaldehyde. Brains were removed, bisected, and post-fixed in 4% paraformaldehyde overnight. Brain tissue was cryoprotected in 30% sucrose for 48 h at 4°C, then frozen in isopentane chilled by dry ice and embedded in OCT (Tissue-Tek). Free floating sections were prepared with a cryostat at 30 μm thickness. Sections were blocked 1 hr with 5% normal goat serum (Sigma) and 1% BSA (Roche) in PBS. They were then incubated overnight in primary antibody diluted in 1/4x blocking solution, washed three times with PBS, and then incubated for 1 hr with AlexaFluor secondary antibodies (Invitrogen). Sections were washed an additional three times in PBS, then transferred to water and mounted onto glass slide. Widefield fluorescent images were captured on a Zeiss Axioplan 2 imaging system, as described above. Confocal microscopy was performed using a Zeiss LSM 510-META Laser Scanning Confocal Microscopy system, with a 63x Zeiss C-Apochromat water immersion objective, NA of 1.2, using Zeiss LSM 510-META software**.**

4.5.8 Autophagosome fusion and degradation assays

Fibroblasts were transfected with mCherry-GFP-LC3 and plated to 6-well culture plates. Cultures were washed thoroughly with PBS the following day and then replated to glass coverslips. After 1-2 days in culture, cells were fixed in 3% paraformaldehyde for 30 min, washed three times in PBS, and then mounted onto glass slides. Cells were

imaged on a Zeiss LSM 510-META Laser Scanning Confocal Microscope, as described above. Images were analyzed using NIH ImageJ software. They were first background subtracted and then thresholded using a tophat transform. The JACoP plugin (Bolte and Cordelieres, 2006) was used to perform object-based colocalization to determine the percent of puncta that are red-only (representing autolysosomes) or green-only (indicative of noise). To correct for noise, data were reported as %red-only - %green-only. To measure autolysosome life-time, cells were instead replated to two-chamber coverglasses and imaging was performed on a Deltavision-RT Live Cell Imaging System equipped with a Photometrics CoolSNAP HQ camera. Images were acquired using a 60x Olympus PlanApo N oil immersion objective, NA of 1.42, at 20 sec intervals in z-stacks spaced at 0.75 μm. Images were deconvolved, and z-stacks were then projected into a 2-D image. SoftWoRx 3.5.1 software was used for image acquisition, deconvolution, and projection. Using NIH ImageJ software, image series were studied manually to identify events where yellow puncta became red, i.e. autophagosome-to-lysosome fusion events. From this point, frames were counted until the red punctum disappeared. This number was multiplied by 20 sec to yield autolysosome lifetime.

4.5.9 Cathepsin assay

Fibroblasts were plated to chambered coverglasses and imaged the following day on a Deltavision-RT Live Cell Imaging System as described above. At the start of imaging, Magic Red reagent was diluted 1:365 into PBS, and then this solution was added at a 1:10 dilution into the cell culture media. Images were acquired using a 20x Olympus UPlan objective, NA of 0.5, at 1 min intervals for a total of 20 min. Three fields of cells per group were imaged simultaneously. Image analysis was performed

using NIH ImageJ software. Images were thresholded to include only the lysosomal compartment, using the same numerical threshold for all images across a single experiment. The total fluorescence above threshold was normalized to the total area of the lysosomal compartment, measured as the area above threshold at t = 20 min. Normalized fluorescence intensities were plotted over time, and the slope of the line of best fit was determined by linear regression. To report relative cathepsin activity, the slope of each line was normalized within each experiment to the control group.

4.5.10 Lysosomal pH

Lysosomal pH was determined using ratiometric imaging of endocytosed Oregon Green Dextran (OGDx), which has a pH-independent excitation maximum at ~440 nm and a pH-dependent excitation maximum at 492 nm with a pK_a of 4.7. Cells growing on chambered coverglasses were pulsed overnight with 150 µg/mL OGDx in the culture medium, then chased for 4 hr with OGDx-free medium to ensure that all OGDx had arrived at its terminal location in the lysosome. Cells were then imaged on a Deltavision-RT Live Cell Imaging System as described above, with a 40x UApo/340 oil immersion objective, NA of 1.35, using two filter pairs. The first (C1) used excitation/emission wavelengths of 436/535 nm; C2 was 492/535 nm. Calibration buffers (130 mM KCl, 1 mM $MgCl_2$, 15 mM Hepes, 15 mM MES) were prepared at pH ranging from 3.0 to 6.0. On the day of use, the ionophores valinomycin and nigericin were added to the calibration buffers at 10 µM each. To construct a standard curve, wild-type fibroblasts were equilibrated for at least 5 minutes in each calibration buffer prior to imaging. Unknowns were then imaged in regular culture medium. All imaging was performed at 37°C under 5% CO_2. Image analysis was performed using NIH ImageJ software. Each

cell was analyzed independently. First, a binary image was generated by multiplying the two images (C1xC2) and adjusting the intensity threshold to include only the labeled lysosomes. This image was then used as a mask for analysis of the original images. The integrated density of each image was measured and the ratio of integrated densities, C2/C1 was recorded. Using GraphPad Prism statistical software, the standards were fit to a sigmoidal curve by the least squares method, and unknowns were interpolated from this curve.

4.5.11 Gene expression analysis

Total RNA was isolated from liver using TRIzol (Invitrogen) per the manufacturer's protocol. cDNA was synthesized using the High Capacity cDNA Archive Kit (Applied Biosystems). Quantitative real time PCR (RT-PCR) was performed on 5 ng cDNA per reaction, in duplicate. Primers and probes for human and mouse *SQSTM1*, and 18S rRNA were purchased from Applied Biosystems. Threshold cycle (Ct) values were determined on an ABI Prism 7900HT Sequence Detection System. Relative expression values were calculated by the standard curve method and normalized to 18S rRNA.

4.5.12 Primary cortical neuron culture and viability assay

C57BL6/J mice were obtained from Jackson Laboratories. Cortices from P0 mouse pups were dissected free of meninges, minced, and then dissociated and cultured as described previously (Jakawich et al., 2010). Neurons were plated in poly-D-lysine (Millipore) treated 96-well plates at a density of $6x10^4$ per well. Cytosine arabinoside (Sigma) was added to the culture media the following day at a final concentration of 5

μM to prevent glial growth. U18666A was added at 2.5 μg/ml at 7 div to induce lipid storage. Neuronal viability was determined by XTT assay (Cell Proliferation Kit II, Roche) following the manufacturer's instructions.

4.5.13 Statistics

Statistical significance was assessed by unpaired Student's *t* test (for comparison of two means) or ANOVA (for comparison of more than two means). The Newman-Keuls post hoc test was performed to carry out pairwise comparisons of group means if ANOVA rejected the null hypothesis. Statistics were performed using the software package Prism 4 (GraphPad Software). *P* values less than 0.05 were considered significant.

Chapter 5

Conclusion

In this dissertation, I have described multiple approaches toward understanding the underlying causes of neurodegeneration in Niemann-Pick type C disease. I have shown that the loss of cerebellar Purkinje cells is a cell autonomous process, and that this phenomenon contributes to motor dysfunction but not other disease phenotypes, including death. Further studies comparing gene expression between vulnerable and resistant populations of Purkinje cells lead to the identification of candidate genes responsible for promoting the death or survival of these neurons. I demonstrated that at least one of these genes, *Hsp27*, is strongly protective in an *in vitro* model of NPC neurodegeneration. Finally, I investigated the role of autophagy in NPC disease. These studies demonstrated that NPC lipid storage causes not only the induction of autophagy, but also decreased lysosomal proteolysis, leading to an impairment of autolysosome maturation. Further, I showed that the autophagic pathway is a major source of stored cholesterol in NPC disease and demonstrated that inhibition of autophagy reversed lysosomal proteolysis deficits and neurodegeneration. In the remainder of this chapter I

will discuss relevant questions that remain open and propose future directions for this work.

5.1 Cell Autonomous Neurodegeneration

In Chapter 2, I utilized a novel conditional knockout mouse model of NPC disease to determine the extent to which Purkinje cell degeneration is a cell autonomous process. Although a prior study suggested that Purkinje cell death was purely cell autonomous (Ko et al., 2005), several others argued for a role of glia in the disease process (German et al., 2002; Griffin et al., 2004; Chen et al., 2007; Phillips et al., 2008; Zhang et al., 2008). My data resolved this issue by demonstrating that deletion of *Npc1* only in Purkinje cells was sufficient to cause their degeneration at the same rate as in mice with global deletion of *Npc1*. Purkinje cell degeneration in NPC disease is therefore a cell autonomous process. Interestingly, these mice displayed moderate motor discoordination and tremors, but no other deficits, including the weight loss and premature death that are characteristic of NPC mice and human NPC patients. These major phenotypes must arise from other brain regions, or perhaps other tissues.

These results raise several new questions: What cell types are responsible for weight loss and death? Is neurodegeneration outside the cerebellum also cell autonomous? Does cell autonomous neurodegeneration reflect a developmental defect, or a continuous requirement for NPC1/NPC2 function? Many of these questions have already been answered through the work of Ting Yu, a fellow graduate student in the Lieberman laboratory. Crossing conditional *Npc1* mice with a line expressing Cre recombinase under the control of an astrocyte promoter lead to lipid accumulation in astrocytes, but did not cause astrocytosis, neurodegeneration, or any gross phenotype.

Conversely, expressing Cre under the *Synapsin 1* promoter, which drives gene expression in virtually all neurons of the brain except cerebellar Purkinje cells (Zhu et al., 2001), was sufficient to cause motor discoordination, weight loss, and death. Finally, the use of a tamoxifen-inducible Cre line demonstrated that global deletion of *Npc1* in adulthood recapitulates all features of NPC disease on a similar timescale to germline deletion (Yu and Lieberman, unpublished data). Collectively, these studies have provided an exceptionally complete picture of neurodegeneration in NPC disease as a post-developmental, cell-autonomous process, and this neurodegeneration underlies the major symptoms of the disease. Further, despite the severity of Purkinje cell loss, most symptoms of NPC arise from the degeneration of neurons outside the cerebellum.

5.2 Disease-modifying genes

The observation of strongly differential vulnerability between Purkinje cells of the anterior and posterior cerebellum in Chapter 2 lead me to wonder what were the factors underlying this phenomenon. In Chapter 3, I developed a method for querying data from the Allen Brain Atlas to identify genes that are differentially expressed between these two subpopulations. From this analysis, I formed a list of 16 high-priority candidate genes with expression patterns that correlate tightly with the pattern of Purkinje cell survival. These genes are primarily members of disparate biochemical pathways; however six of them are involved in some way in the regulation of apoptosis. This observation supported my hypothesis that selective vulnerability arises not from differences in lipid storage or other events proximal to NPC1/NPC2 function, but instead from the neurons' propensities to induce pro-survival or pro-death programs in response to cellular stress. Further supporting this view is the fact that the same pattern of Purkinje cell death is

present in a wide variety of diseases and injuries, many of which do not involve lipid metabolism or lysosome function (Sarna and Hawkes, 2003). Finally, I directly tested the role of my top candidate gene, *Hsp27*, in an *in vitro* model of NPC neurodegeneration and determined that it was strongly preventative of cell death.

This project leaves much future work. Ideally, all of the remaining 15 candidate genes should be tested for their ability to influence neurodegeneration in NPC disease. This may prove technically infeasible, as it is unknown whether candidate pro-death genes are even expressed in the primary cortical neurons used in my experiments. Therefore, attempting to knock down these genes could yield false negative results. Conversely, introducing a known pro-apoptotic gene would be expected to promote neuron death, independent of lipid storage. Perhaps a more feasible strategy would be to limit analyses to candidate neuroprotective genes. This strategy would simply require the introduction of each of the remaining five candidate protective genes into the *in vitro* model system followed by assays to measure a rescue of cell death, analogous to the experiments I performed with *Hsp27*. A further limitation of my approach is the use of U18666A as a model for NPC disease. Although this drug does phenocopy NPC-associated lipid storage, it also has known off-target effects on cholesterol synthesis, and could have other as yet unknown off-target effects that also contribute to cell death (Liscum and Faust, 1989; Cenedella, 2009). Unfortunately, significant efforts to develop an NPC1-dependent *in vitro* model of neurodegeneration from conditional *Npc1* knockout mice failed, as efficient deletion of *Npc1* in cultured neurons could not be achieved. Therefore, promising candidates should be tested further in *in vivo* models with mutations in one of the NPC genes.

Despite these technical challenges, this line of investigation has the potential to yield new and unexpected therapeutic targets. One interesting question will be whether the survival of Purkinje cells in lobule X is the result of a single gene, or of a network of genes acting in concert. The available data suggest that expression of *Hsp27* alone does not completely account for the resilience of these neurons. Protein kinase C delta (PKC^{δ}), another of my candidate genes, is co-expressed with *Hsp27* and is known to phosphorylate Hsp27 (Lee et al., 2005). Because phosphorylation of Hsp27 is required for its neuroprotective effects, expression of PKC^{δ} may have synergistic effects with Hsp27. Further, Hsp27 is not expressed in all parasagittal zones of lobule X, however the Purkinje cells in this lobule appear to be uniformly resistant to degeneration (Sarna et al., 2003). This observation suggests that non-Hsp27 dependent mechanisms of neuronal survival exist. In addition to the expression of pro-survival genes, the relative absence of pro-apoptotic genes may also play a role. To explain the phenomenon of selective vulnerability of Purkinje cells, I favor a model in which differential expression of several genes combines to set a threshold for the induction of apoptosis in response to cellular stress. This threshold must be very low in most Purkinje cells, but is notably quite high in the posterior cerebellar midline.

One final consideration in understanding the differential vulnerability of Purkinje cells is that although my analysis focused on gene expression, other factors could contribute as well. For example, Purkinje cells do not all have equal access to the cerebrospinal fluid (CSF), which is generated by the choroid plexus in close apposition to lobule X. Purkinje cells closest to the surface of the cerebellum or the fourth ventricle also have improved access to CSF. Several circumstances have been documented where

a toxic insult that arrives via CSF, or a protective factor derived from the CSF can influence patterned Purkinje cell loss (Sarna and Hawkes, 2003). These patterns typically differ from the anterior-to-posterior gradient seen in NPC disease, however a contributory effect of CSF access cannot be ruled out. Another, perhaps more relevant, consideration is that not all Purkinje cells make the same synaptic contacts. Most Purkinje cells synapse onto neurons of the deep cerebellar nuclei (DCN). However, Purkinje cells of the flocculonodular zone (lobule X and caudal lobule IX) bypass the DCN and synapse directly onto neurons of the vestibular nuclei in the brain stem (Voogd and Glickstein, 1998). It is possible that these neurons provide better trophic support for their presynaptic partners than do neurons of the DCN. If this were true, it would provide a mechanism for differential survival that is independent of gene transcription. Finally, post-transcriptional mechanisms of regulating survival could also be involved in differential vulnerability, including regulation of protein translation or post-translational modifications.

5.3 Autophagy

In Chapter 4, I presented multiple findings that advanced our understanding of the role of autophagy in NPC disease. First, I showed that Toll-like receptor (TLR) signaling contributes to autophagy induction in NPC disease. Then, I demonstrated that autophagy is a significant source of stored cholesterol, indicating that it plays a predominantly negative role in disease pathogenesis. The final major finding of this chapter was that lipid storage not only causes autophagy induction, but also impairs the clearance of autophagosomes by interfering with lysosomal proteolysis. From these data, I proposed the model of a positive feedback loop wherein lipid storage induces autophagy, which

further enhances lipid storage. I validated this model by utilizing pharmacologic inhibition of autophagy to break the positive feedback loop in *in vitro* models of NPC disease. This manipulation decreased lipid storage by ~50%, rescued lysosomal proteolysis, and restored neuronal viability.

Despite elucidating the contribution of TLR signaling to autophagy induction in NPC disease, our understanding of this phenomenon remains incomplete. Prior studies from our lab have indicated that autophagy induction in NPC is Beclin-1 dependent (Pacheco et al., 2007). Novel mechanisms of regulating autophagy through Beclin-1 continue to be reported, including several which were unknown during my investigation of autophagy in NPC disease. For example, it was recently reported that autophagy induction in a model of Parkinson disease arises from cdk5-dependent phosphorylation of endophilin B1, which recruits the Beclin-1 binding partner UVRAG to induce autophagy (Wong et al., 2011). A separate report indicated an integral role for the generation of reactive oxygen species (ROS) in autophagy induction (Scherz-Shouval et al., 2007). Increased cdk5 activity (Bu et al., 2002) and overproduction of ROS (Porter et al., 2010) have been demonstrated in NPC disease, and these mechanisms may therefore also contribute to autophagy induction. Finally, autophagy induction may be a physiologic response to cholesterol starvation, as it is capable of liberating cholesterol from lipid droplets by macrolipophagy (Cheng et al., 2006; Singh et al., 2009). In NPC disease, the sterol response element binding protein (SREBP) pathway is activated, reflective of decreased trafficking of cholesterol to the ER, where cholesterol sensing proteins reside (Pentchev et al., 1986; Liscum and Faust, 1987). If autophagy induction lies downstream

of SREBP or other potential cholesterol sensing pathways, it provides yet another potential mechanism for autophagy induction in NPC disease.

My study of the autophagic pathway in NPC revealed several features suggestive of a defect in proteostasis. Proteostasis, derived from the phrase "protein homeostasis," refers to the network of biological pathways involved in proper protein folding, constitutive protein turnover, and identification and degradation of irretrievably damaged proteins. Any chronic perturbation of a proteostatic pathway can perturb the whole network, leading eventually to disease. Failure of normal proteostasis is such a common feature in progressive neurological disorders that many have proposed that it is the underlying cause of many, if not all, neurodegenerative diseases (Balch et al., 2008; Douglas and Dillin, 2010). The data presented in Chapter 4 document several alterations of the proteostasis network in NPC disease. For example, I have identified protein aggregates in NPC mice that contain p62 and ubiquitin, a feature identified in practically all well-studied neurodegenerative diseases and thought to be intimately intertwined with pathogenesis (Zatloukal et al., 2002; Komatsu and Ichimura, 2010). Further, I demonstrated decreased lysosomal protease activity as an underlying cause of impaired autolysosome maturation. One would also expect other pathways involving the lysosome to be impaired in NPC disease, including chaperone-mediated autophagy, microautophagy, endocytosis, and phagocytosis. These observations explain how a disease of lipid trafficking could possibly result in cellular phenotypes and neurodegeneration similar to diseases of protein folding, such as Alzheimer, Parkinson, and the polyglutamine diseases. It is possible that these proteostasis defects are the

proximal cause of neurodegeneration in NPC disease. Future experiments will be required to directly test this idea.

5.4 Novel insights for therapeutic strategies

Presently, therapies for NPC disease beyond supportive care are very limited, and no drugs have gained FDA approval for treatment of NPC. The first drug to show any benefit in a clinical trial was miglustat, or *N*-butyldeoxynojirimycin, an inhibitor of glucosylceramide synthase, which catalyzes the first step in the synthesis of glycosphingolipids (Platt et al., 1994). Miglustat treatment was shown to reduce the accumulation of gangliosides in the brain of NPC mice and promote a modest increase in their survival (Zervas et al., 2001). In a small clinical trial, a subset of patients taking miglustat for 1-2 years experienced stabilization of their disease (Wraith et al., 2010). A second potential therapeutic is cyclodextrin. Cyclodextrins are cyclical oligosaccharides originally developed as carriers for hydrophobic drugs in aqueous environments (Uekama et al., 1998). Methyl-β-cyclodextrin and hydroxypropyl-β-cyclodextrin bind and carry cholesterol in a similar manner. They are thought to enter the endolysosomal pathway through bulk phase endocytosis and bypass the need for NPC1 and NPC2 by shuttling cholesterol between the internal and limiting membranes of the lysosome (Rosenbaum et al., 2010). Remarkably, a single injection of cyclodextrin at postnatal day seven extends the lifespan of NPC mice by ~30% (Liu et al., 2008; Liu et al., 2009). Later treatment, following the closure of the blood-brain barrier, was less effective, but also extended the lifespan of NPC mice (Davidson et al., 2009). Based on the strength of these data, a clinical trial of cyclodextrin for NPC disease will begin in the near future (www.nnpdf.org). However, even in the best case scenario, cyclodextrin in its current

form is not a cure, and significant concerns remain over its pharmacokinetics and potential toxicities (Ward et al., 2010). Additional therapeutic strategies will have to be pursued, perhaps in combination with miglustat and cyclodextrin.

Our investigations of *Npc1* conditional knockout mice have revealed several principles which should guide the approach to evaluating therapeutic strategies. Given the cell autonomous and post-developmental nature of neurodegeneration in NPC, only processes initiated within mature neurons should be considered viable therapeutic targets. Further, although Purkinje cell degeneration is a striking and easily measurable feature of NPC disease, it is not responsible for the most significant outcomes of the disease. Therefore, care should be taken to ensure that preclinical trials evaluate the effects of novel therapeutics throughout the brain and at the gross behavioral level.

In chapter 3, I demonstrated that *Hsp27* is a potential therapeutic target in NPC disease, apparently acting through an anti-apoptotic mechanism. Basal *Hsp27* expression is low in most neurons, but is inducible. Agents that promote the expression of *Hsp27* are likely to have value in protecting neurons from lipid storage-induced neurodegeneration, in a manner analogous to lobule X Purkinje cells or in *in vitro* experiments utilizing exogenous expression of *Hsp27*. Several pharmacologic agents are already available that induce *Hsp27* expression. Chief among these are Hsp90 inhibitors. As discussed in Chapter 3, 17-N-allylamino-17-demethoxygeldanamycin (17-AAG) is a drug of this class which has already been demonstrated to induce *Hsp27* expression in the CNS *in vivo* (Egorin et al., 2001; Waza et al., 2005) and is currently in clinical trials for several cancers (www.clinicaltrials.gov). Additionally, I showed that phosphorylation of Hsp27 is important for its neuroprotective abilities, and drugs which promote Hsp27

phosphorylation by activating upstream kinases such as curcumin (Ma et al., 2010) or 12-*O*-tetradecanoylphorbol-13-acetate (TPA) (Takai et al., 2007) may also prove beneficial. It is possible that the inhibition of apoptosis by other means may also have a role in therapy. For example, imatinib, an inhibitor of the c-Abl/p73 pro-apoptotic pathway shown to be activated in Purkinje cells in NPC disease, slowed neurologic disease progression and extended survival in NPC mice (Alvarez et al., 2008). Therefore, any direct inhibitor of apoptosis should be considered a potential NPC therapeutic.

The data presented in Chapter 4 suggest additional therapeutic strategies. I demonstrated that the autophagic pathway is the source of approximately half of the cholesterol stored in the lysosome in NPC disease. It therefore naturally followed that autophagy inhibition would have therapeutic benefit, via clearance of stored lipids. In fact, treatment of cultured neurons with wortmannin was protective against U18666A-induced cell death. Unfortunately, the currently available inhibitors of autophagy induction are non-specific inhibitors of phosphoinositol-3-kinases that are too toxic for *in vivo* use. To effectively target autophagy *in vivo*, novel specific inhibitors will need to be developed.

I also demonstrated several alterations of autophagy and lysosome function that are likely to play a major role in NPC pathogenesis. Lysosomal proteolysis in NPC cells is inefficient, leading to an impairment of autolysosome maturation and probably defects in other lysosomal pathways as well. An additional perturbation of the proteostasis network is caused by the overexpression of p62 and subsequent sequestration of ubiquitinated proteins. The combination of autophagy induction and impaired clearance of autolysosomes is expected to lead to an accumulation of autophagic intermediates. In

addition to reducing lipid storage, inhibition of autophagy by wortmannin treatment would be expected to relieve the accumulation of autophagic intermediates. Further, by reducing the levels of cholesterol in the lysosome, wortmannin improved lysosomal proteolysis. However, it is unclear how much these mechanisms contributed to the neuroprotective affects of wortmannin, and other methods for improving lysosome function should be directly tested.

There are at least two known mechanisms for improving lysosomal protease activity. One of these involves cystatin B, an endogenous inhibitor of multiple cathepsins that is expressed in the lysosome (Turk et al., 2008). Mice lacking cystatin B have increased lysosomal protease activity, and crossing these mice to a model of Alzheimer disease ameliorates the disease phenotype (Yang et al., 2011). Preliminary data from our lab has shown that cystatin B knockdown is sufficient to recue cathepsin B activity in NPC patient fibroblasts and reverses several biochemical markers of the disease phenotype, including elevated levels of Lamp1, LC3-II, and insoluble p62 (Magno, Elrick, and Lieberman, unpublished data). Future work will determine the extent to which increased cathepsin activity via cystatin B knockout is capable of rescuing NPC disease phenotypes in mice. An additional pathway for improving lysosome function is lysosomal biogenesis. The newly characterized transcription factor EB (TFEB) controls the expression of a network of lysosomal genes. Overexpression of TFEB promotes the synthesis of new lysosomes and the exocytosis of older ones (Sardiello et al., 2009). Such a manipulation would be expected to simultaneously expel lipid storage material from the cell and provide a pool of nascent lysosomes that are free of lipid accumulation and are likely to be functionally normal. Promoting such a rapid turnover of lysosomes

may be sufficient to restore normal proteostasis and resolve the accumulation of autophagic intermediates. Such a manipulation has been demonstrated already in culture models of several lysosomal diseases with benefits in the clearance of storage materials and autophagic substrates (Sardiello et al., 2009). Small molecules to manipulate cystatin B and TFEB are currently lacking, but may hold promise for the treatment of NPC and other lysosomal diseases.

5.5 Concluding remarks

Niemann-Pick type C disease is a devastating disorder of childhood, for which effective therapies are still lacking, resulting in continued patient morbidity and mortality, and significant emotional and financial cost for patients, families, and caregivers. The development of treatments for NPC disease will require an improved understanding of the biology underlying neurodegeneration. Through the work described in these pages, I have helped to define the cell types and developmental timing that are critical to disease pathogenesis. Further, I have identified several specific biochemical pathways that influence the survival of neurons in NPC disease, yielding targets for novel therapies. It is my hope that these advances will eventually bear fruit as part of an effective treatment regimen for NPC patients, and perhaps for those suffering from related neurodegenerative diseases as well.

References

Abe A, Arend LJ, Lee L, Lingwood C, Brady RO and Shayman JA. 2000. Glycosphingolipid depletion in fabry disease lymphoblasts with potent inhibitors of glucosylceramide synthase. *Kidney Int* 57(2): 446-454.

Alvarez AR, Klein A, Castro J, Cancino GI, Amigo J, Mosqueira M, Vargas LM, Yevenes LF, Bronfman FC and Zanlungo S. 2008. Imatinib therapy blocks cerebellar apoptosis and improves neurological symptoms in a mouse model of Niemann-Pick type C disease. *FASEB J* 22(10): 3617-3627.

Ames BN. 1966. Assay of inorganic phosphate, total phosphate, and phosphatases. *Methods Enzymol* 8: 115-118.

Amritraj A, Peake K, Kodam A, Salio C, Merighi A, Vance JE and Kar S. 2009. Increased activity and altered subcellular distribution of lysosomal enzymes determine neuronal vulnerability in Niemann-Pick type C1-deficient mice. *Am J Pathol* 175(6): 2540-2556.

Andersen BB, Gundersen HJ and Pakkenberg B. 2003. Aging of the human cerebellum: a stereological study. *J Comp Neurol* 466(3): 356-365.

Anderson L, Rossi D, Linehan J, Brandner S and Weissmann C. 2004. Transgene-driven expression of the Doppel protein in Purkinje cells causes Purkinje cell degeneration and motor impairment. *Proc Natl Acad Sci U S A* 101(10): 3644-3649.

Armstrong CL, Duffin CA, McFarland R and Vogel MW. 2010. Mechanisms of Compartmental Purkinje Cell Death and Survival in the Lurcher Mutant Mouse. *Cerebellum*.

Arrigo AP. 2007. The cellular "networking" of mammalian Hsp27 and its functions in the control of protein folding, redox state and apoptosis. *Adv Exp Med Biol* 594: 14-26.

Auer IA, Schmidt ML, Lee VM, Curry B, Suzuki K, Shin RW, Pentchev PG, Carstea ED and Trojanowski JQ. 1995. Paired helical filament tau (PHFtau) in Niemann-Pick type C disease is similar to PHFtau in Alzheimer's disease. *Acta Neuropathol (Berl)* 90(6): 547-551.

Bach G, Chen CS and Pagano RE. 1999. Elevated lysosomal pH in Mucolipidosis type IV cells. *Clin Chim Acta* 280(1-2): 173-179.

Balch WE, Morimoto RI, Dillin A and Kelly JW. 2008. Adapting proteostasis for disease intervention. *Science* 319(5865): 916-919.

Banerjee R, Beal MF and Thomas B. 2010. Autophagy in neurodegenerative disorders: pathogenic roles and therapeutic implications. *Trends Neurosci* 33(12): 541-549.

Barres BA. 2008. The mystery and magic of glia: a perspective on their roles in health and disease. *Neuron* 60(3): 430-440.

Barski JJ, Dethleffsen K and Meyer M. 2000. Cre recombinase expression in cerebellar Purkinje cells. *Genesis* 28(3-4): 93-98.

Biran V, Heine VM, Verney C, Sheldon RA, Spadafora R, Vexler ZS, Rowitch DH and Ferriero DM. 2011. Cerebellar abnormalities following hypoxia alone compared to hypoxic-ischemic forebrain injury in the developing rat brain. *Neurobiol Dis* 41(1): 138-146.

Boillee S, Yamanaka K, Lobsiger CS, Copeland NG, Jenkins NA, Kassiotis G, Kollias G and Cleveland DW. 2006. Onset and progression in inherited ALS determined by motor neurons and microglia. *Science* 312(5778): 1389-1392.

Bolte S and Cordelieres FP. 2006. A guided tour into subcellular colocalization analysis in light microscopy. *J Microsc* 224(Pt 3): 213-232.

Bruey JM, Ducasse C, Bonniaud P, Ravagnan L, Susin SA, Diaz-Latoud C, Gurbuxani S, Arrigo AP, Kroemer G, Solary E and Garrido C. 2000. Hsp27 negatively regulates cell death by interacting with cytochrome c. *Nat Cell Biol* 2(9): 645-652.

Bu B, Li J, Davies P and Vincent I. 2002. Deregulation of cdk5, hyperphosphorylation, and cytoskeletal pathology in the Niemann-Pick type C murine model. *J Neurosci* 22(15): 6515-6525.

Carbon S, Ireland A, Mungall CJ, Shu S, Marshall B and Lewis S. 2009. AmiGO: online access to ontology and annotation data. *Bioinformatics* 25(2): 288-289.

Carstea ED, Morris JA, Coleman KG, Loftus SK, Zhang D, Cummings C, Gu J, Rosenfeld MA, Pavan WJ, Krizman DB, Nagle J, Polymeropoulos MH, Sturley SL, Ioannou YA, Higgins ME, Comly M, Cooney A, Brown A, Kaneski CR, Blanchette-Mackie EJ, Dwyer NK, Neufeld EB, Chang TY, Liscum L, Tagle DA and et al. 1997. Niemann-Pick C1 disease gene: homology to mediators of cholesterol homeostasis. *Science* 277(5323): 228-231.

Cenedella RJ. 2009. Cholesterol synthesis inhibitor U18666A and the role of sterol metabolism and trafficking in numerous pathophysiological processes. *Lipids* 44(6): 477-487.

Chait A and Kim F. 2010. Saturated fatty acids and inflammation: who pays the toll? *Arterioscler Thromb Vasc Biol* 30(4): 692-693.

Charette SJ and Landry J. 2000. The interaction of HSP27 with Daxx identifies a potential regulatory role of HSP27 in Fas-induced apoptosis. *Ann N Y Acad Sci* 926: 126-131.

Chen FW, Gordon RE and Ioannou YA. 2005. NPC1 late endosomes contain elevated levels of non-esterified ('free') fatty acids and an abnormally glycosylated form of the NPC2 protein. *Biochem J* 390(Pt 2): 549-561.

Chen G, Li HM, Chen YR, Gu XS and Duan S. 2007. Decreased estradiol release from astrocytes contributes to the neurodegeneration in a mouse model of Niemann-Pick disease type C. *Glia* 55(15): 1509-1518.

Cheng J, Ohsaki Y, Tauchi-Sato K, Fujita A and Fujimoto T. 2006. Cholesterol depletion induces autophagy. *Biochem Biophys Res Commun* 351(1): 246-252.

Cheung NS, Koh CH, Bay BH, Qi RZ, Choy MS, Li QT, Wong KP and Whiteman M. 2004. Chronic exposure to U18666A induces apoptosis in cultured murine cortical neurons. *Biochem Biophys Res Commun* 315(2): 408-417.

Choudhury A, Dominguez M, Puri V, Sharma DK, Narita K, Wheatley CL, Marks DL and Pagano RE. 2002. Rab proteins mediate Golgi transport of caveola-

internalized glycosphingolipids and correct lipid trafficking in Niemann-Pick C cells. *J Clin Invest* 109(12): 1541-1550.

Ciesielski KT, Yanofsky R, Ludwig RN, Hill DE, Hart BL, Astur RS and Snyder T. 1994. Hypoplasia of the cerebellar vermis and cognitive deficits in survivors of childhood leukemia. *Arch Neurol* 51(10): 985-993.

Clark HB, Burright EN, Yunis WS, Larson S, Wilcox C, Hartman B, Matilla A, Zoghbi HY and Orr HT. 1997. Purkinje cell expression of a mutant allele of SCA1 in transgenic mice leads to disparate effects on motor behaviors, followed by a progressive cerebellar dysfunction and histological alterations. *J Neurosci* 17(19): 7385-7395.

Clarke G, Collins RA, Leavitt BR, Andrews DF, Hayden MR, Lumsden CJ and McInnes RR. 2000. A one-hit model of cell death in inherited neuronal degenerations. *Nature* 406(6792): 195-199.

Crooks R, Mitchell T and Thom M. 2000. Patterns of cerebellar atrophy in patients with chronic epilepsy: a quantitative neuropathological study. *Epilepsy Res* 41(1): 63-73.

Cruz JC, Sugii S, Yu C and Chang TY. 2000. Role of Niemann-Pick type C1 protein in intracellular trafficking of low density lipoprotein-derived cholesterol. *J Biol Chem* 275(6): 4013-4021.

Custer SK, Garden GA, Gill N, Rueb U, Libby RT, Schultz C, Guyenet SJ, Deller T, Westrum LE, Sopher BL and La Spada AR. 2006. Bergmann glia expression of polyglutamine-expanded ataxin-7 produces neurodegeneration by impairing glutamate transport. *Nat Neurosci* 9(10): 1302-1311.

Davidson CD, Ali NF, Micsenyi MC, Stephney G, Renault S, Dobrenis K, Ory DS, Vanier MT and Walkley SU. 2009. Chronic cyclodextrin treatment of murine Niemann-Pick C disease ameliorates neuronal cholesterol and glycosphingolipid storage and disease progression. *PLoS One* 4(9): e6951.

Dietschy JM and Turley SD. 2001. Cholesterol metabolism in the brain. *Curr Opin Lipidol* 12(2): 105-112.

Dietschy JM, Turley SD and Spady DK. 1993. Role of liver in the maintenance of cholesterol and low density lipoprotein homeostasis in different animal species, including humans. *J Lipid Res* 34(10): 1637-1659.

Double KL, Reyes S, Werry EL and Halliday GM. 2010. Selective cell death in neurodegeneration: why are some neurons spared in vulnerable regions? *Prog Neurobiol* 92(3): 316-329.

Douglas PM and Dillin A. 2010. Protein homeostasis and aging in neurodegeneration. *J Cell Biol* 190(5): 719-729.

Du X, Kumar J, Ferguson C, Schulz TA, Ong YS, Hong W, Prinz WA, Parton RG, Brown AJ and Yang H. 2011. A role for oxysterol-binding protein-related protein 5 in endosomal cholesterol trafficking. *J Cell Biol* 192(1): 121-135.

Duchala CS, Shick HE, Garcia J, Deweese DM, Sun X, Stewart VJ and Macklin WB. 2004. The toppler mouse: a novel mutant exhibiting loss of Purkinje cells. *J Comp Neurol* 476(2): 113-129.

Egorin MJ, Zuhowski EG, Rosen DM, Sentz DL, Covey JM and Eiseman JL. 2001. Plasma pharmacokinetics and tissue distribution of 17-(allylamino)-17-

demethoxygeldanamycin (NSC 330507) in CD2F1 mice1. *Cancer Chemother Pharmacol* 47(4): 291-302.
Ehrnsperger M, Gaestel M and Buchner J. 2000. Analysis of chaperone properties of small Hsp's. *Methods Mol Biol* 99: 421-429.
Elleder M, Jirasek A, Smid F, Ledvinova J and Besley GT. 1985. Niemann-Pick disease type C. Study on the nature of the cerebral storage process. *Acta Neuropathol (Berl)* 66(4): 325-336.
Elrick MJ, Pacheco CD, Yu T, Dadgar N, Shakkottai VG, Ware C, Paulson HL and Lieberman AP. 2010. Conditional Niemann-Pick C mice demonstrate cell autonomous Purkinje cell neurodegeneration. *Hum Mol Genet* 19(5): 837-847.
Evgrafov OV, Mersiyanova I, Irobi J, Van Den Bosch L, Dierick I, Leung CL, Schagina O, Verpoorten N, Van Impe K, Fedotov V, Dadali E, Auer-Grumbach M, Windpassinger C, Wagner K, Mitrovic Z, Hilton-Jones D, Talbot K, Martin JJ, Vasserman N, Tverskaya S, Polyakov A, Liem RK, Gettemans J, Robberecht W, De Jonghe P and Timmerman V. 2004. Mutant small heat-shock protein 27 causes axonal Charcot-Marie-Tooth disease and distal hereditary motor neuropathy. *Nat Genet* 36(6): 602-606.
Fink JK, Filling-Katz MR, Sokol J, Cogan DG, Pikus A, Sonies B, Soong B, Pentchev PG, Comly ME, Brady RO and et al. 1989. Clinical spectrum of Niemann-Pick disease type C. *Neurology* 39(8): 1040-1049.
Fischer H, Ellstrom P, Ekstrom K, Gustafsson L, Gustafsson M and Svanborg C. 2007. Ceramide as a TLR4 agonist; a putative signalling intermediate between sphingolipid receptors for microbial ligands and TLR4. *Cell Microbiol* 9(5): 1239-1251.
Fujita K, Maeda D, Xiao Q and Srinivasula SM. 2011. Nrf2-mediated induction of p62 controls Toll-like receptor-4-driven aggresome-like induced structure formation and autophagic degradation. *Proc Natl Acad Sci U S A* 108(4): 1427-1432.
Fukuda T, Ewan L, Bauer M, Mattaliano RJ, Zaal K, Ralston E, Plotz PH and Raben N. 2006. Dysfunction of endocytic and autophagic pathways in a lysosomal storage disease. *Ann Neurol* 59(4): 700-708.
Gallala HD, Breiden B and Sandhoff K. 2011. Regulation of the NPC2 protein-mediated cholesterol trafficking by membrane lipids. *J Neurochem* 116(5): 702-707.
Ganley IG and Pfeffer SR. 2006. Cholesterol accumulation sequesters Rab9 and disrupts late endosome function in NPC1-deficient cells. *J Biol Chem* 281(26): 17890-17899.
Gelsthorpe ME, Baumann N, Millard E, Gale SE, Langmade SJ, Schaffer JE and Ory DS. 2008. Niemann-Pick type C1 I1061T mutant encodes a functional protein that is selected for endoplasmic reticulum-associated degradation due to protein misfolding. *J Biol Chem* 283(13): 8229-8236.
Genet S and Kado RT. 1997. Hyperpolarizing current of the Na/K ATPase contributes to the membrane polarization of the Purkinje cell in rat cerebellum. *Pflugers Arch* 434(5): 559-567.
German DC, Liang CL, Song T, Yazdani U, Xie C and Dietschy JM. 2002. Neurodegeneration in the Niemann-Pick C mouse: glial involvement. *Neuroscience* 109(3): 437-450.

German DC, Quintero EM, Liang C, Xie C and Dietschy JM. 2001. Degeneration of neurons and glia in the Niemann-Pick C mouse is unrelated to the low-density lipoprotein receptor. *Neuroscience* 105(4): 999-1005.
German DC, Quintero EM, Liang CL, Ng B, Punia S, Xie C and Dietschy JM. 2001. Selective neurodegeneration, without neurofibrillary tangles, in a mouse model of Niemann-Pick C disease. *J Comp Neurol* 433(3): 415-425.
Goldstein JL and Brown MS. 2009. The LDL receptor. *Arterioscler Thromb Vasc Biol* 29(4): 431-438.
Gong YH, Parsadanian AS, Andreeva A, Snider WD and Elliott JL. 2000. Restricted expression of G86R Cu/Zn superoxide dismutase in astrocytes results in astrocytosis but does not cause motoneuron degeneration. *J Neurosci* 20(2): 660-665.
Goodman JM. 2008. The gregarious lipid droplet. *J Biol Chem* 283(42): 28005-28009.
Griffin LD, Gong W, Verot L and Mellon SH. 2004. Niemann-Pick type C disease involves disrupted neurosteroidogenesis and responds to allopregnanolone. *Nat Med* 10(7): 704-711.
Gu X, Li C, Wei W, Lo V, Gong S, Li SH, Iwasato T, Itohara S, Li XJ, Mody I, Heintz N and Yang XW. 2005. Pathological cell-cell interactions elicited by a neuropathogenic form of mutant Huntingtin contribute to cortical pathogenesis in HD mice. *Neuron* 46(3): 433-444.
Hara T, Nakamura K, Matsui M, Yamamoto A, Nakahara Y, Suzuki-Migishima R, Yokoyama M, Mishima K, Saito I, Okano H and Mizushima N. 2006. Suppression of basal autophagy in neural cells causes neurodegenerative disease in mice. *Nature* 441(7095): 885-889.
Havasi A, Li Z, Wang Z, Martin JL, Botla V, Ruchalski K, Schwartz JH and Borkan SC. 2008. Hsp27 inhibits Bax activation and apoptosis via a phosphatidylinositol 3-kinase-dependent mechanism. *J Biol Chem* 283(18): 12305-12313.
He C and Levine B. The Beclin 1 interactome. *Curr Opin Cell Biol* 22(2): 140-149.
He C and Levine B. 2010. The Beclin 1 interactome. *Curr Opin Cell Biol* 22(2): 140-149.
Heckroth JA and Abbott LC. 1994. Purkinje cell loss from alternating sagittal zones in the cerebellum of leaner mutant mice. *Brain Res* 658(1-2): 93-104.
Heng MY, Tallaksen-Greene SJ, Detloff PJ and Albin RL. 2007. Longitudinal evaluation of the Hdh(CAG)150 knock-in murine model of Huntington's disease. *J Neurosci* 27(34): 8989-8998.
Higashi Y, Murayama S, Pentchev PG and Suzuki K. 1993. Cerebellar degeneration in the Niemann-Pick type C mouse. *Acta Neuropathol (Berl)* 85(2): 175-184.
Higgins JJ, Patterson MC, Dambrosia JM, Pikus AT, Pentchev PG, Sato S, Brady RO and Barton NW. 1992. A clinical staging classification for type C Niemann-Pick disease. *Neurology* 42(12): 2286-2290.
Holopainen JM, Saarikoski J, Kinnunen PK and Jarvela I. 2001. Elevated lysosomal pH in neuronal ceroid lipofuscinoses (NCLs). *Eur J Biochem* 268(22): 5851-5856.
Hughes ED, Qu YY, Genik SJ, Lyons RH, Pacheco CD, Lieberman AP, Samuelson LC, Nasonkin IO, Camper SA, Van Keuren ML and Saunders TL. 2007. Genetic variation in C57BL/6 ES cell lines and genetic instability in the Bruce4 C57BL/6 ES cell line. *Mamm Genome* 18(8): 549-558.

Huot J, Houle F, Spitz DR and Landry J. 1996. HSP27 phosphorylation-mediated resistance against actin fragmentation and cell death induced by oxidative stress. *Cancer Res* 56(2): 273-279.

Infante RE, Radhakrishnan A, Abi-Mosleh L, Kinch LN, Wang ML, Grishin NV, Goldstein JL and Brown MS. 2008. Purified NPC1 protein: II. Localization of sterol binding to a 240-amino acid soluble luminal loop. *J Biol Chem* 283(2): 1064-1075.

Infante RE, Wang ML, Radhakrishnan A, Kwon HJ, Brown MS and Goldstein JL. 2008. NPC2 facilitates bidirectional transfer of cholesterol between NPC1 and lipid bilayers, a step in cholesterol egress from lysosomes. *Proc Natl Acad Sci U S A* 105(40): 15287-15292.

Ioannou YA. 2001. Multidrug permeases and subcellular cholesterol transport. *Nat Rev Mol Cell Biol* 2(9): 657-668.

Isaacs AM, Oliver PL, Jones EL, Jeans A, Potter A, Hovik BH, Nolan PM, Vizor L, Glenister P, Simon AK, Gray IC, Spurr NK, Brown SD, Hunter AJ and Davies KE. 2003. A mutation in Af4 is predicted to cause cerebellar ataxia and cataracts in the robotic mouse. *J Neurosci* 23(5): 1631-1637.

Jakawich SK, Neely RM, Djakovic SN, Patrick GN and Sutton MA. 2010. An essential postsynaptic role for the ubiquitin proteasome system in slow homeostatic synaptic plasticity in cultured hippocampal neurons. *Neuroscience* 171(4): 1016-1031.

Jakob U, Gaestel M, Engel K and Buchner J. 1993. Small heat shock proteins are molecular chaperones. *J Biol Chem* 268(3): 1517-1520.

Jennings JJ, Jr., Zhu JH, Rbaibi Y, Luo X, Chu CT and Kiselyov K. 2006. Mitochondrial aberrations in mucolipidosis Type IV. *J Biol Chem* 281(51): 39041-39050.

Josephs KA, Van Gerpen MW and Van Gerpen JA. 2003. Adult onset Niemann-Pick disease type C presenting with psychosis. *J Neurol Neurosurg Psychiatry* 74(4): 528-529.

Karten B, Peake KB and Vance JE. 2009. Mechanisms and consequences of impaired lipid trafficking in Niemann-Pick type C1-deficient mammalian cells. *Biochim Biophys Acta* 1791(7): 659-670.

Kihara A, Kabeya Y, Ohsumi Y and Yoshimori T. 2001. Beclin-phosphatidylinositol 3-kinase complex functions at the trans-Golgi network. *EMBO Rep* 2(4): 330-335.

Klionsky DJ. 2005. The molecular machinery of autophagy: unanswered questions. *J Cell Sci* 118(Pt 1): 7-18.

Klionsky DJ, Abeliovich H, Agostinis P, Agrawal DK, Aliev G, et al. 2007. Guidelines for the use and interpretation of assays for monitoring autophagy in higher eukaryotes. *Autophagy* 4(2).

Ko DC, Milenkovic L, Beier SM, Manuel H, Buchanan J and Scott MP. 2005. Cell-autonomous death of cerebellar purkinje neurons with autophagy in Niemann-Pick type C disease. *PLoS Genet* 1(1): 81-95.

Koike M, Shibata M, Waguri S, Yoshimura K, Tanida I, Kominami E, Gotow T, Peters C, von Figura K, Mizushima N, Saftig P and Uchiyama Y. 2005. Participation of autophagy in storage of lysosomes in neurons from mouse models of neuronal ceroid-lipofuscinoses (Batten disease). *Am J Pathol* 167(6): 1713-1728.

Komatsu M and Ichimura Y. 2010. Physiological significance of selective degradation of p62 by autophagy. *FEBS Lett* 584(7): 1374-1378.
Komatsu M and Ichimura Y. 2010. Selective autophagy regulates various cellular functions. *Genes Cells* 15(9): 923-933.
Komatsu M, Waguri S, Chiba T, Murata S, Iwata J, Tanida I, Ueno T, Koike M, Uchiyama Y, Kominami E and Tanaka K. 2006. Loss of autophagy in the central nervous system causes neurodegeneration in mice. *Nature* 441(7095): 880-884.
Komatsu M, Waguri S, Koike M, Sou YS, Ueno T, Hara T, Mizushima N, Iwata JI, Ezaki J, Murata S, Hamazaki J, Nishito Y, Iemura SI, Natsume T, Yanagawa T, Uwayama J, Warabi E, Yoshida H, Ishii T, Kobayashi A, Yamamoto M, Yue Z, Uchiyama Y, Kominami E and Tanaka K. 2007. Homeostatic Levels of p62 Control Cytoplasmic Inclusion Body Formation in Autophagy-Deficient Mice. *Cell* 131(6): 1149-1163.
Korolchuk VI, Mansilla A, Menzies FM and Rubinsztein DC. 2009. Autophagy inhibition compromises degradation of ubiquitin-proteasome pathway substrates. *Mol Cell* 33(4): 517-527.
Kubota C, Torii S, Hou N, Saito N, Yoshimoto Y, Imai H and Takeuchi T. 2010. Constitutive reactive oxygen species generation from autophagosome/lysosome in neuronal oxidative toxicity. *J Biol Chem* 285(1): 667-674.
Kuma A, Hatano M, Matsui M, Yamamoto A, Nakaya H, Yoshimori T, Ohsumi Y, Tokuhisa T and Mizushima N. 2004. The role of autophagy during the early neonatal starvation period. *Nature* 432(7020): 1032-1036.
Kume A, Takahashi A, Hashizume Y and Asai J. 1991. A histometrical and comparative study on Purkinje cell loss and olivary nucleus cell loss in multiple system atrophy. *J Neurol Sci* 101(2): 178-186.
Kwon HJ, Abi-Mosleh L, Wang ML, Deisenhofer J, Goldstein JL, Brown MS and Infante RE. 2009. Structure of N-terminal domain of NPC1 reveals distinct subdomains for binding and transfer of cholesterol. *Cell* 137(7): 1213-1224.
Lakso M, Pichel JG, Gorman JR, Sauer B, Okamoto Y, Lee E, Alt FW and Westphal H. 1996. Efficient in vivo manipulation of mouse genomic sequences at the zygote stage. *Proc Natl Acad Sci U S A* 93(12): 5860-5865.
Lavoie JN, Lambert H, Hickey E, Weber LA and Landry J. 1995. Modulation of cellular thermoresistance and actin filament stability accompanies phosphorylation-induced changes in the oligomeric structure of heat shock protein 27. *Mol Cell Biol* 15(1): 505-516.
Lee YJ, Lee DH, Cho CK, Bae S, Jhon GJ, Lee SJ, Soh JW and Lee YS. 2005. HSP25 inhibits protein kinase C delta-mediated cell death through direct interaction. *J Biol Chem* 280(18): 18108-18119.
Lein ES, Hawrylycz MJ, Ao N, Ayres M, Bensinger A, et al. 2007. Genome-wide atlas of gene expression in the adult mouse brain. *Nature* 445(7124): 168-176.
Levine B and Kroemer G. 2008. Autophagy in the pathogenesis of disease. *Cell* 132(1): 27-42.
Levine B and Yuan J. 2005. Autophagy in cell death: an innocent convict? *J Clin Invest* 115(10): 2679-2688.

Lino MM, Schneider C and Caroni P. 2002. Accumulation of SOD1 mutants in postnatal motoneurons does not cause motoneuron pathology or motoneuron disease. *J Neurosci* 22(12): 4825-4832.

Liscum L and Faust JR. 1987. Low density lipoprotein (LDL)-mediated suppression of cholesterol synthesis and LDL uptake is defective in Niemann-Pick type C fibroblasts. *J Biol Chem* 262(35): 17002-17008.

Liscum L and Faust JR. 1989. The intracellular transport of low density lipoprotein-derived cholesterol is inhibited in Chinese hamster ovary cells cultured with 3-beta-[2-(diethylamino)ethoxy]androst-5-en-17-one. *J Biol Chem* 264(20): 11796-11806.

Liscum L, Ruggiero RM and Faust JR. 1989. The intracellular transport of low density lipoprotein-derived cholesterol is defective in Niemann-Pick type C fibroblasts. *J Cell Biol* 108(5): 1625-1636.

Liu B, Li H, Repa JJ, Turley SD and Dietschy JM. 2008. Genetic variations and treatments that affect the lifespan of the NPC1 mouse. *J Lipid Res* 49(3): 663-669.

Liu B, Turley SD, Burns DK, Miller AM, Repa JJ and Dietschy JM. 2009. Reversal of defective lysosomal transport in NPC disease ameliorates liver dysfunction and neurodegeneration in the npc1-/- mouse. *Proc Natl Acad Sci U S A* 106(7): 2377-2382.

Lloyd-Evans E, Morgan AJ, He X, Smith DA, Elliot-Smith E, Sillence DJ, Churchill GC, Schuchman EH, Galione A and Platt FM. 2008. Niemann-Pick disease type C1 is a sphingosine storage disease that causes deregulation of lysosomal calcium. *Nat Med* 14(11): 1247-1255.

Lobsiger CS and Cleveland DW. 2007. Glial cells as intrinsic components of non-cell-autonomous neurodegenerative disease. *Nat Neurosci* 10(11): 1355-1360.

Loftus SK, Erickson RP, Walkley SU, Bryant MA, Incao A, Heidenreich RA and Pavan WJ. 2002. Rescue of neurodegeneration in Niemann-Pick C mice by a prion-promoter-driven Npc1 cDNA transgene. *Hum Mol Genet* 11(24): 3107-3114.

Loftus SK, Morris JA, Carstea ED, Gu JZ, Cummings C, Brown A, Ellison J, Ohno K, Rosenfeld MA, Tagle DA, Pentchev PG and Pavan WJ. 1997. Murine model of Niemann-Pick C disease: mutation in a cholesterol homeostasis gene. *Science* 277(5323): 232-235.

Love S, Bridges LR and Case CP. 1995. Neurofibrillary tangles in Niemann-Pick disease type C. *Brain* 118 (Pt 1): 119-129.

Lowenthal AC, Cummings JF, Wenger DA, Thrall MA, Wood PA and de Lahunta A. 1990. Feline sphingolipidosis resembling Niemann-Pick disease type C. *Acta Neuropathol (Berl)* 81(2): 189-197.

Luan Z, Saito Y, Miyata H, Ohama E, Ninomiya H and Ohno K. 2008. Brainstem neuropathology in a mouse model of Niemann-Pick disease type C. *J Neurol Sci* 268(1-2): 108-116.

Ma J, Phillips L, Wang Y, Dai T, LaPage J, Natarajan R and Adler SG. 2010. Curcumin activates the p38MPAK-HSP25 pathway in vitro but fails to attenuate diabetic nephropathy in DBA2J mice despite urinary clearance documented by HPLC. *BMC Complement Altern Med* 10: 67.

Magistretti J, Mantegazza M, Guatteo E and Wanke E. 1996. Action potentials recorded with patch-clamp amplifiers: are they genuine? *Trends Neurosci* 19(12): 530-534.

Matsuda J, Kido M, Tadano-Aritomi K, Ishizuka I, Tominaga K, Toida K, Takeda E, Suzuki K and Kuroda Y. 2004. Mutation in saposin D domain of sphingolipid activator protein gene causes urinary system defects and cerebellar Purkinje cell degeneration with accumulation of hydroxy fatty acid-containing ceramide in mouse. *Hum Mol Genet* 13(21): 2709-2723.

Mattson MP. 2000. Apoptosis in neurodegenerative disorders. *Nat Rev Mol Cell Biol* 1(2): 120-129.

Mattsson N, Zetterberg H, Bianconi S, Yanjanin NM, Fu R, Mansson JE, Porter FD and Blennow K. 2011. Gamma-secretase-dependent amyloid-beta is increased in Niemann-Pick type C: a cross-sectional study. *Neurology* 76(4): 366-372.

Maxfield FR and van Meer G. 2010. Cholesterol, the central lipid of mammalian cells. *Curr Opin Cell Biol* 22(4): 422-429.

McMahon A, Fowler SC, Perney TM, Akemann W, Knopfel T and Joho RH. 2004. Allele-dependent changes of olivocerebellar circuit properties in the absence of the voltage-gated potassium channels Kv3.1 and Kv3.3. *Eur J Neurosci* 19(12): 3317-3327.

Miller YI, Choi SH, Fang L and Harkewicz R. 2009. Toll-like receptor-4 and lipoprotein accumulation in macrophages. *Trends Cardiovasc Med* 19(7): 227-232.

Mizutani T, Maeda S, Hayakawa K, Tanaka U, Hirahata S, Kamoshita H, Taketani T and Morimatsu Y. 1988. Paraneoplastic cortical cerebellar degeneration. A neuropathological study of an autopsy case in comparison with cortical cerebellar degeneration in alcoholics. *Acta Neuropathol* 77(2): 206-212.

Morris MD, Bhuvaneswaran C, Shio H and Fowler S. 1982. Lysosome lipid storage disorder in NCTR-BALB/c mice. I. Description of the disease and genetics. *Am J Pathol* 108(2): 140-149.

Mukherjee S and Maxfield FR. 2004. Lipid and cholesterol trafficking in NPC. *Biochim Biophys Acta* 1685(1-3): 28-37.

Naureckiene S, Sleat DE, Lackland H, Fensom A, Vanier MT, Wattiaux R, Jadot M and Lobel P. 2000. Identification of HE1 as the second gene of Niemann-Pick C disease. *Science* 290(5500): 2298-2301.

Nishiyama J, Matsuda K, Kakegawa W, Yamada N, Motohashi J, Mizushima N and Yuzaki M. 2010. Reevaluation of neurodegeneration in lurcher mice: constitutive ion fluxes cause cell death with, not by, autophagy. *J Neurosci* 30(6): 2177-2187.

Ogawa C, Kihara A, Gokoh M and Igarashi Y. 2003. Identification and characterization of a novel human sphingosine-1-phosphate phosphohydrolase, hSPP2. *J Biol Chem* 278(2): 1268-1272.

Orenstein SJ and Cuervo AM. 2010. Chaperone-mediated autophagy: molecular mechanisms and physiological relevance. *Semin Cell Dev Biol* 21(7): 719-726.

Pacheco CD, Kunkel R and Lieberman AP. 2007. Autophagy in Niemann-Pick C disease is dependent upon Beclin-1 and responsive to lipid trafficking defects. *Hum Mol Genet* 16(12): 1495-1503.

Pacheco CD and Lieberman AP. 2007. Lipid trafficking defects increase Beclin-1 and activate autophagy in Niemann-Pick type C disease. *Autophagy* 3(5): 487-489.

Pacheco CD and Lieberman AP. 2008. The pathogenesis of Niemann-Pick type C disease: a role for autophagy? *Expert Rev Mol Med* 10: e26.

Pandey P, Farber R, Nakazawa A, Kumar S, Bharti A, Nalin C, Weichselbaum R, Kufe D and Kharbanda S. 2000. Hsp27 functions as a negative regulator of cytochrome c-dependent activation of procaspase-3. *Oncogene* 19(16): 1975-1981.

Pankiv S, Clausen TH, Lamark T, Brech A, Bruun JA, Outzen H, Overvatn A, Bjorkoy G and Johansen T. 2007. p62/SQSTM1 binds directly to Atg8/LC3 to facilitate degradation of ubiquitinated protein aggregates by autophagy. *J Biol Chem* 282(33): 24131-24145.

Pattingre S, Tassa A, Qu X, Garuti R, Liang XH, Mizushima N, Packer M, Schneider MD and Levine B. 2005. Bcl-2 antiapoptotic proteins inhibit Beclin 1-dependent autophagy. *Cell* 122(6): 927-939.

Paul C, Simon S, Gibert B, Virot S, Manero F and Arrigo AP. 2010. Dynamic processes that reflect anti-apoptotic strategies set up by HspB1 (Hsp27). *Exp Cell Res* 316(9): 1535-1552.

Paul CA, Boegle AK and Maue RA. 2004. Before the loss: neuronal dysfunction in Niemann-Pick Type C disease. *Biochim Biophys Acta* 1685(1-3): 63-76.

Pentchev PG, Comly ME, Kruth HS, Vanier MT, Wenger DA, Patel S and Brady RO. 1985. A defect in cholesterol esterification in Niemann-Pick disease (type C) patients. *Proc Natl Acad Sci U S A* 82(23): 8247-8251.

Pentchev PG, Kruth HS, Comly ME, Butler JD, Vanier MT, Wenger DA and Patel S. 1986. Type C Niemann-Pick disease. A parallel loss of regulatory responses in both the uptake and esterification of low density lipoprotein-derived cholesterol in cultured fibroblasts. *J Biol Chem* 261(35): 16775-16780.

Phillips SE, Woodruff EA, 3rd, Liang P, Patten M and Broadie K. 2008. Neuronal loss of Drosophila NPC1a causes cholesterol aggregation and age-progressive neurodegeneration. *J Neurosci* 28(26): 6569-6582.

Pipalia NH, Huang A, Ralph H, Rujoi M and Maxfield FR. 2006. Automated microscopy screening for compounds that partially revert cholesterol accumulation in Niemann-Pick C cells. *J Lipid Res* 47(2): 284-301.

Platt FM, Neises GR, Dwek RA and Butters TD. 1994. N-butyldeoxynojirimycin is a novel inhibitor of glycolipid biosynthesis. *J Biol Chem* 269(11): 8362-8365.

Porter FD, Scherrer DE, Lanier MH, Langmade SJ, Molugu V, Gale SE, Olzeski D, Sidhu R, Dietzen DJ, Fu R, Wassif CA, Yanjanin NM, Marso SP, House J, Vite C, Schaffer JE and Ory DS. 2010. Cholesterol oxidation products are sensitive and specific blood-based biomarkers for Niemann-Pick C1 disease. *Sci Transl Med* 2(56): 56ra81.

Preville X, Salvemini F, Giraud S, Chaufour S, Paul C, Stepien G, Ursini MV and Arrigo AP. 1999. Mammalian small stress proteins protect against oxidative stress through their ability to increase glucose-6-phosphate dehydrogenase activity and by maintaining optimal cellular detoxifying machinery. *Exp Cell Res* 247(1): 61-78.

Raman IM and Bean BP. 1999. Ionic currents underlying spontaneous action potentials in isolated cerebellar Purkinje neurons. *J Neurosci* 19(5): 1663-1674.

Ravikumar B, Sarkar S, Davies JE, Futter M, Garcia-Arencibia M, Green-Thompson ZW, Jimenez-Sanchez M, Korolchuk VI, Lichtenberg M, Luo S, Massey DC, Menzies FM, Moreau K, Narayanan U, Renna M, Siddiqi FH, Underwood BR,

Winslow AR and Rubinsztein DC. 2010. Regulation of mammalian autophagy in physiology and pathophysiology. *Physiol Rev* 90(4): 1383-1435.
Ravikumar B, Vacher C, Berger Z, Davies JE, Luo S, Oroz LG, Scaravilli F, Easton DF, Duden R, O'Kane CJ and Rubinsztein DC. 2004. Inhibition of mTOR induces autophagy and reduces toxicity of polyglutamine expansions in fly and mouse models of Huntington disease. *Nat Genet* 36(6): 585-595.
Rosenbaum AI, Zhang G, Warren JD and Maxfield FR. 2010. Endocytosis of beta-cyclodextrins is responsible for cholesterol reduction in Niemann-Pick type C mutant cells. *Proc Natl Acad Sci U S A* 107(12): 5477-5482.
Rossi D, Cozzio A, Flechsig E, Klein MA, Rulicke T, Aguzzi A and Weissmann C. 2001. Onset of ataxia and Purkinje cell loss in PrP null mice inversely correlated with Dpl level in brain. *Embo J* 20(4): 694-702.
Saeed AI, Sharov V, White J, Li J, Liang W, Bhagabati N, Braisted J, Klapa M, Currier T, Thiagarajan M, Sturn A, Snuffin M, Rezantsev A, Popov D, Ryltsov A, Kostukovich E, Borisovsky I, Liu Z, Vinsavich A, Trush V and Quackenbush J. 2003. TM4: a free, open-source system for microarray data management and analysis. *Biotechniques* 34(2): 374-378.
Saito Y, Suzuki K, Hulette CM and Murayama S. 2004. Aberrant phosphorylation of alpha-synuclein in human Niemann-Pick type C1 disease. *J Neuropathol Exp Neurol* 63(4): 323-328.
Saito Y, Suzuki K, Nanba E, Yamamoto T, Ohno K and Murayama S. 2002. Niemann-Pick type C disease: accelerated neurofibrillary tangle formation and amyloid beta deposition associated with apolipoprotein E epsilon 4 homozygosity. *Ann Neurol* 52(3): 351-355.
Sardiello M, Palmieri M, di Ronza A, Medina DL, Valenza M, Gennarino VA, Di Malta C, Donaudy F, Embrione V, Polishchuk RS, Banfi S, Parenti G, Cattaneo E and Ballabio A. 2009. A gene network regulating lysosomal biogenesis and function. *Science* 325(5939): 473-477.
Sarna J, Miranda SR, Schuchman EH and Hawkes R. 2001. Patterned cerebellar Purkinje cell death in a transgenic mouse model of Niemann Pick type A/B disease. *Eur J Neurosci* 13(10): 1873-1880.
Sarna JR and Hawkes R. 2003. Patterned Purkinje cell death in the cerebellum. *Prog Neurobiol* 70(6): 473-507.
Sarna JR, Larouche M, Marzban H, Sillitoe RV, Rancourt DE and Hawkes R. 2003. Patterned Purkinje cell degeneration in mouse models of Niemann-Pick type C disease. *J Comp Neurol* 456(3): 279-291.
Scherz-Shouval R, Shvets E, Fass E, Shorer H, Gil L and Elazar Z. 2007. Reactive oxygen species are essential for autophagy and specifically regulate the activity of Atg4. *Embo J* 26(7): 1749-1760.
Schulze H, Kolter T and Sandhoff K. 2009. Principles of lysosomal membrane degradation: Cellular topology and biochemistry of lysosomal lipid degradation. *Biochim Biophys Acta* 1793(4): 674-683.
Scott C and Ioannou YA. 2004. The NPC1 protein: structure implies function. *Biochim Biophys Acta* 1685(1-3): 8-13.

Settembre C, Fraldi A, Jahreiss L, Spampanato C, Venturi C, Medina D, de Pablo R, Tacchetti C, Rubinsztein DC and Ballabio A. 2008. A block of autophagy in lysosomal storage disorders. *Hum Mol Genet* 17(1): 119-129.

Shakkottai VG and Paulson HL. 2009. Physiologic alterations in ataxia: channeling changes into novel therapies. *Arch Neurol* 66(10): 1196-1201.

Shi CS and Kehrl JH. 2008. MyD88 and Trif target Beclin 1 to trigger autophagy in macrophages. *J Biol Chem* 283(48): 33175-33182.

Shu L, Lee L and Shayman JA. 2002. Regulation of phospholipase C-gamma activity by glycosphingolipids. *J Biol Chem* 277(21): 18447-18453.

Shu L, Murphy HS, Cooling L and Shayman JA. 2005. An in vitro model of Fabry disease. *J Am Soc Nephrol* 16(9): 2636-2645.

Singh R, Kaushik S, Wang Y, Xiang Y, Novak I, Komatsu M, Tanaka K, Cuervo AM and Czaja MJ. 2009. Autophagy regulates lipid metabolism. *Nature* 458(7242): 1131-1135.

Sleat DE, Wiseman JA, El-Banna M, Kim KH, Mao Q, Price S, Macauley SL, Sidman RL, Shen MM, Zhao Q, Passini MA, Davidson BL, Stewart GR and Lobel P. 2004. A mouse model of classical late-infantile neuronal ceroid lipofuscinosis based on targeted disruption of the CLN2 gene results in a loss of tripeptidyl-peptidase I activity and progressive neurodegeneration. *J Neurosci* 24(41): 9117-9126.

Spiegel S and Milstien S. 2003. Sphingosine-1-phosphate: an enigmatic signalling lipid. *Nat Rev Mol Cell Biol* 4(5): 397-407.

Spillantini MG, Tolnay M, Love S and Goedert M. 1999. Microtubule-associated protein tau, heparan sulphate and alpha-synuclein in several neurodegenerative diseases with dementia. *Acta Neuropathol (Berl)* 97(6): 585-594.

Spires-Jones TL, Stoothoff WH, de Calignon A, Jones PB and Hyman BT. 2009. Tau pathophysiology in neurodegeneration: a tangled issue. *Trends Neurosci* 32(3): 150-159.

Suzuki K, Parker CC, Pentchev PG, Katz D, Ghetti B, D'Agostino AN and Carstea ED. 1995. Neurofibrillary tangles in Niemann-Pick disease type C. *Acta Neuropathol* 89(3): 227-238.

Suzuki M, Sugimoto Y, Ohsaki Y, Ueno M, Kato S, Kitamura Y, Hosokawa H, Davies JP, Ioannou YA, Vanier MT, Ohno K and Ninomiya H. 2007. Endosomal accumulation of Toll-like receptor 4 causes constitutive secretion of cytokines and activation of signal transducers and activators of transcription in Niemann-Pick disease type C (NPC) fibroblasts: a potential basis for glial cell activation in the NPC brain. *J Neurosci* 27(8): 1879-1891.

Swensen AM and Bean BP. 2003. Ionic mechanisms of burst firing in dissociated Purkinje neurons. *J Neurosci* 23(29): 9650-9663.

Syntichaki P and Tavernarakis N. 2003. The biochemistry of neuronal necrosis: rogue biology? *Nat Rev Neurosci* 4(8): 672-684.

Takahashi H, Ikeuchi T, Honma Y, Hayashi S and Tsuji S. 1998. Autosomal dominant cerebellar ataxia (SCA6): clinical, genetic and neuropathological study in a family. *Acta Neuropathol* 95(4): 333-337.

Takai S, Matsushima-Nishiwaki R, Tokuda H, Yasuda E, Toyoda H, Kaneoka Y, Yamaguchi A, Kumada T and Kozawa O. 2007. Protein kinase C delta regulates

the phosphorylation of heat shock protein 27 in human hepatocellular carcinoma. *Life Sci* 81(7): 585-591.
Tamboli IY, Hampel H, Tien NT, Tolksdorf K, Breiden B, Mathews PM, Saftig P, Sandhoff K and Walter J. 2011. Sphingolipid storage affects autophagic metabolism of the amyloid precursor protein and promotes Abeta generation. *J Neurosci* 31(5): 1837-1849.
Tanaka Y, Guhde G, Suter A, Eskelinen EL, Hartmann D, Lullmann-Rauch R, Janssen PM, Blanz J, von Figura K and Saftig P. 2000. Accumulation of autophagic vacuoles and cardiomyopathy in LAMP-2-deficient mice. *Nature* 406(6798): 902-906.
Tavani F, Zimmerman RA, Berry GT, Sullivan K, Gatti R and Bingham P. 2003. Ataxia-telangiectasia: the pattern of cerebellar atrophy on MRI. *Neuroradiology* 45(5): 315-319.
Tillman TS and Cascio M. 2003. Effects of membrane lipids on ion channel structure and function. *Cell Biochem Biophys* 38(2): 161-190.
Tolbert DL, Ewald M, Gutting J and La Regina MC. 1995. Spatial and temporal pattern of Purkinje cell degeneration in shaker mutant rats with hereditary cerebellar ataxia. *J Comp Neurol* 355(4): 490-507.
Torvik A and Torp S. 1986. The prevalence of alcoholic cerebellar atrophy. A morphometric and histological study of an autopsy material. *J Neurol Sci* 75(1): 43-51.
Trudeau MM, Dalton JC, Day JW, Ranum LP and Meisler MH. 2006. Heterozygosity for a protein truncation mutation of sodium channel SCN8A in a patient with cerebellar atrophy, ataxia, and mental retardation. *J Med Genet* 43(6): 527-530.
Turk V, Stoka V and Turk D. 2008. Cystatins: biochemical and structural properties, and medical relevance. *Front Biosci* 13: 5406-5420.
Tusher VG, Tibshirani R and Chu G. 2001. Significance analysis of microarrays applied to the ionizing radiation response. *Proc Natl Acad Sci U S A* 98(9): 5116-5121.
Uekama K, Hirayama F and Irie T. 1998. Cyclodextrin Drug Carrier Systems. *Chem Rev* 98(5): 2045-2076.
Uttenweiler A and Mayer A. 2008. Microautophagy in the yeast Saccharomyces cerevisiae. *Methods Mol Biol* 445: 245-259.
Vance JE, Hayashi H and Karten B. 2005. Cholesterol homeostasis in neurons and glial cells. *Semin Cell Dev Biol* 16(2): 193-212.
Vanier MT and Millat G. 2003. Niemann-Pick disease type C. *Clin Genet* 64(4): 269-281.
Voikar V, Rauvala H and Ikonen E. 2002. Cognitive deficit and development of motor impairment in a mouse model of Niemann-Pick type C disease. *Behav Brain Res* 132(1): 1-10.
Voogd J and Glickstein M. 1998. The anatomy of the cerebellum. *Trends Cogn Sci* 2(9): 307-313.
Walkley SU. 1995. Pyramidal neurons with ectopic dendrites in storage diseases exhibit increased GM2 ganglioside immunoreactivity. *Neuroscience* 68(4): 1027-1035.
Walkley SU and Suzuki K. 2004. Consequences of NPC1 and NPC2 loss of function in mammalian neurons. *Biochim Biophys Acta* 1685(1-3): 48-62.

Wang ML, Motamed M, Infante RE, Abi-Mosleh L, Kwon HJ, Brown MS and Goldstein JL. 2010. Identification of surface residues on Niemann-Pick C2 essential for hydrophobic handoff of cholesterol to NPC1 in lysosomes. *Cell Metab* 12(2): 166-173.

Wang T and Morgan JI. 2007. The Purkinje cell degeneration (pcd) mouse: an unexpected molecular link between neuronal degeneration and regeneration. *Brain Res* 1140: 26-40.

Ward S, O'Donnell P, Fernandez S and Vite CH. 2010. 2-hydroxypropyl-beta-cyclodextrin raises hearing threshold in normal cats and in cats with Niemann-Pick type C disease. *Pediatr Res* 68(1): 52-56.

Waza M, Adachi H, Katsuno M, Minamiyama M, Sang C, Tanaka F, Inukai A, Doyu M and Sobue G. 2005. 17-AAG, an Hsp90 inhibitor, ameliorates polyglutamine-mediated motor neuron degeneration. *Nat Med* 11(10): 1088-1095.

Weintraub H, Abramovici A, Sandbank U, Booth AD, Pentchev PG and Sela B. 1987. Dysmyelination in NCTR-Balb/C mouse mutant with a lysosomal storage disorder. Morphological survey. *Acta Neuropathol* 74(4): 374-381.

Welsh JP, Yuen G, Placantonakis DG, Vu TQ, Haiss F, O'Hearn E, Molliver ME and Aicher SA. 2002. Why do Purkinje cells die so easily after global brain ischemia? Aldolase C, EAAT4, and the cerebellar contribution to posthypoxic myoclonus. *Adv Neurol* 89: 331-359.

Wilcox WR. 2004. Lysosomal storage disorders: the need for better pediatric recognition and comprehensive care. *J Pediatr* 144(5 Suppl): S3-14.

Winkelman MD and Hines JD. 1983. Cerebellar degeneration caused by high-dose cytosine arabinoside: a clinicopathological study. *Ann Neurol* 14(5): 520-527.

Wong AS, Lee RH, Cheung AY, Yeung PK, Chung SK, Cheung ZH and Ip NY. 2011. Cdk5-mediated phosphorylation of endophilin B1 is required for induced autophagy in models of Parkinson's disease. *Nat Cell Biol* 13(5): 568-579.

Wraith JE, Baumgartner MR, Bembi B, Covanis A, Levade T, Mengel E, Pineda M, Sedel F, Topcu M, Vanier MT, Widner H, Wijburg FA and Patterson MC. 2009. Recommendations on the diagnosis and management of Niemann-Pick disease type C. *Mol Genet Metab* 98(1-2): 152-165.

Wraith JE, Vecchio D, Jacklin E, Abel L, Chadha-Boreham H, Luzy C, Giorgino R and Patterson MC. 2010. Miglustat in adult and juvenile patients with Niemann-Pick disease type C: long-term data from a clinical trial. *Mol Genet Metab* 99(4): 351-357.

Xu S, Zhou S, Xia D, Xia J, Chen G, Duan S and Luo J. 2010. Defects of synaptic vesicle turnover at excitatory and inhibitory synapses in Niemann-Pick C1-deficient neurons. *Neuroscience* 167(3): 608-620.

Xu Y, Liu XD, Gong X and Eissa NT. 2008. Signaling pathway of autophagy associated with innate immunity. *Autophagy* 4(1): 110-112.

Xu Z, Farver W, Kodukula S and Storch J. 2008. Regulation of sterol transport between membranes and NPC2. *Biochemistry* 47(42): 11134-11143.

Yamamoto M, Sato S, Hemmi H, Hoshino K, Kaisho T, Sanjo H, Takeuchi O, Sugiyama M, Okabe M, Takeda K and Akira S. 2003. Role of adaptor TRIF in the MyD88-independent toll-like receptor signaling pathway. *Science* 301(5633): 640-643.

Yamanaka K, Chun SJ, Boillee S, Fujimori-Tonou N, Yamashita H, Gutmann DH, Takahashi R, Misawa H and Cleveland DW. 2008. Astrocytes as determinants of disease progression in inherited amyotrophic lateral sclerosis. *Nat Neurosci* 11(3): 251-253.

Yang DS, Stavrides P, Mohan PS, Kaushik S, Kumar A, Ohno M, Schmidt SD, Wesson D, Bandyopadhyay U, Jiang Y, Pawlik M, Peterhoff CM, Yang AJ, Wilson DA, St George-Hyslop P, Westaway D, Mathews PM, Levy E, Cuervo AM and Nixon RA. 2011. Reversal of autophagy dysfunction in the TgCRND8 mouse model of Alzheimer's disease ameliorates amyloid pathologies and memory deficits. *Brain* 134(Pt 1): 258-277.

Yang Z and Klionsky DJ. 2010. Eaten alive: a history of macroautophagy. *Nat Cell Biol* 12(9): 814-822.

Yoneshige A, Suzuki K and Matsuda J. 2010. A mutation in the saposin C domain of the sphingolipid activator protein (Prosaposin) gene causes neurodegenerative disease in mice. *J Neurosci Res* 88(10): 2118-2134.

Yu L, Alva A, Su H, Dutt P, Freundt E, Welsh S, Baehrecke EH and Lenardo MJ. 2004. Regulation of an ATG7-beclin 1 program of autophagic cell death by caspase-8. *Science* 304(5676): 1500-1502.

Yu WH, Cuervo AM, Kumar A, Peterhoff CM, Schmidt SD, Lee JH, Mohan PS, Mercken M, Farmery MR, Tjernberg LO, Jiang Y, Duff K, Uchiyama Y, Naslund J, Mathews PM, Cataldo AM and Nixon RA. 2005. Macroautophagy--a novel Beta-amyloid peptide-generating pathway activated in Alzheimer's disease. *J Cell Biol* 171(1): 87-98.

Yue Z, Horton A, Bravin M, DeJager PL, Selimi F and Heintz N. 2002. A novel protein complex linking the delta 2 glutamate receptor and autophagy: implications for neurodegeneration in lurcher mice. *Neuron* 35(5): 921-933.

Zampieri S, Mellon SH, Butters TD, Nevyjel M, Covey DF, Bembi B and Dardis A. 2009. Oxidative stress in NPC1 deficient cells: protective effect of allopregnanolone. *J Cell Mol Med* 13(9B): 3786-3796.

Zatloukal K, Stumptner C, Fuchsbichler A, Heid H, Schnoelzer M, Kenner L, Kleinert R, Prinz M, Aguzzi A and Denk H. 2002. p62 Is a common component of cytoplasmic inclusions in protein aggregation diseases. *Am J Pathol* 160(1): 255-263.

Zervas M, Somers KL, Thrall MA and Walkley SU. 2001. Critical role for glycosphingolipids in Niemann-Pick disease type C. *Curr Biol* 11(16): 1283-1287.

Zhang M, Strnatka D, Donohue C, Hallows JL, Vincent I and Erickson RP. 2008. Astrocyte-only Npc1 reduces neuronal cholesterol and triples life span of Npc1-/- mice. *J Neurosci Res* 86(13): 2848-2856.

Zhu Y, Romero MI, Ghosh P, Ye Z, Charnay P, Rushing EJ, Marth JD and Parada LF. 2001. Ablation of NF1 function in neurons induces abnormal development of cerebral cortex and reactive gliosis in the brain. *Genes Dev* 15(7): 859-876.

Zhuchenko O, Bailey J, Bonnen P, Ashizawa T, Stockton DW, Amos C, Dobyns WB, Subramony SH, Zoghbi HY and Lee CC. 1997. Autosomal dominant cerebellar ataxia (SCA6) associated with small polyglutamine expansions in the alpha 1A-voltage-dependent calcium channel. *Nat Genet* 15(1): 62-69.